Project Title: An Integrated Approach to Characterizing Bypassed Oil in Heterogeneous and Fractured Reservoirs Using Partitioning Tracers

ANNUAL REPORT
Reporting Period Start Date: June 2003
Reporting Period End Date: June 2004

Principal Author: Akhil Datta-Gupta
August, 2004

DOE Contract No. DE-FC26-02NT15345

Submitting Organization:
Texas Engineering Experiment Station
Texas A&M University, College Station, TX

Subcontractor: Gary A. Pope
Petroleum and Geosystems Engineering
University of Texas, Austin, TX

DISCLAIMER

ABSTRACT

We explore the use of efficient streamline-based simulation approaches for modeling and analysis partitioning interwell tracer tests in heterogeneous and fractured hydrocarbon reservoirs. The streamline approach is generalized to model water injection in naturally fractured reservoirs through the use of a dual media approach. The fractures and matrix are treated as separate continua that are connected through a transfer function, as in conventional finite difference simulators for modeling fractured systems. A detailed comparison with a commercial finite difference simulator shows very good agreement. Furthermore, an examination of the scaling behavior of the computation time indicates that the streamline approach is likely to result in significant savings for large-scale field applications. We also propose a novel approach to history matching finite-difference models that combines the advantage of the streamline models with the versatility of finite-difference simulation. In our approach, we utilize the streamline-derived sensitivities to facilitate history matching during finite-difference simulation. The use of finite-difference model allows us to account for detailed process physics and compressibility effects. The approach is very fast and avoids much of the subjective judgments and time-consuming trial-and-errors associated with manual history matching. We demonstrate the power and utility of our approach using a synthetic example and two field examples. Finally, we discuss several alternative ways of using partitioning interwell tracer tests (PITTs) in oil fields for the calculation of oil saturation, swept pore volume and sweep efficiency, and assess the accuracy of such tests under a variety of reservoir conditions.

TABLE OF CONTENTS

Title page	1
Disclaimer	2
Abstract	3
Executive Summary	5
Introduction	7
Experimental	9
Results and Discussion-Part I	10
Results and Discussion-Part II	45
Results and Discussion-Part III	65
Conclusions	118
References	121
List of Acronyms and Abbreviations	126

EXECUTIVE SUMMARY

During the second year of the project, we have generalized streamline-based simulation to describe fluid transport in naturally fractured reservoirs through a dual-media approach. Describing fluid transport in naturally fractured reservoirs entails additional challenge because of the complicated physics arising from matrix-fracture interactions. The fractures and matrix are treated as separate continua that are connected through a transfer function, as in conventional finite difference simulators for modeling fractured systems. The transfer functions that describe fluid exchange between the fracture and matrix system can be implemented easily within the framework of the current single-porosity streamline models. In particular, the streamline time of flight concept is utilized to develop a general dual porosity dual permeability system of equations for water injection in naturally fractured reservoirs. We compare our results with a commercial finite-difference simulator for waterflooding in five spot and nine-spot patterns. For both dual porosity and dual permeability formulation, the streamline approach shows close agreement in terms of recovery histories and saturation profiles with a marked reduction in numerical dispersion and grid orientation effects. An examination of the scaling behavior of the computation time indicates that the streamline approach is likely to result in significant savings for large-scale field applications.

We also propose a novel approach to history matching finite-difference models that combines the advantage of the streamline models with the versatility of finite-difference simulation. In our approach, we utilize the streamline-derived sensitivities to facilitate history matching during finite-difference simulation. First, the velocity field from the finite-difference model is used to compute streamline trajectories, time of flight and parameter sensitivities. The sensitivities are then utilized in an inversion algorithm to update the reservoir model during finite-difference simulation. The use of finite-difference model allows us to account for detailed process physics and compressibility effects. Although the streamline-derived sensitivities are only approximate, they do not seem to noticeably impact the quality of the match or efficiency of the approach. For history matching, we use ‘a generalized travel-time inversion’ that is shown to be extremely robust because of its quasi-linear properties and converges in only a few iterations. The approach is very fast and avoids much of the subjective judgments and time-consuming trial-and-errors associated with manual history matching. We demonstrate the power and utility of our approach using a synthetic example and two field examples.

We discuss several alternative ways of using partitioning interwell tracer tests (PITTs) in oil fields for the calculation of oil saturation, swept pore volume and sweep efficiency, and assess the accuracy of such tests under a variety of reservoir conditions. The method of moments is used for the interpretation of PITTs in heterogeneous reservoirs with spatially variable residual oil saturation and extends the method to cases with mobile oil saturation. The feasibility of using partitioning tracers to estimate oil saturation at different depths in the reservoir was investigated assuming that the tracer concentrations could be measured with downhole chemical sensors or any other suitable method. The possibility of using natural organic tracers (dissolved components of the crude oil) as a low-cost alternative to injected tracers was also simulated and the method of moments was used to interpret the results for both single porosity and dual porosity reservoirs. All of these applications point to a much greater potential for the PITT technology than is commonly recognized or practiced in the oil field. The results clearly demonstrate that the

method of moments is a very simple, fast and robust method to estimate oil saturation and swept pore volumes from either injected or natural partitioning tracer data.

This report is divided into three major parts. The first part describes the mathematical formulation and numerical implementation of the streamline-based simulation of water injection in naturally fractured reservoirs. The second part of the report develops a novel history matching approach that combines the efficiency of streamline-based sensitivity computations with a 'full physics' finite difference simulator. This considerably broadens the applicability of the streamline-based analysis of tracer data for characterization of heterogeneous and fractured reservoirs. The third part of the report is devoted to the field scale design and optimization of tracer tests using a combination of analytic method of moments and numerical simulation.

The following papers were published based on the work from the second year of this research project.

1. Al-Huthali, A. and Datta-Gupta, A., "Streamline Simulation of Water Injection in Naturally Fractured Reservoirs," SPE 89443 presented at the SPE/DOE fourteenth symposium on Improved Oil Recovery, Tulsa, OK, April 17-21, 2004. (also in *Journal of Petroleum Science and Engineering, August,* 2004*)*

2. Cheng, H, Khargoria, A., He, Z. and Datta-Gupta, A., "Fast History Matching of Finite-difference Models Using Streamline-derived Sensitivities," SPE 89447 presented at the SPE/DOE fourteenth symposium on Improved Oil Recovery, Tulsa, OK, April 17-21, 2004

Also, we have developed a 3D streamline simulator for modeling tracer tests in fractured reservoirs. A user-friendly interface with basic graphics capabilities have been added to facilitate use of the model by practicing engineers.

INTRODUCTION

Streamline Simulation of Water Injection in Naturally Fractured Reservoirs

Until recently streamline simulators were limited to single-porosity systems and not suitable for modeling fluid flow and transport in naturally fractured reservoirs. Describing fluid transport in naturally fractured reservoirs entails additional challenge because of the complicated physics arising from matrix-fracture interactions. In this paper the streamline-based simulation is generalized to describe fluid transport in naturally fractured reservoirs through a dual-media approach. The fractures and matrix are treated as separate continua that are connected through a transfer function, as in conventional finite difference simulators for modeling fractured systems. The transfer functions that describe fluid exchange between the fracture and matrix system can be implemented easily within the framework of the current single-porosity streamline models. In particular, the streamline time of flight concept is utilized to develop a general dual porosity dual permeability system of equations for water injection in naturally fractured reservoirs. We solve the saturations equations using an operator splitting approach that involves 'convection' along streamline followed 'matrix-fracture' exchange calculations on the grid. Our formulation reduces to the commonly used dual porosity model when the flow in the matrix is considered negligible.

We have accounted for the matrix-fracture interactions using two different transfer functions: the conventional transfer function (CTF) and an empirical transfer function (ETF). The ETF allows for analytical solution of the saturation equation for dual porosity systems and is used to validate the numerical implementation. We also compare our results with a commercial finite-difference simulator for waterflooding in five spot and nine-spot patterns. For both dual porosity and dual permeability formulation, the streamline approach shows close agreement in terms of recovery histories and saturation profiles with a marked reduction in numerical dispersion and grid orientation effects. An examination of the scaling behavior of the computation time indicates that the streamline approach is likely to result in significant savings for large-scale field applications.

Fast and Robust History Matching of Field Tracer Tests: A Comparison of Travel Time vs. Amplitude Inversion

We propose a novel approach to history matching finite-difference models that combines the advantage of the streamline models with the versatility of finite-difference simulation. Current streamline models are limited in their ability to incorporate complex physical processes and cross-streamline mechanisms in a computationally efficient manner. A unique feature of streamline models is their ability to efficiently compute the sensitivity of the production data with respect to reservoir parameters using a single flow simulation. These sensitivities define the relationship between changes in production response because of small changes in reservoir parameters and thus, form the basis for many history matching algorithms. In our approach, we utilize the streamline-derived sensitivities to facilitate history matching during finite-difference simulation. First, the velocity field from the finite-difference model is used to compute streamline trajectories, time of flight and parameter sensitivities. The sensitivities are then utilized in an inversion algorithm to update the reservoir model during finite-difference simulation.

The use of finite-difference model allows us to account for detailed process physics and compressibility effects. Although the streamline-derived sensitivities are only approximate, they do not seem to noticeably impact the quality of the match or efficiency of the approach. For history matching, we use 'a generalized travel-time inversion' that is shown to be extremely robust because of its quasi-linear properties and converges in only a few iterations. The approach is very fast and avoids much of the subjective judgments and time-consuming trial-and-errors associated with manual history matching. We demonstrate the power and utility of our approach using a synthetic example and two field examples. The first one is from a CO2 pilot area in the Goldsmith San Andreas Unit, a dolomite formation in west Texas with over 20 years of waterflood production history. The second example is from a giant middle-eastern reservoir and involves history matching a multimillion cell geologic model with 16 injectors and 70 producers. The final model preserved all of the prior geologic constraints while matching 30 years of production history.

Field-Scale Design and Interpretation via Analytic Methods and Numerical Simulation

To complement the streamline-based studies carried out at Texas A&M, a parallel effort has been ongoing using analytic methods and a finite difference model for field-scale design and optimization of tracer tests. This work is carried out under the supervision of Dr. Gary A. Pope at the University of Texas, a subcontractor to the project and discusses several alternative ways of using partitioning interwell tracer tests (PITTs) in oil fields for the calculation of oil saturation, swept pore volume and sweep efficiency, and assesses the accuracy of such tests under a variety of reservoir conditions. The method of moments is used for the interpretation of PITTs in heterogeneous reservoirs with spatially variable residual oil saturation and extends the method to cases with mobile oil saturation. The feasibility of using partitioning tracers to estimate oil saturation at different depths in the reservoir was investigated assuming that the tracer concentrations could be measured with downhole chemical sensors or any other suitable method. The possibility of using natural organic tracers (dissolved components of the crude oil) as a low-cost alternative to injected tracers was also simulated and the method of moments was used to interpret the results for both single porosity and dual porosity reservoirs. All of these applications point to a much greater potential for the PITT technology than is commonly recognized or practiced in the oil field. The results clearly demonstrate that the method of moments is a very simple, fast and robust method to estimate oil saturation and swept pore volumes from either injected or natural partitioning tracer data.

EXPERIMENTAL

No experiments were performed during the second year of the project.

RESULTS AND DISCUSSION: PART I

Streamline Simulation of Water Injection in Naturally Fractured Reservoirs

Introduction

Streamline-based flow simulation has experienced rapid development and industry acceptance in recent years. The approach has been shown to be highly efficient for modeling fluid flow in large, geologically complex systems where the dominant flow patterns are governed by well positions and heterogeneity.[3-6] Streamline simulation has been applied successfully to a wide range of reservoir engineering problems such as ranking geological models[5,6], 'upscaling' from fine-scale models[7], well- allocation factors and pore volumes[5], integration of water-cut and tracer data into reservoir description[8], and history matching[5,8]. The streamline approach provides sub-grid resolution and minimizes numerical dispersion and grid orientation effects compared to conventional finite-difference methods. Also, it offers efficient use of memory and high computational speed.

Until recently[1,2] streamline simulators have been limited to single-porosity system and thus, are not able to explicitly account for the differences in the matrix/fracture transport and more importantly, matrix/fracture exchange mechanisms that can play an importantly role in naturally fractured systems. A common way to circumvent this limitation is to use the dual media approach whereby the matrix and fractures are treated as separate continua throughout the reservoir.[1,2,9,10] The fracture system is typically associated with high permeabilities and low effective porosities whereas the matrix system is assigned low permeabilitites and high porosities. Thus, fluid flow occurs mostly in fracture system and the matrix serves primarily as fluid storage. Additionally, the matrix and the fracture system interact through exchange terms that depend on the differences in fluid pressure between the two systems. Such matrix-fracture exchange is typically modeled using 'transfer functions'.[9,10]

Several authors have studied the matrix-fracture interactions using experimental and theoretical means. Both capillary and gravitational forces can play important role in determining the matrix-fracture exchange rate. Kazemi *et al*.[9] introduced the first multiphase transfer function. Many authors[10,11,12] have reported successful modeling of fluid flow in fractured systems using this type of transfer functions. In this study, we will refer to such transfer functions as the conventional transfer function (CTF). Sonier *et al*.[13] and Litvak[14] modified the CTF by including the gravitational effects from partially water-filled fractures. When water imbibition is the predominant mechanism for displacing oil from the matrix, empirical transfer functions (ETF) have been used to describe the matrix-fracture exchange mechanisms[15-19]. Such empirical models are conceptually simple and can be calibrated against laboratory experiments. Also, these models can be coupled to Buckley-Leverett equation through a fast convolution to describe displacement in fractures surrounded by matrix block. In our streamline implementation, we will utilize both CTF and ETF to describe flow in naturally fractured systems.

Our objective in this paper is to present a streamline-based approach for modeling fluid flow and transport in naturally fractured reservoirs. We extend the streamline approach to fractured media by deriving the saturation equations for dual porosity dual permeability systems using the streamline time of flight as the spatial coordinate. In the absence of matrix flow, the

approach reduces to the commonly used dual porosity system of equations and is identical to the formulation recently proposed by Di Donato et al.[2] We discuss numerical implementation of the saturation equations within the framework of the current streamline models and validate our results by extensive comparison with a commercial finite- difference simulator under fracture flow conditions.

Mathematical Formulation

Fluid Flow Equations in Naturally Fractured Systems. In naturally fractured reservoirs fluids generally exist in two systems (1) the rock matrix, which provides the main bulk of the reservoir volume and storage and (2) the highly permeable rock fractures which provide the main path for fluid flow. If the fracture system is assumed to provide the main path and storage for fluid, i.e. it is not connected to the matrix system, this can be considered as a single-porosity single-permeability system (SPSP) as in **Fig. 1**. On the other hand, if we assume that the fluid flow in the reservoir takes place primarily through the fracture networks while the matrix-blocks are linked only through the fracture system, this could be regarded as a dual-porosity single-permeability system (DPSP) as in **Fig. 2**. In addition, if there is flow between matrix-blocks, this can be considered as a dual-porosity dual-permeability system (DPDP) as in **Fig. 3**. Clearly, the dual-porosity dual-permeability system is the most general approach to modeling fractured reservoirs and will reduce to the dual-porosity system when flow in the matrix block is assumed to be negligible. The applicability and limitations of these approaches have been discussed by Dean and Lo.[10]

Consider two-phase incompressible flow in a DPDP system. The governing equations that describe fluid flow consist of two sets of equations[9,10,11,12]. The first set deals with the fluid transport in the fractured system, **Eq. 1**, and the second set deals with the fluid transport in the matrix system, **Eq. 2**. Each set consists of one equation for each phase.

$$\begin{aligned}
\nabla \cdot \vec{\vec{k}}_f \cdot \left(\lambda_{of} \nabla P_{of} + \lambda_{ogf} \nabla D\right) - \Gamma_o + q_{of} &= \phi_f \frac{\partial S_{of}}{\partial t} \\
\nabla \cdot \vec{\vec{k}}_f \cdot \left(\lambda_{wf} \nabla P_{wf} + \lambda_{wgf} \nabla D\right) - \Gamma_w + q_{wf} &= \phi_f \frac{\partial S_{wf}}{\partial t}
\end{aligned} \tag{1}$$

$$\begin{aligned}
\nabla \cdot \vec{\vec{k}}_m \cdot \left(\lambda_{om} \nabla P_{om} + \lambda_{ogm} \nabla D\right) + \Gamma_o + q_{om} &= \phi_m \frac{\partial S_{om}}{\partial t} \\
\nabla \cdot \vec{\vec{k}}_m \cdot \left(\lambda_{wm} \nabla P_{wm} + \lambda_{wgm} \nabla D\right) + \Gamma_w + q_{wm} &= \phi_m \frac{\partial S_{wm}}{\partial t}
\end{aligned} \tag{2}$$

The subscripts *m* and *f* represent matrix and fracture system respectively. The mobility of oil and water in each system, λ_o and λ_w, are defined, as follows:

$$\lambda_o = \frac{k_{ro}}{\mu_o}$$
$$\lambda_w = \frac{k_{rw}}{\mu_w} \tag{3}$$

The gravity terms, λ_{og} and λ_{wg}, are defined, as follows:

$$\lambda_{og} = \frac{k_{ro}\rho_o g}{\mu_o}$$
$$\lambda_{wg} = \frac{k_{rw}\rho_w g}{\mu_w} \tag{4}$$

The transfer terms, Γ_o and Γ_w, represent the volumetric oil and water rate transferred between fracture and matrix systems. Clearly, these transfer terms describe the matrix-fracture interactions and we will discuss them in a later section.

Streamline Modeling of Fractured Reservoirs. The underlying principle of streamline simulation is to first trace streamlines through the reservoir using a velocity field and then to transport fluid along these streamlines. In this section, we first discuss the formulation of the pressure equations that form the basis for the velocity fields and streamline trajectories. Next, we transform the saturation equations to the streamline time of flight coordinates to facilitate analytical and numerical calculations of saturations along streamlines.

Pressure Equation for Tracing Streamlines. The first step toward tracing streamlines is to generate a pressure field by solving the pressure equation using a finite difference or finite element scheme. The pressure field can then be converted to a total-velocity field using Darcy's law. Once the total-velocity field is generated, streamlines can be traced easily because they are locally tangential to the total-velocity.[3-6] If we neglect capillarity and add the water-oil equations for each system, we obtain the pressure equations for the fracture and matrix systems as follows:

$$\nabla \cdot \vec{\vec{k}}_f \cdot \left(\lambda_{tf} \nabla P_f + \lambda_{gf} \nabla D\right) - \Gamma_t = -q_{sf} \tag{5}$$

$$\nabla \cdot \vec{\vec{k}}_m \cdot \left(\lambda_{tm} \nabla P_m + \lambda_{gm} \nabla D\right) + \Gamma_t = -q_{sm} \tag{6}$$

where

$$\lambda_t = \lambda_o + \lambda_w$$
$$\lambda_g = \lambda_{og} + \lambda_{wg} \tag{7}$$

The total transfer term, Γ_t, is given as:

$$\Gamma_t = \Gamma_o + \Gamma_w \tag{8}$$

Because we have flow in both matrix and fracture systems in the DPDP formulation, we have to trace streamlines in both the systems. **Eq.5** and **Eq.6** together provide the pressure fields in these systems.

In the DPSP approach, we assume no flow between matrix-blocks. So, the flow and sink terms in **Eq.6** will vanish. **Eq.6** can be written as:

$$\Gamma_t = 0 \tag{9}$$

If we combine **Eq.8** and **Eq.9**, we conclude that the transfer terms, Γ_o and Γ_w, have equal magnitudes and opposite directions.

$$\Gamma_o = -\Gamma_w \tag{10}$$

Because there is no flow in the matrix system, streamlines will be generated and traced only in the fracture system using the following pressure equation:

$$\nabla \cdot \vec{\vec{k}}_f \cdot \left(\lambda_{tf} \nabla P_f + \lambda_{gf} \nabla D\right) = -q_{sf} \tag{11}$$

It is important to point out that the transfer term doesn't appear in the pressure equation. Thus, the transfer term will not affect streamline trajectories and the trajectory computations for the DPSP system is identical to that of a conventional SPSP streamline simulator. However, for the DPDP system, the pressure distribution in the matrix and the fracture system need to be solved for simultaneously in the same manner as in conventional finite-difference simulation and the details have been discussed by Dean and Lo.[10]

Transformation of Saturation Equations to Streamline Coordinates. The equations that describe the evolution of water saturation in a DPDP system (**Eqs. 1** and **2**) can be re-written as follows:

$$\phi_f \frac{\partial S_{wf}}{\partial t} + \vec{u}_{tf} \cdot \nabla f_{wf} + f_{wf} \nabla . \vec{u}_{tf} + \nabla \cdot \vec{G}_f + \Gamma_w = 0 \tag{12}$$

$$\phi_m \frac{\partial S_{wm}}{\partial t} + \vec{u}_{tm} \cdot \nabla f_{wm} + f_{wm} \nabla . \vec{u}_{tm} + \nabla \cdot \vec{G}_m - \Gamma_w = 0 \tag{13}$$

In **Eq.12** and **Eq.13** f_w is the fractional flow of water given by

$$f_w = \frac{\lambda_w}{\lambda_t} \tag{14}$$

and G represents the gravity term defined as,

$$\vec{G} = k \cdot \frac{\lambda_w \lambda_o}{\lambda_t} (\rho_o - \rho_w) g \nabla D \tag{15}$$

To write **Eq.12** and **Eq.13** in terms of streamline time of flight (TOF), the following coordinate transformation is applied[3-6,20]

$$\vec{u}_t \cdot \nabla = \phi \frac{\partial}{\partial \tau} \tag{16}$$

where the TOF, τ, is the time required by a neutral tracer to travel along the streamline, ψ

$$\tau = \int_{along\ \psi} \frac{\phi}{\|u_t\|} \partial \zeta \tag{17}$$

The saturation equations for fracture and matrix systems now reduce to the following

$$\frac{\partial S_{wf}}{\partial t} + \frac{\partial f_{wf}}{\partial \tau_f} + f_{wf} \nabla . \vec{u}_{tf} + \frac{\nabla \cdot \vec{G}_f}{\phi_f} + \frac{\Gamma_w}{\phi_f} = 0 \tag{18}$$

$$\frac{\partial S_{wm}}{\partial t} + \frac{\partial f_{wm}}{\partial \tau_m} + f_{wm} \nabla . \vec{u}_{tm} + \frac{\nabla \cdot \vec{G}_m}{\phi_m} - \frac{\Gamma_w}{\phi_m} = 0 \tag{19}$$

Eq.18 and **Eq.19** can be used to solve for saturation along the streamlines in fracture and matrix systems in a DPDP model. Notice that the terms $f_{wf} \nabla . \vec{u}_{tf}$ and $f_{wm} \nabla . \vec{u}_{tm}$ represent additional cross-flux in the matrix and the fracture system in the DPDP model. Also, $\vec{u}_{tf}$ and $\vec{u}_{tm}$ may not be defined over the entire spatial domain. Under such conditions, we revert back to the total velocity (matrix + fracture) for tracing streamlines.

For the DPSP model the flow in the matrix is ignored and we will trace streamlines only in the fracture system. So, the main transport equation is the saturation equation in the fracture system, **Eq.18**. In addition, the fracture velocity represents the total system velocity which is a conserved quantity, that is $\nabla . \vec{u}_{tf} = 0$. The saturation equations for the fracture and matrix systems for the DPSP model now reduce to the following

$$\frac{\partial S_{wf}}{\partial t}+\frac{\partial f_{wf}}{\partial \tau_f}+\frac{\nabla\cdot\vec{G}_f}{\phi_f}+\frac{\Gamma_w}{\phi_f}=0 \tag{20}$$

$$\Gamma_w=\phi_m\frac{\partial S_{wm}}{\partial t} \tag{21}$$

Finally, for the SPSP system, both fluid flow and storage are assumed to be in the fracture system only and the interaction with the matrix is not included. The saturation equation reduces to the one currently used in conventional streamline simulators.

Matrix-Fracture Transfer Functions

In the previous sections we have discussed the derivation of the saturation equations for the DPDP and the DPSP systems in terms of streamline TOF coordinates. We now focus on describing the interactions between the matrix and the fracture systems through the use of transfer functions. A detailed discussion of several transfer functions and their implementation in streamline simulation can be found in Di Donato et al.[2] The conventional transfer function (CTF), which is the most common form of transfer function used in fractured reservoir simulations, has the following form for water and oil phases[9,10,11,12]:

$$\Gamma_w=F_s k_m \lambda_{wmf}\left(P_{wf}-P_{wm}\right) \tag{22}$$

$$\Gamma_o=F_s k_m \lambda_{omf}\left(P_{of}-P_{om}\right) \tag{23}$$

where

$$\begin{aligned} P_{wf}&=P_{of}-P_{cf}\\ P_{wm}&=P_{om}-P_{cm}\end{aligned} \tag{24}$$

In **Eqs. 22** and **23**, we ignore the gravitational forces and assume a pseudo-steady state behavior in the matrix block. Also, the mobility ratios, λ_{wmf} and λ_{omf}, represent the upstream mobility between fracture and matrix systems and F_s is a shape factor that defines the connectivity between the matrix block and the surrounding fractures.

Note that **Eq.22** and **Eq.23** are functions of phase saturation and pressure. In DPSP system, the dependency of these equations on the phase pressure can be eliminated using **Eq.9** and the capillary pressure relations as follows,

$$\left(P_{of}-P_{om}\right)=\frac{\lambda_{wmf}}{\lambda_{omf}+\lambda_{wmf}}\left(P_{cf}-P_{cm}\right) \tag{25}$$

By substituting **Eq.25** into **Eq.23**, we arrive at the following transfer function for the DPSP streamline simulator,

$$\Gamma_w = F_S k_m \frac{\lambda_{wmf}\lambda_{omf}}{\lambda_{omf} + \lambda_{wmf}}\left(P_{cm} - P_{cf}\right) \tag{26}$$

For a rectangular matrix block with all sides exposed to imbibing water, the shape factor has the following form[9]:

$$F_s = 4\left(\frac{1}{l_x^2} + \frac{1}{l_y^2} + \frac{1}{l_z^2}\right) \tag{27}$$

When countercurrent imbibition is the dominant force for displacing oil from the matrix, empirical transfer functions (ETF) have also been used to describe the matrix-fracture exchange in DPSP systems. The advantage of the ETF is that we can derive an analytical solution to the Buckley-Leverett displacement for saturation calculations in the fracture system.[19] We will utilize the analytical solution to validate our numerical computations of saturations along streamlines. In the ETF, the cumulative oil recovery from a matrix-block surrounded by water can be approximated by the following[21]

$$Q = Q_\infty\left(1 - e^{-\omega t}\right) \tag{28}$$

where ω is a rate constant that is defined as the reciprocal of the time required by the matrix-block to expel 63% of the recoverable oil[19]. This constant can also be determined empirically from laboratory experiments. By differentiating **Eq.28**, the volumetric rate of water transferred from the fracture system to the matrix-blocks is given by:

$$\Gamma_{w@S_w=1.0} = Q_\infty \omega e^{-\omega t} \tag{29}$$

Eq.29 assumes 100% water saturation in the fracture system. This implies that the oil transferred from the matrix is rapidly carried away by the water flowing in the fracture system. To account for changing water saturation in the fracture, a fast convolution can be utilized as suggested by DeSwaan[17]:

$$\Gamma_w = Q_\infty \omega \int_0^t e^{-\omega(t-\varepsilon)} \frac{\partial S_{wf}(\varepsilon)}{\partial \varepsilon} \partial\varepsilon \tag{30}$$

So far we have assumed that the primary recovery mechanism is counter-current imbibition in the DPSP system. This applies when the vertical dimension, l_z of the matrix-block is small. If l_z is large, a gravity head between the matrix-block and the fracture system also will cause fluid movement. **Fig. 4** illustrates the gravity head concept in a single matrix-block surrounded by fractures. If gravity is included in the transfer function, the volumetric oil and water rate can be expressed as[13,14]

$$\Gamma_w = F_s k_m \lambda_{wmf} \left(P_{of} - P_{om} - P_{cf} + P_{mf} + \frac{\Delta P_{gh}}{2} \right)$$
$$\Gamma_o = F_s k_m \lambda_{omf} \left(P_{of} - P_{om} - \frac{\Delta P_{gh}}{2} \right) \tag{31}$$

where

$$\Delta P_{gh} = l_z \left(S_{wnf} - S_{wnm} \right)\left(\rho_w - \rho_o \right) g$$
$$S_{wnf} = \frac{S_{wf} - S_{wcf}}{1 - S_{orf} - S_{wcf}} \tag{32}$$
$$S_{wnm} = \frac{S_{wm} - S_{wcm}}{1 - S_{orm} - S_{wcm}}$$

and S_{wnf}, S_{wnm} are the normalized water saturation in the fracture system and the matrix-block**.**

Finally, utilizing **Eq.9**, the volumetric water transfer rate between fracture and matrix system including gravity is

$$\Gamma_w = F_s k_m \frac{\lambda_{wmf} \lambda_{omf}}{\lambda_{omf} + \lambda_{wmf}} \left(P_{cm} - P_{cf} + \Delta P_{gh} \right) \tag{33}$$

Numerical Solution To Saturation Equations

Dual-Porosity Dual-Permeability System. In the DPDP system, we assume that fluid flow occurs both in the matrix and fracture systems. Thus, we need to generate streamlines for both the systems and compute water saturation along these streamlines. For clarity, we will ignore gravity and cross-flux terms in this discussion. Both of these terms can be included as part of the 'corrective step' in the numerical solution discussed later in this section. Now **Eq.18** and **Eq.19** lead to the following saturation equations for the matrix and fracture systems,

$$\frac{\partial S_{wf}}{\partial t} + \frac{\partial f_{wf}}{\partial \tau_f} + \frac{\Gamma_w}{\phi_f} = 0 \tag{34}$$

$$\frac{\partial S_{wm}}{\partial t} + \frac{\partial f_{wm}}{\partial \tau_m} - \frac{\Gamma_w}{\phi_m} = 0 \tag{35}$$

In general, the streamlines in the fracture and matrix systems will be quite different and this results in difficulties in solving **Eq.34** and **Eq.35** because of their coupling through the transfer terms. We circumvent these difficulties using an operator splitting procedure.[22,23] The underlying idea here is to represent the time derivative in **Eq.34** and **Eq.35** as a convective time step followed by a corrective time step.[24]

$$\begin{aligned} \frac{\partial S_{wf}}{\partial t} &\rightarrow \frac{\partial S_{wf}}{\partial t_1} + \frac{\partial S_{wf}}{\partial t_2} \\ \frac{\partial S_{wm}}{\partial t} &\rightarrow \frac{\partial S_{wm}}{\partial t_1} + \frac{\partial S_{wm}}{\partial t_2} \end{aligned} \tag{36}$$

The convective time-step includes the saturation evolution along the streamlines because of the viscous forces. The corrective time-step incorporates the transfer term between the fracture and the matrix systems.

Thus, the convective terms are given as,

$$\frac{\partial S_{wf}}{\partial t_1} + \frac{\partial f_{wf}}{\partial \tau_f} = 0 \tag{37}$$

$$\frac{\partial S_{wm}}{\partial t_1} + \frac{\partial f_{wm}}{\partial \tau_m} = 0 \tag{38}$$

and the corrective terms are given as,

$$\frac{\partial S_{wf}}{\partial t_2} + \frac{\Gamma_w}{\phi_f} = 0 \tag{39}$$

$$\frac{\partial S_{wm}}{\partial t_2} - \frac{\Gamma_w}{\phi_m} = 0 \tag{40}$$

The convective part can be solved using similar procedures as in single-porosity streamline simulation.[3-6] The streamline saturation resulting form the convective calculations are then mapped back onto the grid and used as initial conditions for the corrective step. The corrective equations accounting for the exchange are then solved on the grid-blocks.

We used an explicit finite-difference scheme to discretize the convective term in the fracture system, **Eq.37**

$$S_{wf,i}^{n+1} - S_{wf,i}^{n} = -\Delta t \frac{f_{wf,i}^{n} - f_{wf,i-1}^{n}}{\Delta \tau_f} \tag{41}$$

Note that *i*-index represents nodes along the streamline. In a similar way, we can discretize the convective term in the matrix system.

We can use the same numerical scheme for the corrective term for the fracture system, **Eq.39**.

$$S_{wf,i}^{n+1} - S_{wf,i}^{n} = -\Delta t \left\{ \begin{array}{l} \left(\frac{F_s k_m}{\phi_f} \right)_i \left(\frac{\lambda_{wmf} \lambda_{omf}}{\lambda_{omf} + \lambda_{wmf}} \right)_i^n \\ \left(P_{cm} - P_{cf} \right)_i^n \end{array} \right\} \tag{42}$$

In **Eq.42**, *i*-index represents the grid-block numbers. Similarly, the same formulation can be used for the corrective term for the matrix system, **Eq.40**. An iterative calculation of matrix-fracture saturations will probably make the approach more robust but is likely to be more time consuming.[2] For example cases presented here, we did not see the need for such an iterative procedure.

As mentioned before, the fracture and matrix saturations from the convective step are mapped onto the grid and used as an initial condition for the corrective step. The following weighted average is used to map fracture saturation,

$$S_{wf,grid} = \frac{\sum_{i=1}^{nsl} S_{wf,i} \Delta \tau_{f,i}}{\sum_{i=1}^{nsl} \Delta \tau_{f,i}} \tag{43}$$

where *nsl* is the number of streamlines passing through a grid-block, $\Delta\tau$ is the time of flight across the grid-block. We use the same averaging scheme to map the matrix saturation back onto the grids.

Dual-Porosity Single-Permeability System. In the DPSP system, streamlines will be generated and traced only through the fracture system. So the convective and transfer terms in the saturation equation can be solved together in a coupled fashion along the streamline and no time-splitting is required. Using the CTF the saturation equation in the fracture system will have the following numerical form:

$$S_{wf,i}^{n+1} - S_{wf,i}^{n} = -\Delta t \left\{ \begin{array}{l} \dfrac{f_{wf,i}^{n} - f_{wf,i-1}^{n}}{\Delta \tau_f} + \\ \left(\dfrac{F_s k_m}{\phi_f} \right)_i \left(\dfrac{\lambda_{wmf} \lambda_{omf}}{\lambda_{omf} + \lambda_{wmf}} \right)_i^n \\ \left(P_{cm} - P_{cf} \right)_i^n \end{array} \right\} \tag{44}$$

Matrix saturation can be calculated from the mass conservation equation, **Eq.21**. The explicit numerical form of this equation is

$$S_{wm,i}^{n+1} - S_{wm,i}^{n} = -\Delta t \left\{ \begin{array}{l} \left(\dfrac{F_s k_m}{\phi_f} \right)_i \left(\dfrac{\lambda_{wmf} \lambda_{omf}}{\lambda_{omf} + \lambda_{wmf}} \right)_i^n \\ \left(P_{cm} - P_{cf} \right)_i^n \end{array} \right\} \tag{45}$$

If the ETF is used in the saturation equations, the fracture saturation equation will have the following numerical form:

$$\begin{aligned} S_{wf,i}^{n+1} - S_{wf,i}^{n} &= \left\{ \begin{array}{l} -\left(\dfrac{1}{\Delta t} + \dfrac{Q_\infty \omega}{\phi_f} e^{-\omega \Delta t} \right)^{-1} \\ \left(\dfrac{f_{wf,i}^{n} - f_{wf,i-1}^{n}}{\Delta \tau_f} + \right. \\ \left. \dfrac{Q_\infty \omega}{\phi_f} SUM^{n-1} e^{-\omega \Delta t} \right) \end{array} \right\} \\ SUM^{n-1} &= \left[SUM^{n-2} + \left(S_{wf,i}^{n} - S_{wf,i}^{n-1} \right) \right] e^{-\omega \Delta t}, n \geq 1 \\ SUM^{n-1} &= 0 \end{aligned} \tag{46}$$

where we have used a difference scheme proposed by Kazemi *et al*.[19] to estimate the convolution term in the ETF. Matrix saturation equation, **Eq.21**, can be solved numerically using similar procedure

$$S_{wm,i}^{n+1} - S_{wm,i}^{n} = -\Delta t \left(\frac{Q_\infty \omega}{\phi_f} SUM^{n-1} e^{-\omega \Delta t} \right) \tag{47}$$

Fracture system water saturation along streamlines can be mapped back onto the grid using **Eq.43**. Matrix saturation along streamlines can be mapped onto the grid-blocks using the following arithmetic average

$$S_{wm,grid} = \frac{1}{nsl}\sum_{i=1}^{nsl} S_{wm,i} \tag{48}$$

If **Eq.46** were used to compute the saturation evolution, the summation term, SUM^{n-1}, is mapped onto the grid-block for the next time update calculations. A weighted average can be used to map the summation term.

$$SUM_{grid}^{n-1} = \frac{\sum_{i=1}^{nsl} SUM_i^{n-1}\Delta\tau_{f,i}}{\sum_{i=1}^{nsl}\Delta\tau_{f,i}} \tag{49}$$

Validating Numerical Solution of the Saturation Equation with ETF. The saturation equation with the ETF for displacement in the fracture can be written as

$$\frac{\partial S_{wf}}{\partial t} + H\frac{\partial S_{wf}}{\partial \tau_f} + \frac{Q_\infty}{\phi_f}\omega\int_0^t e^{-\omega(t-\varepsilon)}\frac{\partial S_{wf}(\varepsilon)}{\partial \varepsilon}\partial\varepsilon = 0$$
$$H = \frac{\partial f_{wf}}{\partial S_{wf}} \tag{50}$$

with the following initial and boundary conditions:

$$S_{wf}(\tau_f, 0) = 0$$
$$S_{wf}(0, t) = 1 \tag{51}$$

For constant H, we can solve **Eq.50** analytically for saturation distribution in the fracture.[19] This allows us to validate our numerical computations of saturations along streamlines by comparing the results from the numerical and analytical solutions. The example used to perform this comparison involves water injection in a heterogeneous quarter five-spot pattern. **Fig. 5** shows a 2D permeability field which represents the fracture distribution. Other parameters are presented in **Table 1**. **Fig. 6** shows the fracture-water saturation at two different times for the numerical and the analytical solutions. The results are in excellent agreement which indicates the validity of the numerical solution of the saturation equation.

RESULTS AND DISCUSSION

In this section, we discuss the implementation of the DPSP and DPDP streamline formulation using several examples involving waterflood in five-spot and nine-spot patterns. We examine the effects of the transfer term on the saturation evolution and production histories and compare our results with a commercial DPSP/DPDP simulator viz. ECLIPSE.[25]

Dual-Porosity Single-Permeability System without Gravity Effects. Here we use the CTF without the gravity terms and compare the results from the DPSP streamline simulator with those from the fully implicit DPSP ECLIPSE in terms of water cut and recovery histories and water saturation distributions. The comparison is based on two examples involving waterflood in homogeneous and heterogeneous quarter five spot patterns.

Homogenous Case: Quarter Five Spot Pattern. This example was first presented by Kazemi *et al*.[9] and later used by Thomas *et al*.[12]. **Table 2** shows the reservoir parameters. **Figs. 7** and **8** show relative permeability and capillary pressure curves used in this example. Streamlines for this case are shown in **Fig. 9**. To start with, we investigate the impact of the transfer function on the streamline simulation results. **Figs. 10** and **11** show the water saturation map and the water cut history from the DPSP streamline simulator with and without the CTF. The case without CTF represents the conventional single porosity streamline formulation. Here the water cut is higher and the water saturation advances faster because the interaction with the matrix system is not included. Next, we compare the DPSP streamline simulation to the DPSP ECLIPSE. **Fig. 12** shows water cut and recovery histories from the two simulators indicating an excellent agreement. **Figs. 13** and **14** show the water saturation in fracture and matrix system at two different times from both the simulators. The saturation maps are clearly in good agreement.

Heterogeneous Case: Quarter Five Spot Pattern. We now extend our discussion to a heterogeneous quarter five spot case. The parameters used here are the same as in **Table 2**, except for the fracture permeability. The permeability field is the one shown in **Fig. 5**. **Fig. 15** shows the water saturation in the fracture system with and without the transfer function. As before, the dual porosity formulation slows down the water advancement in the fracture because of the interaction with the matrix. **Fig. 16** compares the water cut response indicating the significance of the dual porosity formulation. The streamline trajectories are shown in **Fig. 17** and reflect the permeability heterogeneity in the fracture system. The water cut and recovery histories for the DPSP streamline simulator and the DPSP ECLIPSE are in good agreement as shown in **Fig. 18**. Similar agreements are found in the fracture and matrix water saturation from both simulators as illustrated in **Fig. 19** and **Fig. 20**. However, the saturation fronts from ECLIPSE are somewhat smeared because of numerical dispersion. The streamline saturation calculations are decoupled from the simulation grid and the effects of permeability heterogeneity on the saturation front are more prominent here.

Dual-Porosity Single Permeability System with Gravity Effects. In this section we examine the impact of gravity terms in the transfer function and again, compare our results with DPSP ECLIPSE using two examples: a homogenous quarter five-spot pattern, and a heterogeneous nine-spot pattern.

Homogenous Case: Quarter Five Spot Pattern. **Table 3** presents the reservoir parameters, and **Fig. 7** and **Fig. 8** show relative permeability and capillary pressure curves used in this example. **Fig. 21** presents the water cut histories for three scenarios using ECLIPSE. These are: (1) no transfer function, (2) a transfer function including the imbibition only, and (3) a transfer function including the gravity and imbibition. As before, the simulation run without transfer function shows the highest water cut response and the earliest breakthrough time. The simulation run with imbibition transfer function shows the lowest water cut response in this case. Including the gravity effects tend to reduce the recovery from the matrix for these examples. **Fig. 22** shows that the DPSP streamline simulator predicts the same behavior as ECLIPSE. In **Fig. 23**, we have superimposed the results indicating the close agreement between the simulators.

Heterogeneous Case: Nine Spot Pattern. We now extend the discussion in the previous section to a heterogeneous nine spot example. The fracture permeability field is the same 2D permeability map shown in **Fig. 5**. **Table 4** presents the reservoir parameters used in this example. We used the same relative permeability and capillary curves as the previous examples. **Fig. 24** shows the streamline pattern in the reservoir. The water cut and recovery histories for the DPSP streamline simulator and the DPSP ECLIPSE are almost identical as shown in **Fig. 25**. For individual wells, the water cut and recovery histories from both simulators are also in good agreement as shown in **Fig. 26**. Fracture and matrix water saturation for both the simulators also show a good match as illustrated in **Fig. 27**. **Fig. 27** again shows the effects of numerical dispersion in the ECLIPSE results leading to smearing of sharp fronts in the saturation map.

Dual-Porosity Dual-Permeability System. We now discuss applications of the dual porosity dual-permeability streamline formulation for modeling fractured systems. Such a model is appropriate when the contrast between the matrix and the fracture permeability is not large enough to justify a DPSP approach.[10] Unlike the previous results, now flow occurs both in the matrix and fracture systems and streamlines need to be generated for both the systems. The saturation advancement along streamlines is carried out using the operator splitting approach as outlined before. We will compare our results with DPDP ECLIPSE for water injection in homogeneous and heterogeneous nine-spot patterns.

Homogeneous Case: Nine-spot Pattern. The reservoir parameters used here are presented in **Table 4** except for the matrix permeability which was increased to 100 md to allow more flow. The fracture permeability used in this example was 500 md. The relative permeability and capillary curves are shown in **Fig. 7** and **Fig. 8**. Recall that in the operator splitting approach, first a time interval is selected during which we update the saturation using the convective term followed by a second update using a corrective step that includes the transfer term. We will refer to this time interval as 'splitting time-step' (SPT). During the SPT, we solve the convective terms using a 'convective time-step' (CVT). Once the convective terms are solved along

streamlines, fracture and matrix water saturations are mapped back onto the grid block. Now the corrective equations can be solved on the grid for the same SPT using a 'corrective time-step' (CRT). The choice of the CVT and CRT depends on the stability of the numerical solution of the convective and corrective terms. The choice of the SPT depends, among others, on transverse fluxes arising from mobility and unsteady state effects and some guidelines are provided by Osako et al.[24]

To start with we choose SPT equal to 250 days. **Fig. 28** shows the water cut response from two producing wells during the convective step for each SPT interval. On the same plot, we indicated the water cut responses after the corrective step. The water cut response shows close agreement with the DPDP ECLIPSE after we incorporate the corrective terms in the saturation calculations. These results clearly indicate the validity of the operator splitting approach. We also examined the sensitivity of the results on the split-time interval using a longer SPT of 500 days. **Fig. 29** shows that this choice of time step clearly leads to erroneous results. However, detailed investigation of error estimates or stability criterion was beyond the scope of this study and remains an area of future research. **Fig. 30** presents a comparison between the DPDP Streamline simulator and ECLIPSE in terms of water saturation distribution after 1000 days. The SPT was chosen to be equal to 250 days. Both simulators show comparable results.

Heterogeneous Case: Nine Spot Pattern. We now extend the discussion for a heterogeneous case with the fracture permeability field in **Fig. 5**. A comparison between the DPDP streamline simulator and the DPDP ECLIPSE in terms of water cut response shows good agreement for all eight producers as shown in **Fig. 31**. Fracture and matrix water saturation from both the simulators also show good match as illustrated in **Fig. 32**. As before, some impact of grid orientation and numerical smearing are evident in the ECLIPSE results.

CPU Time and Scaling. In this section, we compare the CPU time and its scaling behavior for DPSP streamline simulation, fully implicitly DPSP ECLIPSE and IMPES DPSP ECLIPSE. We performed multiple runs on a 3D homogenous case with different number of grid blocks to examine the scaling behavior of the CPU time. **Table 5** shows the parameters used to perform this task.

Fig. 33 shows the CPU time comparison. The CPU time for the IMPES DPSP ECLIPSE has a quadratic relationship with the grid-block numbers. This indicates that using this type of simulation for large models is not computationally efficient. The fully implicit DPSP shows some improvement in CPU time with a scaling exponent of 1.69. On the other, the DPSP streamline simulator CPU time increases linearly as the number of grid-block increases. The results are in agreement with the findings of Di Donato *et al*.[2] and tend to affirm that the streamline simulation will be particularly advantageous for field-scale simulation using high resolution geologic models.

Table 1- Parameters for Quarter Five Spot Example Used to Validate the Numerical Solution of the Saturation Equation with ETF.

Parameters	*Values*
Area, ft2	1,440,000
Thickness, ft	30
Injection and Production Rates, STB/Day	100
ω, 1/Day	0.001
ϕ_f	0.01
ϕ_m	0.16
S_{wcm} & S_{orm}	0.25
k_{rwf}	S_{wf}
k_{rof}	1- S_{wf}
μ_w	1
μ_o	1
k_f, *md*	10000

Table 2-Quarter Five Spot Parameters, Homogenous Case (Imbibition Only).

Parameters	*Values*
Dimension In I-Direction, ft	600
Dimension In J-Direction, ft	600
Thickness, ft	30 ft
Reservoir Grid	40 × 40×1
Injection Rates, STB/Day	210
Production Rate, STB/Day	200
k_m, *md*	1
k_f, *md*	10000
F_s, *ft2*	0.08
ϕ_f	0.01
ϕ_m	0.19
μ_w, *cp*	0.5
μ_o, *cp*	2
ρ_w, *psi/ft*	0.44
ρ_o, *psi/ft*	0.3611
P_i, *psi*	396.89

Table 3-Quarter Five Spot Pattern Parameters, Homogenous Case (Gravity and Imbibition).

Parameters	*Values*
Dimension in I-Direction, ft	2000
Dimension In J-Direction, ft	2000
Matrix-Block Thickness, l_z, ft	30 ft
Reservoir Grid	40 × 40×1
Injection Rates, STB/Day	400
Production Rate, STB/Day	400
k_f, *md*	500
k_m, *md*	1
F_s, ft^2	0.12
ϕ_f	0.05
ϕ_m	0.19
μ_w, *cp*	0.5
μ_o, *cp*	2
ρ_w, *psi/ft*	0.44
ρ_o, *psi/ft*	0.3611
P_i, *psi*	4000

Table 4-Nine Spot Pattern Parameters, Heterogeneous Case (Gravity and Imbibition).

Parameters	*Values*
Dimension In I-Direction, ft	2000
Dimension In J-Direction, ft	2000
Thickness, ft	30 ft
Matrix-Block Thickness, l_z, ft	30 ft
Reservoir Grid	41 × 41×1
Injection Rates, STB/Day	800
Production Rate for each Well, STB/Day	100
k_m, *md*	1
F_s, ft^2	0.0844
ϕ_f	0.05
ϕ_m	0.2
μ_w, *cp*	0.5
μ_o, *cp*	2
ρ_w, *psi/ft*	0.44
ρ_o, *psi/ft*	0.3611
P_i, *psi*	4000

Table 5-Quarter Five Spot Pattern Parameters, Homogenous Case, CPU Time.

Parameters	*Values*
Dimension In I-Direction, ft	1000
Dimension In J-Direction, ft	1000
Thickness, ft	100 ft
Injection Rates, STB/Day	1000
Production Rate, STB/Day	1000
k_f, *md*	500
k_m, *md*	1
F_s, ft^2	0.05
ϕ_f	0.05
ϕ_m	0.25
μ_w, *cp*	0.5
μ_o, *cp*	2
ρ_w, *psi/ft*	0.44
ρ_o, *psi/ft*	0.3611
P_i, *psi*	4000

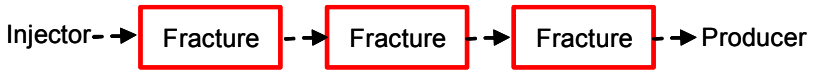

Figure 1-Single-Porosity Single-Permeability System.

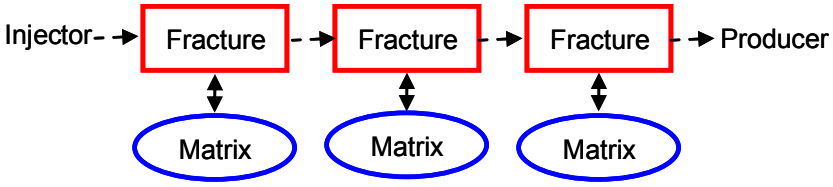

Figure 2-Dual-Porosity Single-Permeability System.

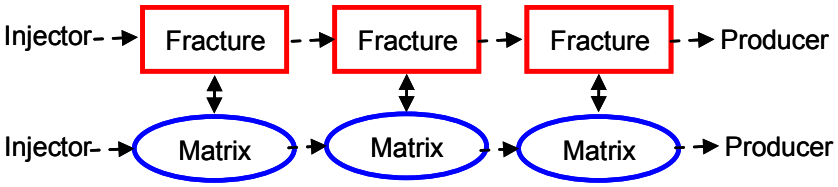

Figure 3-Dual-Porosity Dual-Permeability System.

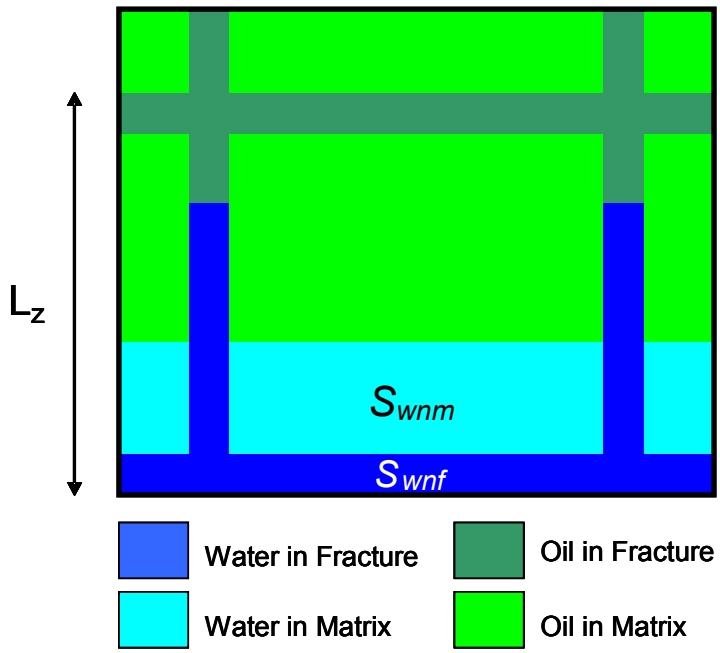

Figure 4 - Gravity Effect in a Single Matrix-Block Surrounded by Fractures Partially Filled with Water.

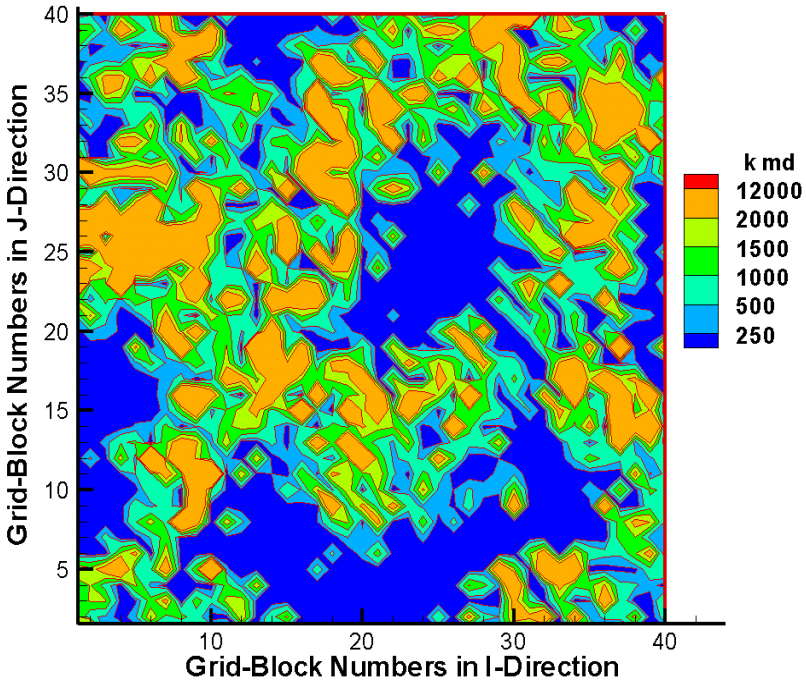

Figure 5 - 2D Fracture Permeability Field

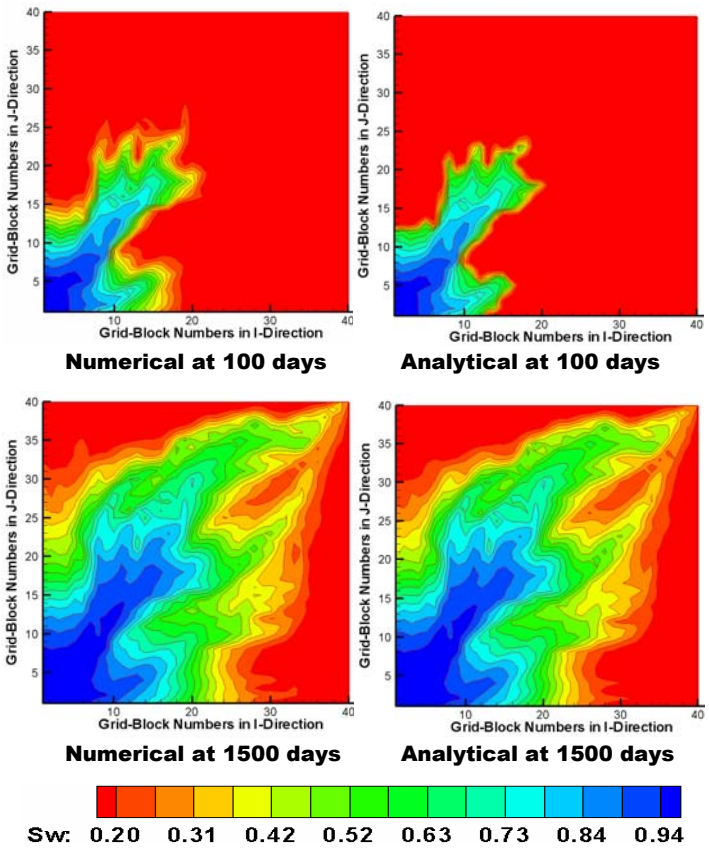

Figure 6-Comparison between the Numerical and Analytical Solutions of the Saturation Equation with ETF.

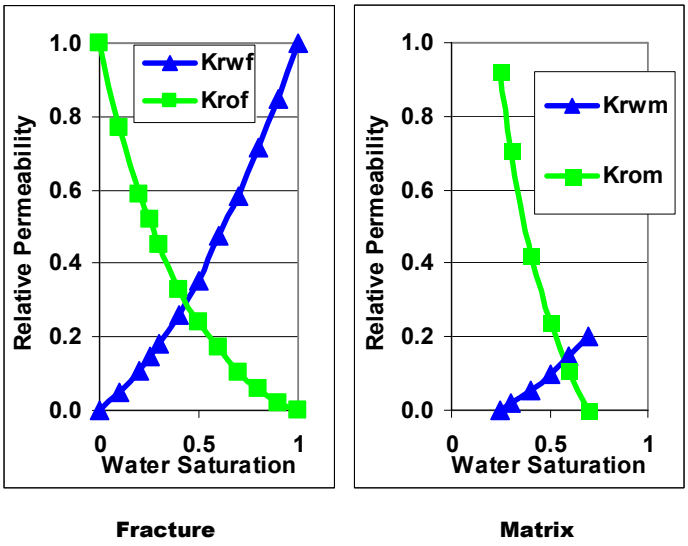

Figure 7-Fracture and Matrix Relative Permeability Curves (after Kazemi et al., 1976).

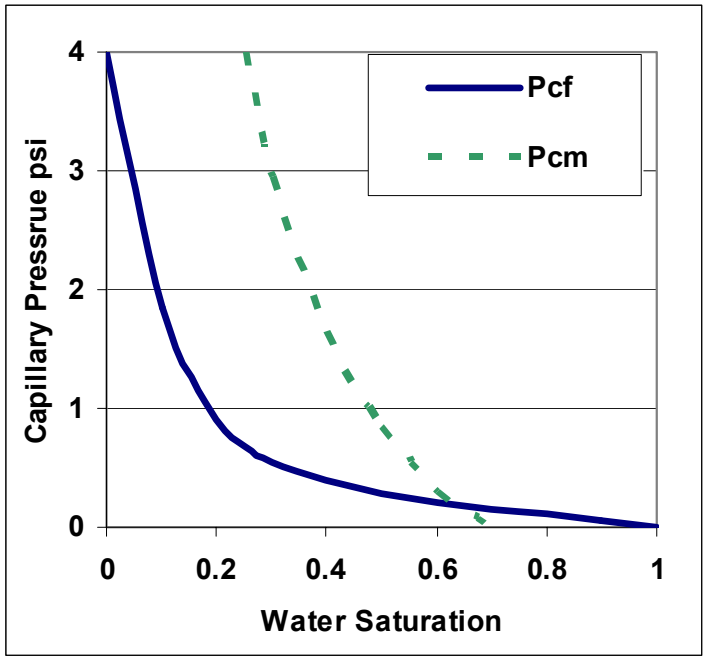

Figure 8-Fracture and Matrix Capillary Pressure Curves (after Kazemi et al. 1976).

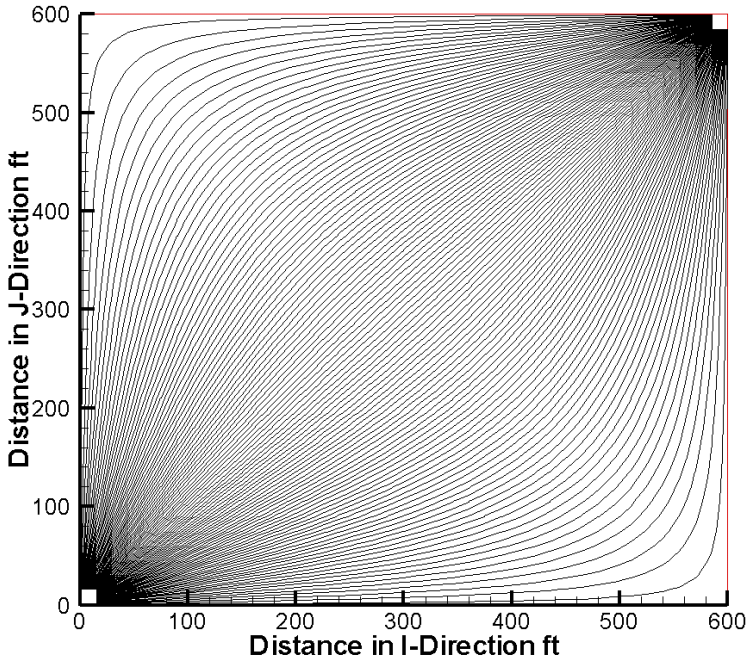

Figure 9-Streamlines in a Quarter Five Spot Pattern, Homogenous Case, Imbibition Process.

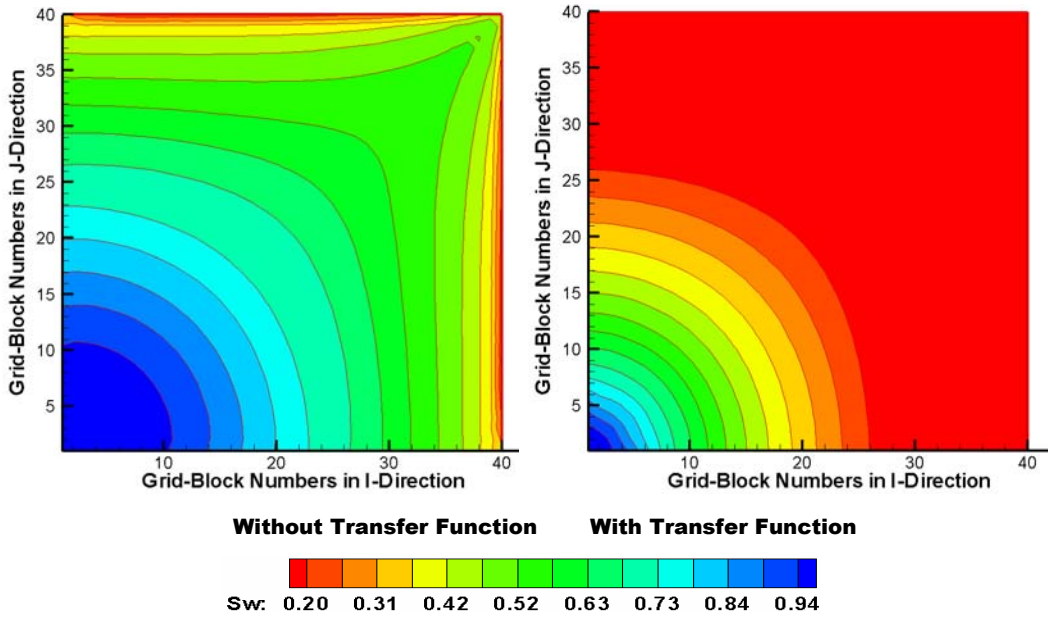

Figure 10-Fracture Water Saturation from DPSP Streamline Simulator with and without Transfer Function at 100 days, Homogenous Case, Imbibition Only.

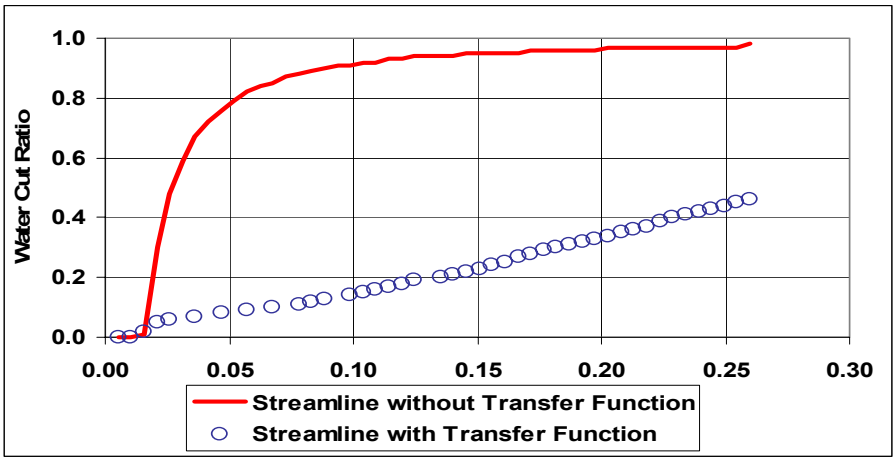

Figure 11-Water-cut Histories From the DPSP Streamline Simulation with and without Transfer Function, Homogenous Case, Imbibition Only.

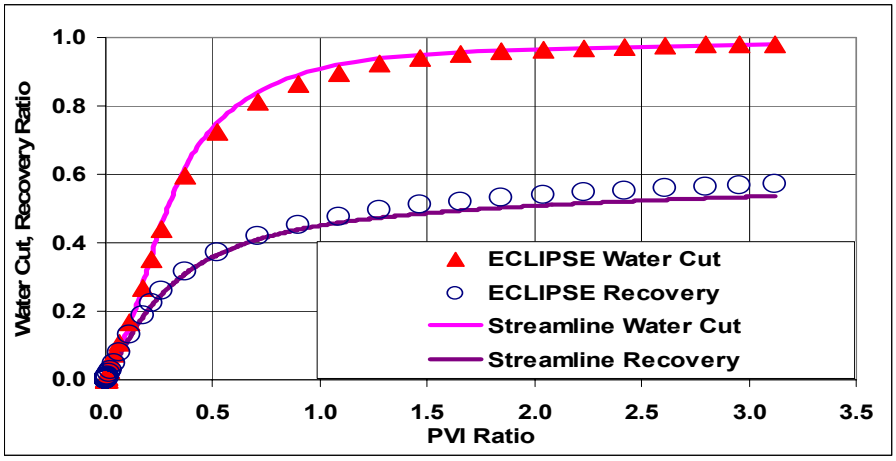

Figure 12-Comparison between the DPSP Streamline Simulator and the DPSP ECLIPSE in Terms of Water Cut and Recovery Histories, Homogenous Case, Imbibition Only.

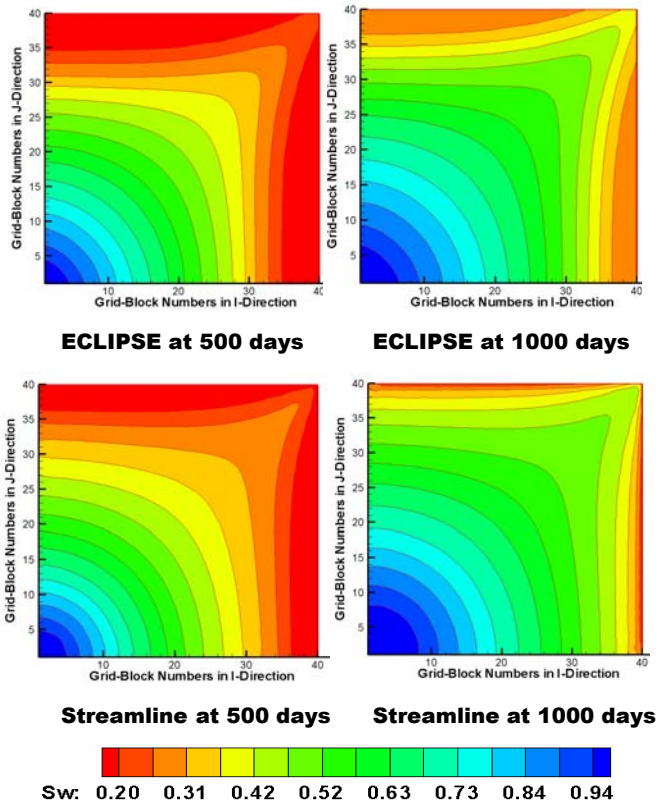

Figure 13-Comparison between the DPSP Streamline Simulator and the DPSP ECLIPSE in Terms of Fracture Water Saturation, Homogenous Case, Imbibition Only.

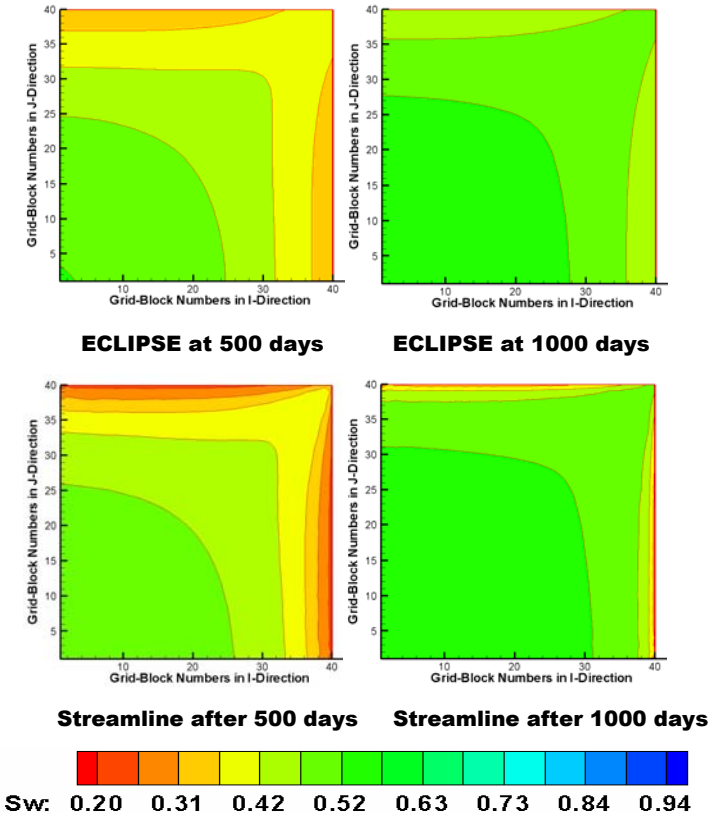

Figure 14-Comparison between the DPSP Streamline Simulator and the DPSP ECLIPSE in Terms of Matrix Water Saturation, Homogenous Case, Imbibition Only.

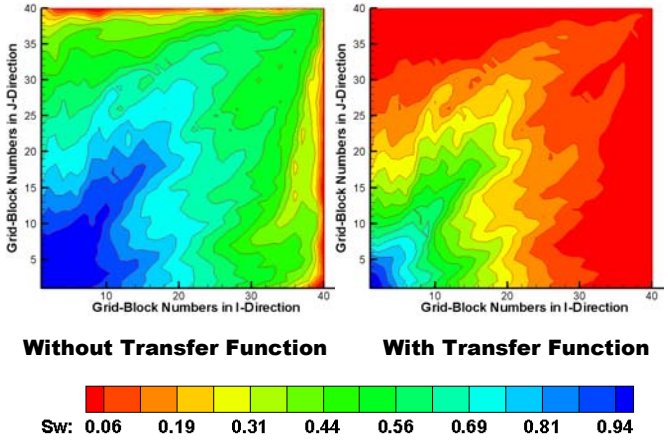

Figure 15- Fracture Water Saturation from the DPSP Streamline Simulator with and without Transfer Function at 100 days, Heterogeneous Case, Imbibition only.

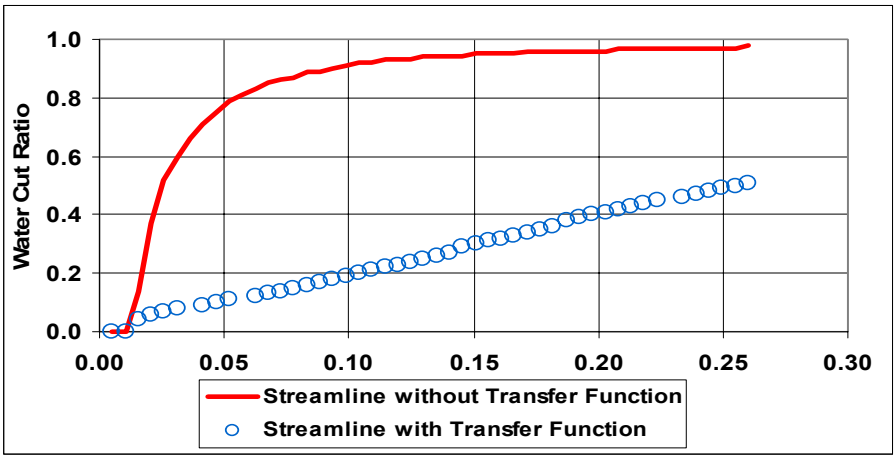

Figure 16-Water-cut Histories From the DPSP Streamline Simulation with and without Transfer Function , Heterogeneous Case, Imbibition Only.

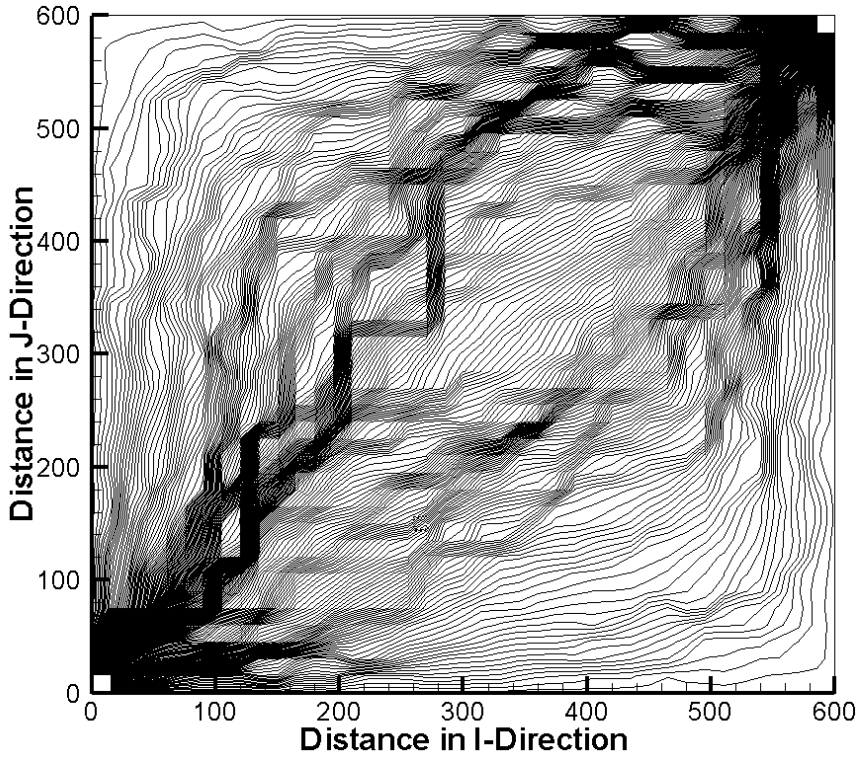

Figure 17-Streamlines in a Quarter Five Spot Pattern, Heterogenous Case, Imbibition Process.

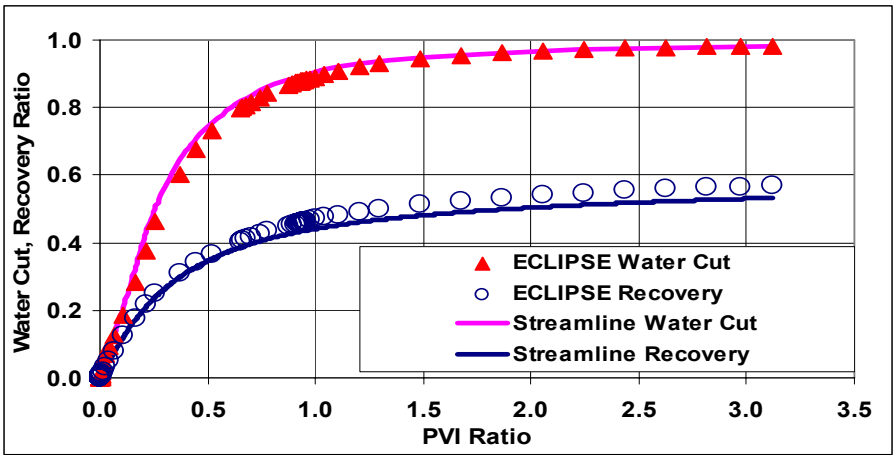

Figure 18-Comparison between the DPSP Streamline Simulator and the DPSP ECLIPSE in Terms of Water Cut and Recovery Ratios, Heterogeneous Case, Imbibition Process.

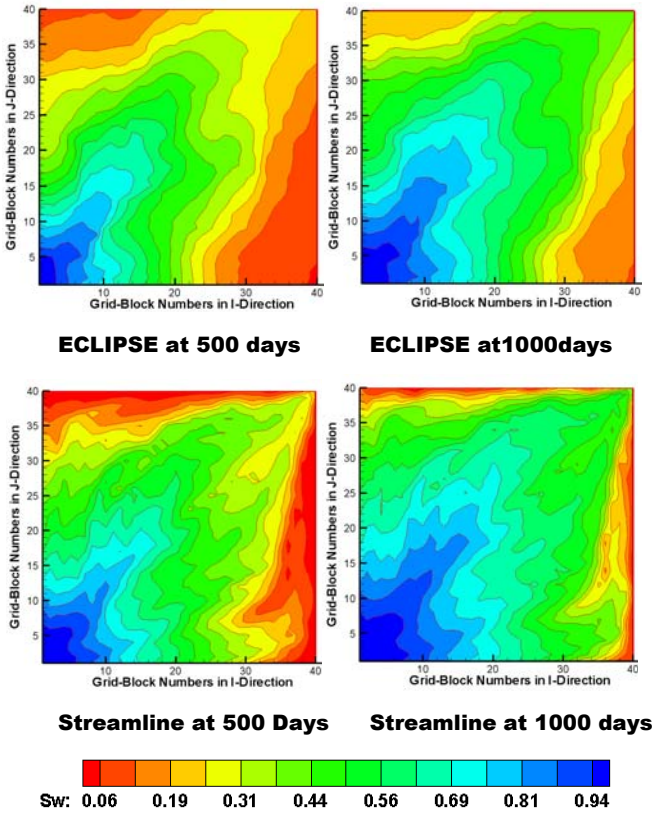

Figure 19-Comparison between the DPSP Streamline Simulator and the DPSP ECLIPSE in Terms of Fracture Water Saturation, Heterogeneous Case, Imbibition Process.

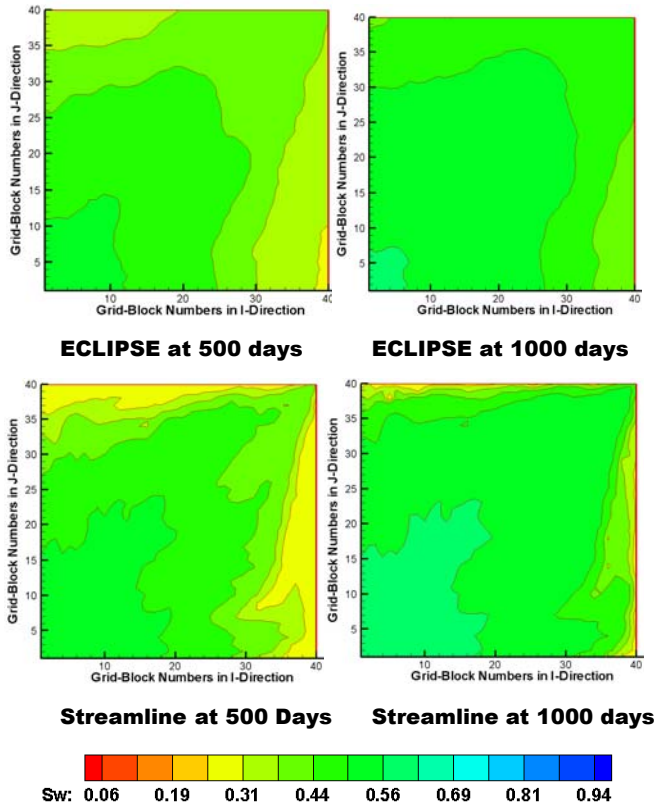

Figure 20-Comparison between the DPSP Streamline Simulator and the DPSP ECLIPSE in Terms of Matrix Water Saturation, Homogenous Case, Imbibition Process.

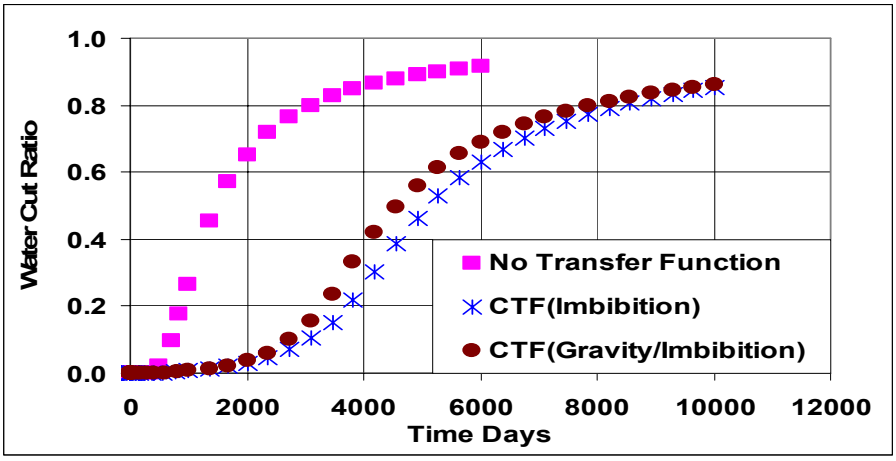

Figure 21-ECLIPSE Water Cut History, Quarter Five Spot Pattern, Gravity/Imbibition Process.

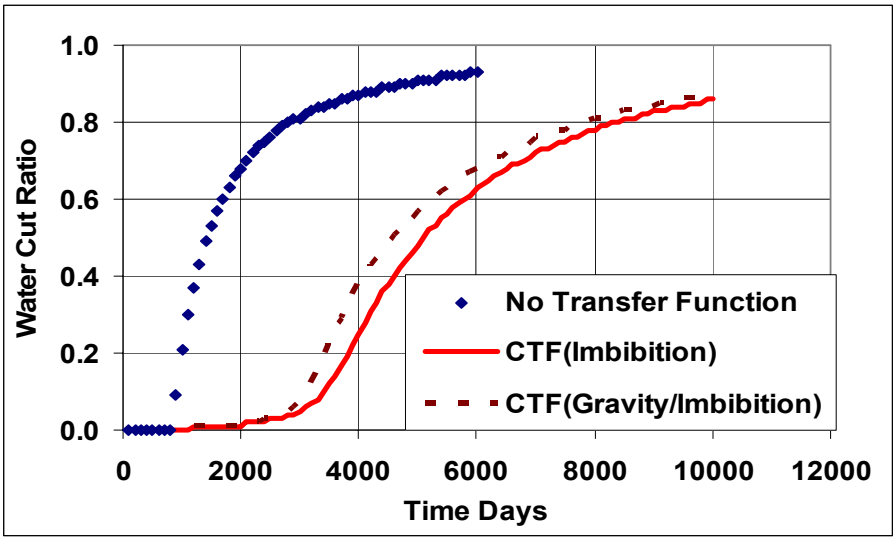

Figure 22-Streamline Simulation Water Cut History, Quarter Five Spot Pattern, Gravity/Imbibition Process.

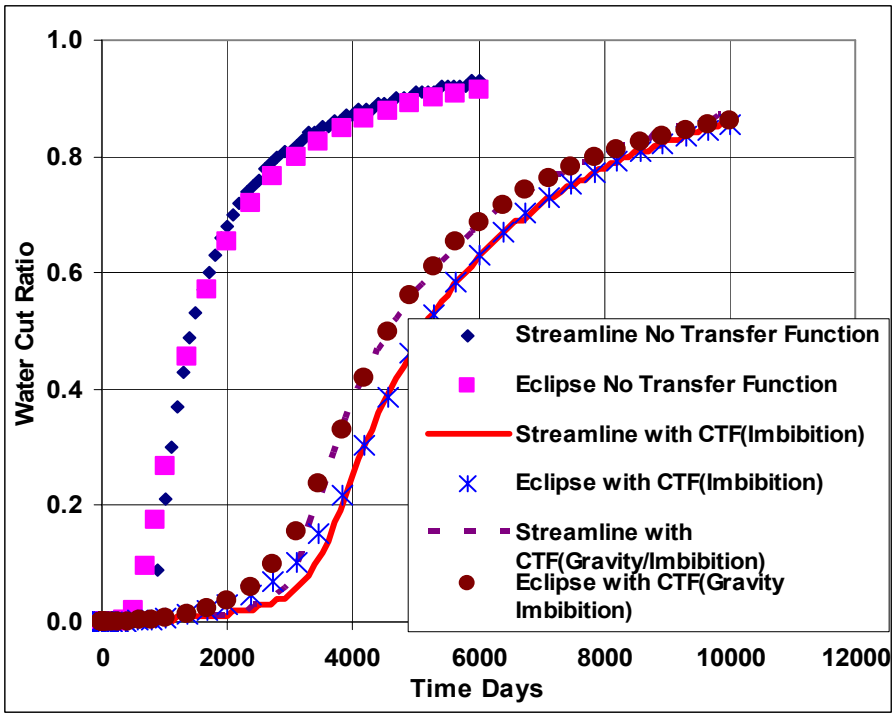

Figure 23- Comparison between the DPSP Streamline Simulator and the DPSP ECLIPSE in Terms of Water Cut History, Quarter Five Spot Pattern, Gravity/Imbibition Process.

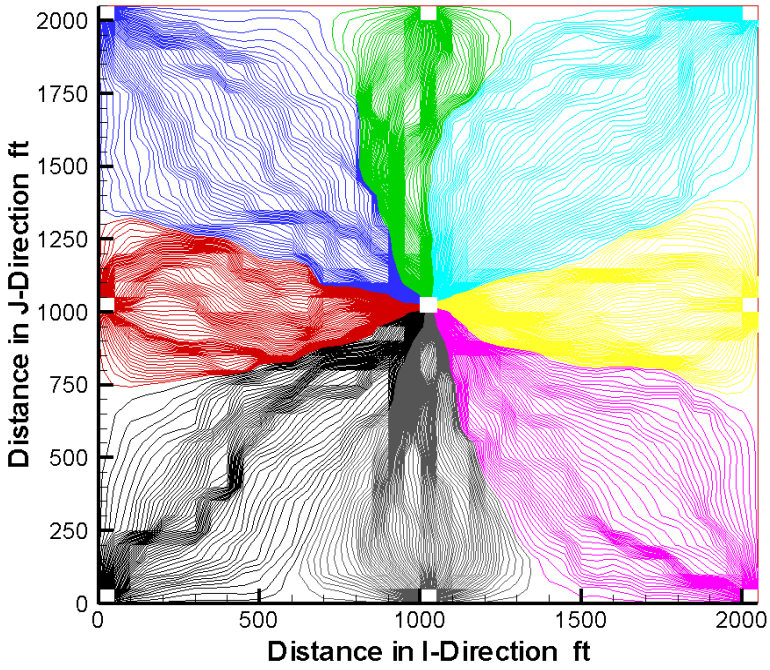

Figure 24-Streamlines in a Nine Spot Pattern, Heterogenous Nine Spot Case, Gravity/Imbibition Process.

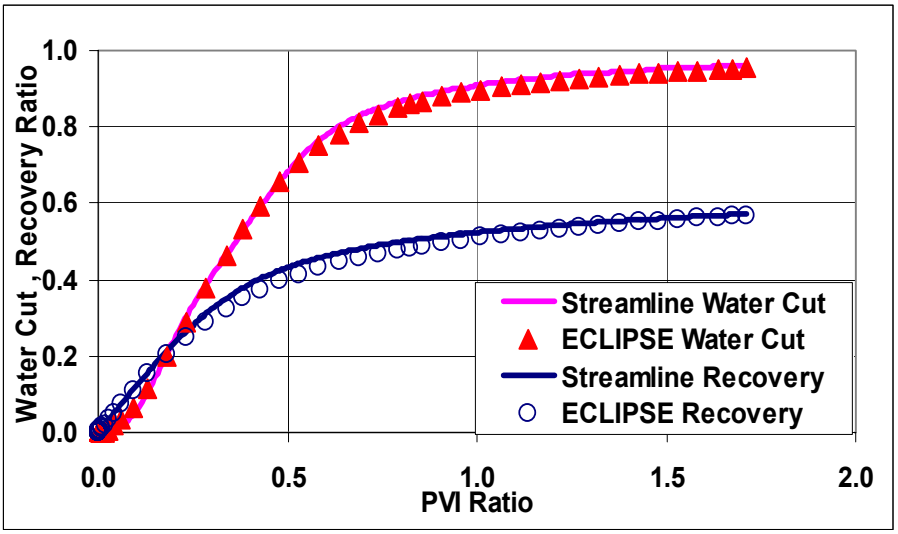

Figure 25- Comparison between the DPSP Streamline Simulator and the DPSP ECLIPSE in Terms of Field Water Cut and Recovery Ratios, Heterogeneous Nine Spot Case, Gravity/Imbibition Process.

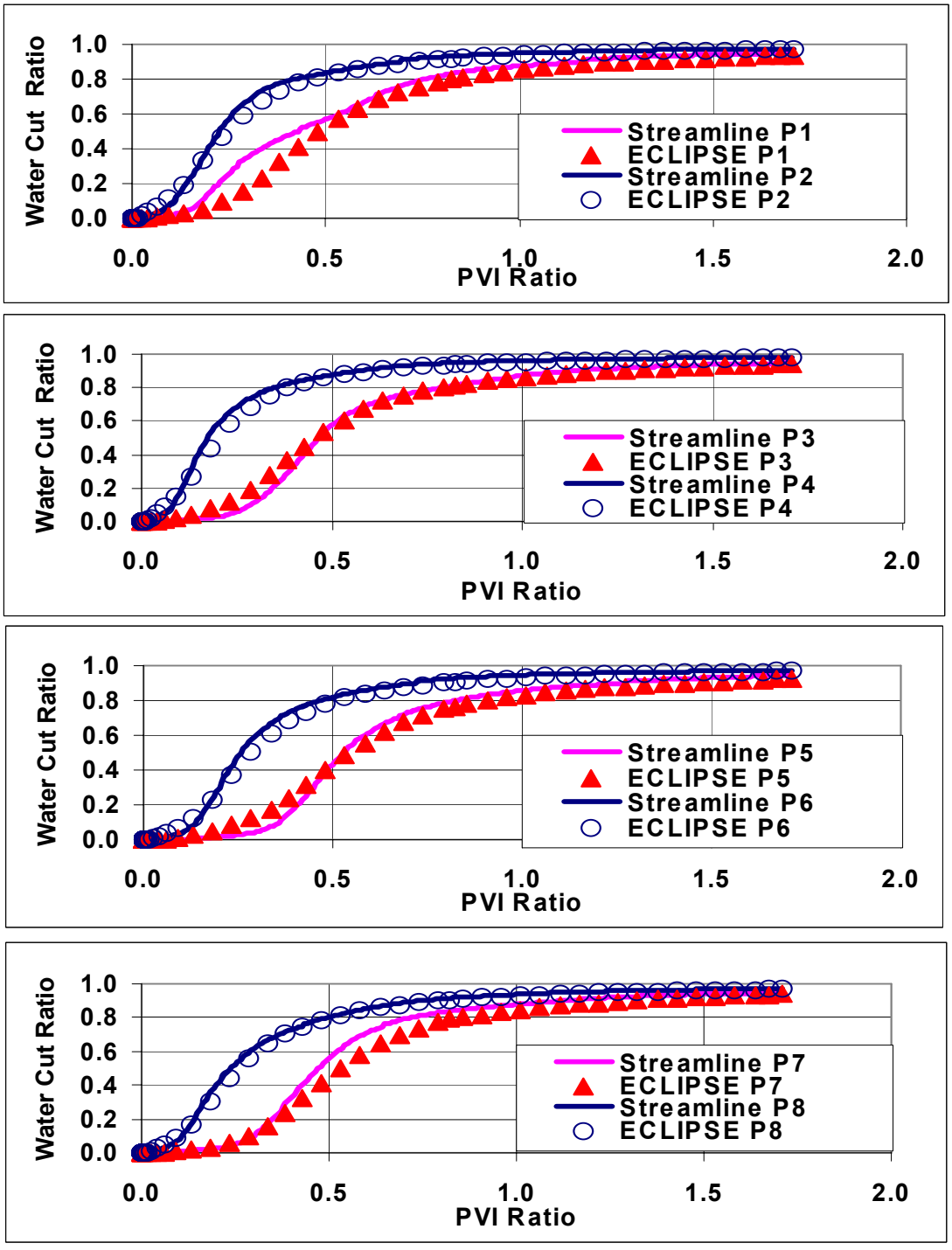

Figure 26- Comparison between the DPSP Streamline Simulator and the DPSP ECLIPSE in terms of Water Cut in Individual Producers, Heterogeneous Nine Spot Case, Gravity/Imbibition Process.

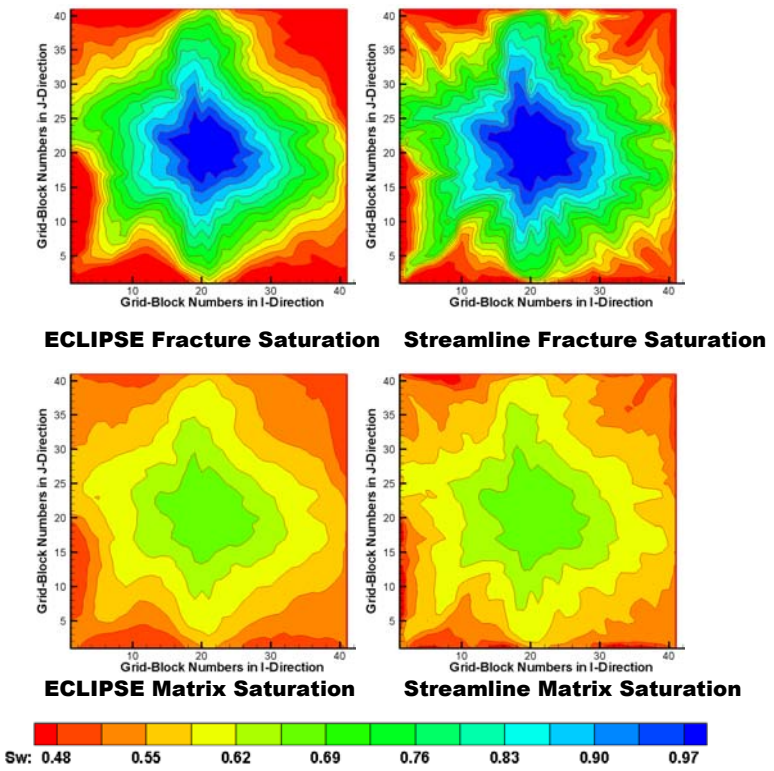

Figure 27- Comparison between the DPSP Streamline Simulator and the DPSP ECLIPSE in terms of Fracture Water Saturation after 6000 Days, Heterogeneous Nine Spot Case, Gravity/Imbibition Process.

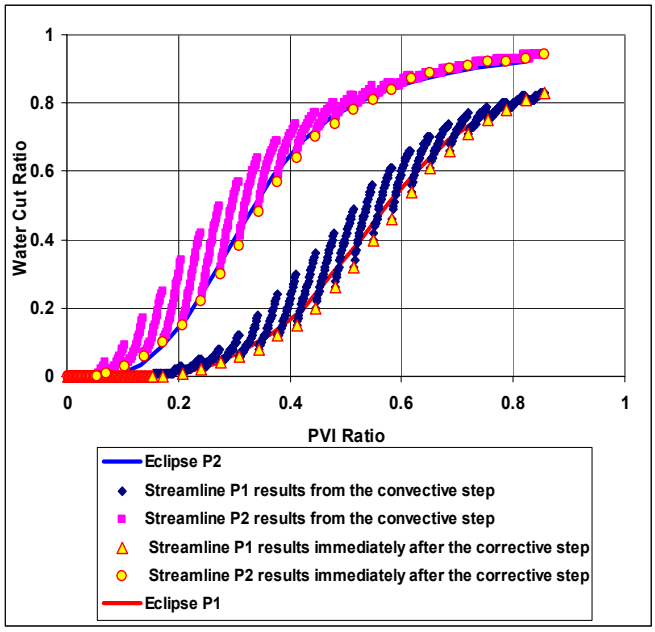

Figure 28-Comparison between the DPDP Streamline Simulator and the DPDP ECLIPSE in terms of Water Cut Ratio, Homogenous Case, Imbibition Process (SPT=250 days).

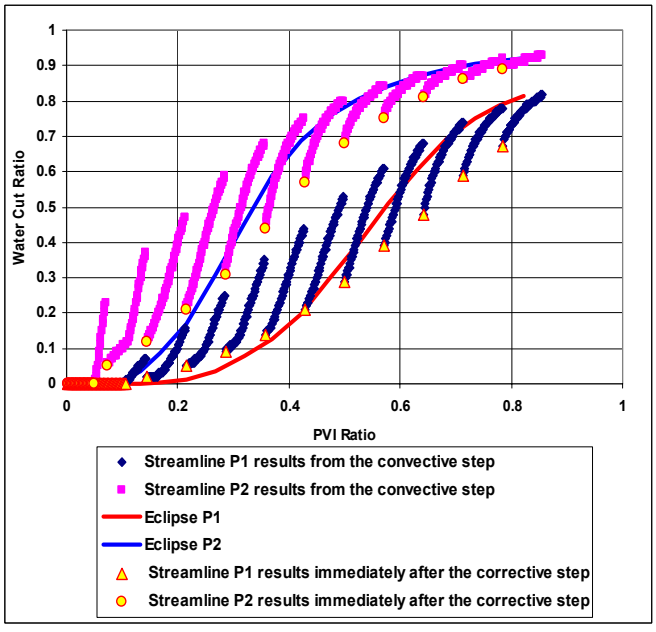

Figure 29-Comparison between the DPDP Streamline Simulator and the DPDP ECLIPSE in terms of Water Cut Ratio, Homogenous Case, Imbibition Process (SPT=500 days).

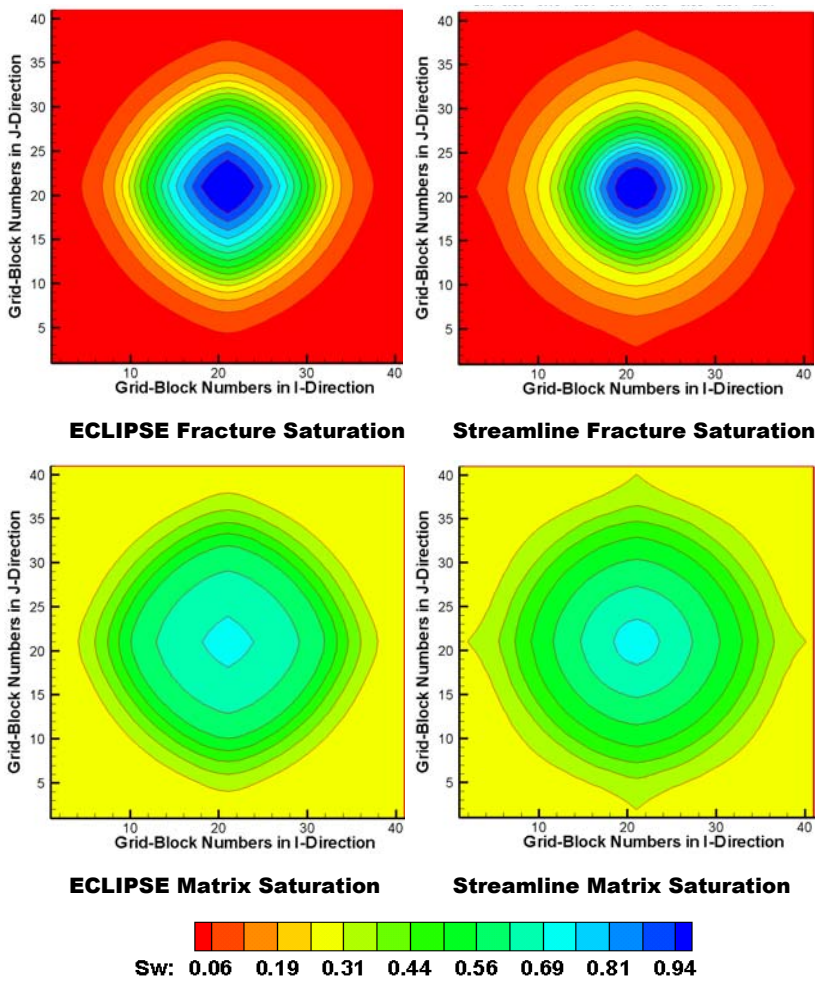

Figure 30-Comparison between the DPDP Streamline Simulator and the DPDP ECLIPSE in terms of Water Saturation after 1000 Days, Homogenous Nine Spot Case, Imbibition Process.

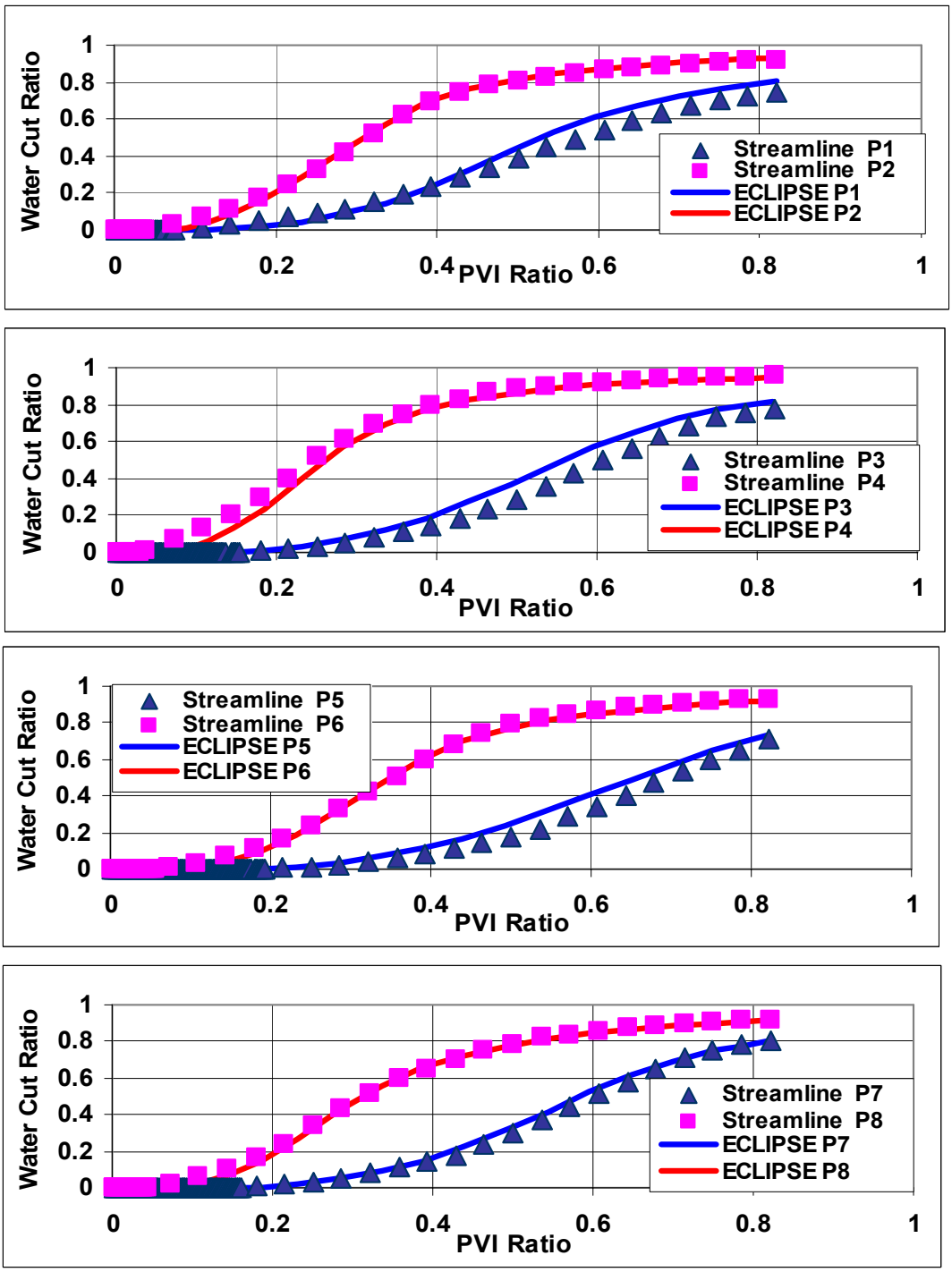

Figure 31- Comparison between the DPDP Streamline Simulator and the DPDP ECLIPSE in Terms of Water Cut Ratio, Heterogeneous Case, Imbibition Process.

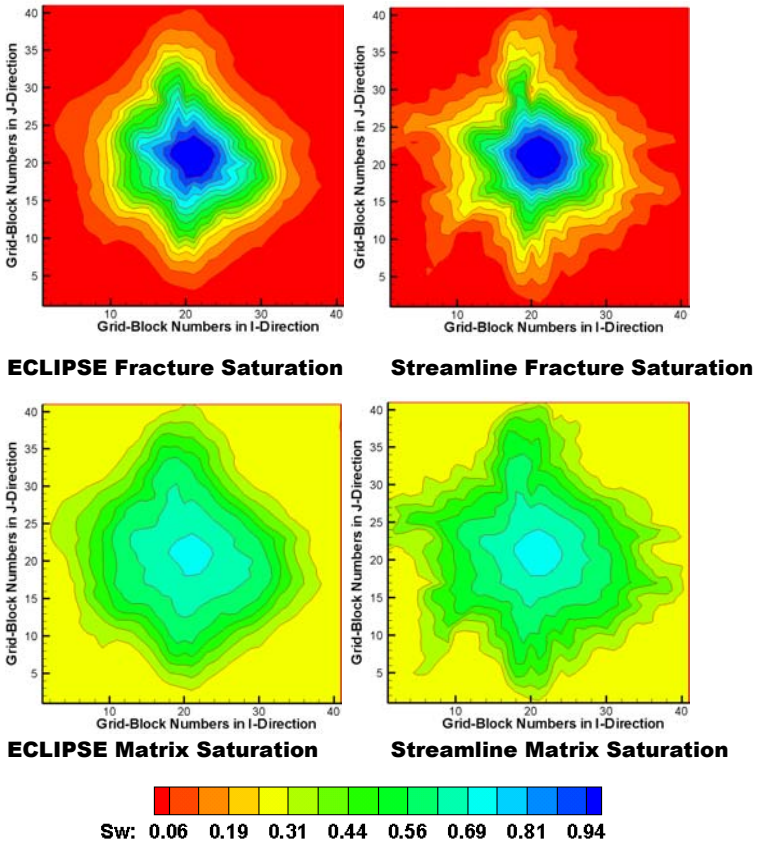

Figure 32- Comparison between the DPDP Streamline Simulator and the DPDP ECLIPSE in terms of Water Saturation after 1000 Days, Heterogeneous Nine Spot Case, Imbibition Process.

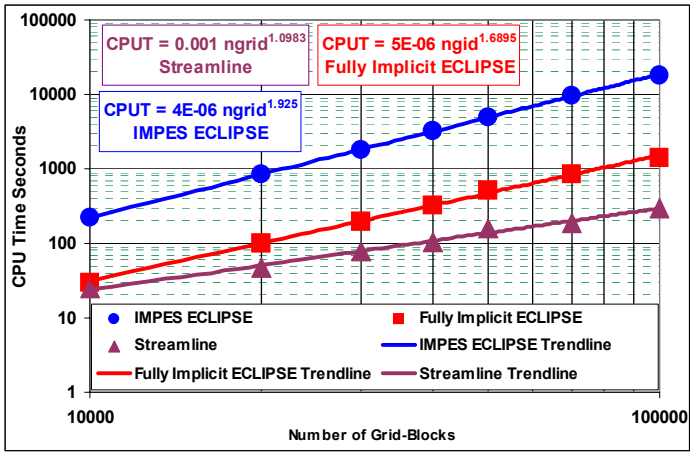

Figure 33-CPU Time Comparison the Fully Implicit DPSP ECLIPSE, The IMPES DPSP ECLIPSE, and the DPSP Streamline Simulation.

RESULTS AND DISCUSSION: PART II

Fast History Matching of Finite-Difference Models Using Streamline-Derived Sensitivities

Introduction

Geological models derived from static data alone often fail to reproduce the field production history. Reconciling geologic models to the dynamic response of the reservoir is critical to building reliable reservoir models. Classical history matching procedures whereby reservoir parameters are adjusted manually by trail-and-error can be tedious and often yield a reservoir description that is not realistic and no longer consistent with the geologic interpretation. In recent years, several techniques have been developed for integrating production data into reservoir models.[1-15] Integration of dynamic data typically requires a least-square based minimization to match the observed and calculated production response. There are several approaches to such minimization and these can be broadly classified into three categories: gradient-based methods, sensitivity-based methods and derivative-free methods. The derivative-free approaches such as simulated annealing or genetic algorithms require numerous flow simulations and can be computationally prohibitive for field-scale applications.[15] Gradient-based methods have been widely used for automatic history matching, although the convergence rates of these methods are typically slower than the sensitivity-based methods such as the Gauss-Newton or the LSQR method.[1,3,6,10] An integral part of the sensitivity-based methods is the computation of sensitivity coefficients. These sensitivities are simply partial derivatives that define the change in production response because of a small change in reservoir parameters.

There are several approaches to calculating sensitivity coefficients and these generally fall into one of the three categories: perturbation method, direct method and adjoint state methods.[16] Conceptually, the perturbation approach is the simplest and requires the fewest changes in an existing code. Sensitivities are estimated by simply perturbing the model parameters one at a time by a small amount and then computing the corresponding production response. Such an approach requires (N+1) forward simulations where N is the number of parameters. Obviously, this can be computationally prohibitive for reservoir models with many parameters. In the direct or sensitivity equation method,[16] the flow and transport equations are differentiated to obtain expressions for the sensitivity coefficients. Because there is one equation for each parameter, this approach can require the same amount of work. A variation of this method, called the gradient simulator method,[17] utilizes the discretized version of the flow equations and takes advantage of the fact that the coefficient matrix remains unchanged for all the parameters and needs to be decomposed only once. Thus, sensitivity computation for each parameter now requires a matrix-vector multiplication.[14,18] This method can also be computationally expensive for large number of parameters. Finally, the adjoint state method requires derivation and solution of adjoint equations that can be significantly smaller in number compared to the sensitivity equations. The adjoint equations are obtained by minimizing the production data misfit with flow equations as constraint and can be quite cumbersome for multiphase flow applications.19 Furthermore, the number of adjoint solutions will generally depend on the amount of production data and thus, length of the production history.

Recently, the streamline approach has provided an extremely efficient means for computing parameter sensitivities. With the streamline method, the sensitivities can be computed analytically using a single flow simulation.2,12 Because the sensitivity calculations involve evaluation of 1-D integrals along streamlines, the method scales very well with respect to model size or the number of parameters. Although the streamline models have been extremely successful in bridging the gap between geologic modeling and flow simulation, they are currently limited in their ability to incorporate complex physical processes and cross-streamline mechanisms in a computationally efficient manner.13 Thus, an efficient and robust approach to production data integration using finite-difference models will be particularly useful in characterizing reservoirs dominated by mechanisms such as compressibility and gravity effects, transverse dispersion and other complex physical mechanisms.

In this paper we propose a novel approach to history matching finite-difference models that combines the advantage of the streamline models with the versatility of finite-difference simulation. We first generate streamlines using the velocity field derived from a finite-difference simulator. The streamlines are then used to compute the parameter sensitivities for updating the reservoir model. The updated model is then used in the finite-difference simulation to predict reservoir performance and the process is repeated until a satisfactory history match is obtained. For history matching, we use 'a generalized travel-time inversion' that is shown to be extremely robust because of its quasi-linear properties and converges in only a few iterations. The approach is very fast and avoids much of the subjective judgments and time-consuming trial-and-errors associated with manual history matching. It is based upon proven techniques from geophysical inversion and is designed to preserve geologic realism during history matching. We have illustrated the power and practical feasibility of the method using synthetic and field examples.

Approach

An outline of the procedure in our proposed approach is given in a flow chart in **Fig. 1**. Briefly, the major steps are as follows:

Flow Simulation Using Finite-Difference Simulator. We have utilized a commercial finite-difference simulator (viz. ECLIPSE[20]) for modeling fluid flow in the reservoir. The two-phase black oil model used here is completely general and includes comprehensive physical mechanisms such as compressibility, gravity effects and other cross-streamline fluxes such as mobility effects, rate changes, infill drilling etc.

Generalized Travel-Time Computations. Production data misfit is represented by a 'generalized travel-time' at each producing well. The 'generalized travel-time' is computed by systematically shifting the computed production response towards the observed data until the cross-correlation between the two is maximized. This is illustrated in **Fig. 2** and is discussed further later. By defining a generalized travel time, we effectively reduce the data mismatch at a well into a single 'travel time shift' and thus, are able to retain many of the desirable properties of travel time inversion.[19]

Streamline-based Sensitivity Computations. The fluid fluxes obtained from the finite-difference simulator are utilized to trace streamline trajectories and calculate time of flight. These calculations can account for complex geology and faulted systems.[21,22] The time of flight is then utilized to compute the sensitivity of the generalized travel-time with respect to reservoir

parameters as discussed later. Note that the sensitivity computations require a single flow simulation regardless of the number of parameters.

Model Updating via Generalized Travel-Time Inversion. This step involves computing the changes in the model parameters via a least-squared minimization technique that utilizes the streamline-derived sensitivity coefficients. Additional constraints are imposed to penalize deviation from a prior model to preserve geologic realism and also, to restrict permeability changes to large-scale trends consistent with the low resolution of the production data.[2]

Note that the streamline-based sensitivity computations are completely general and can account for changing conditions such as infill drilling and rate changes via streamline updating.[12] However, these sensitivities are only approximations in the presence of compressibility and cross-streamline mechanisms. A basic premise of our approach is that these approximate sensitivities are adequate for inverse modeling. All our results indicate that this is a reasonable assumption. We store the pressure and flux information from finite-difference simulation for each streamline update for the entire simulation run. Thus, only one finite-difference simulation is required for each model update. The process is repeated until a satisfactory history match is obtained.

Illustration of the Procedure: A Synthetic Example. Before discussing the mathematical formulation we will first illustrate the procedure using a simple example. This involves history matching water-cut response from a 5-spot pattern with infill drilling. **Fig. 3a** shows the reference permeability field and well locations. The mesh size used is 21×21×1. The reference permeability distribution consists of a low-permeability trend towards north and a high-permeability trend towards south. Four infill wells (Wells 5-8) were introduced at 600 days of production. The water-cut responses from ECLIPSE for the eight producers using the reference permeability field are shown in **Fig. 4**. We treat this as the observed data. Next, starting from a homogeneous initial permeability model (**Fig. 3b**) we match the water-cut response via the generalized travel-time inversion. The permeability for each grid block is treated as an adjustable parameter for this example (a total of 441 parameters). The initial and final water-cut matches are shown in **Figs. 4a** and **4b**. The final permeability distribution is shown in **Fig. 3c**. Clearly, the final permeability model captured the large-scale trend of the reference permeability field. The permeability multipliers resulting from the history matching are shown in **Fig. 3d**. The production data integration process is very efficient and takes only a few iterations to converge (**Fig. 5**). The CPU time required for this case is less than 4 minutes for 16 iterations in a PC (Intel Xeon 3.06 GHz Processor).

Mathematical Background: Generalized Travel-Time Inversion and Sensitivity Computations

In this section we discuss the mathematical details related to streamline-based sensitivity computations and generalized travel-time inversion. Much of the work has been presented in our earlier papers.[2,12] We provide a summary for completeness.

Streamline-Based Sensitivity Calculation. The sensitivity calculations assume two-phase incompressible flow. However, we utilize these sensitivities for model updating during black-oil finite-difference simulation. The basic premise here is that the approximate sensitivities, for most purposes, are adequate for inverse modeling.

Two-phase incompressible flow equation in the streamline time of flight coordinate is given by Eq. 1.

$$\frac{\partial S_w}{\partial t} + \frac{\partial F_w}{\partial \tau} = 0 \tag{1}$$

In Eq. 1, the time of flight can be defined in terms of 'slowness', $s(\mathbf{x})$

$$\tau = \int_{\psi} s(\mathbf{x}) dr \tag{2}$$

and the 'slowness' which is the reciprocal of interstitial velocity, is given by

$$s(\mathbf{x}) = \frac{\phi(\mathbf{x})}{\lambda_t k(\mathbf{x}) |\nabla P(\mathbf{x})|} \tag{3}$$

We assume that streamlines do not shift significantly because of small perturbations in reservoir properties. For steady velocity fields, this assumption is strictly valid for porosity and quite satisfactory for permeability changes.[23] We can now compute the sensitivity of fractional flow to reservoir parameters through a variation in the streamline time of flight as follows:

$$\delta F_w = \frac{\partial F_w}{\partial \tau} \delta \tau \tag{4}$$

The change in the time of flight can be expressed in terms of the slowness change as

$$\delta \tau = \int_{\psi} \delta s(\mathbf{x}) dr \tag{5}$$

Now, the slowness is a composite response and its variation can be related to changes in reservoir properties as follows

$$\delta s(\mathbf{x}) = \frac{\partial s(\mathbf{x})}{\partial k} \delta k(\mathbf{x}) + \frac{\partial s(\mathbf{x})}{\partial \phi} \delta \phi(\mathbf{x}) \tag{6}$$

where the partial derivatives are

$$\frac{\partial s(\mathbf{x})}{\partial k} = \frac{-\phi(\mathbf{x})}{\lambda_t k^2(\mathbf{x}) |\nabla P|} = -\frac{s(\mathbf{x})}{k(\mathbf{x})} \tag{7}$$

$$\frac{\partial s(\mathbf{x})}{\partial \phi} = \frac{1}{\lambda_t k(\mathbf{x}) |\nabla P|} = \frac{s(\mathbf{x})}{\phi(\mathbf{x})} \tag{8}$$

The time of flight sensitivities can be obtained analytically in terms of simple integrals along streamline. For example, the time of flight sensitivity with respect to permeability will be given by[23]

$$\frac{\partial \tau}{\partial k(\mathbf{x})} = \int_{\Sigma} \frac{\partial s(\mathbf{x})}{\partial k(\mathbf{x})} dx = -\int_{\Sigma} \frac{s(\mathbf{x})}{k(\mathbf{x})} dx \tag{9}$$

where the integrals are evaluated along the streamline trajectory. It is to be noted that the quantities in the sensitivity expressions are either contained in the initial reservoir model or are produced by a single simulation run.

Data Misfit and the Concept of a Generalized Travel-Time. Production data integration typically involves the minimization of a least squares functional representing the difference between the observed data and the calculated response from a simulator. Additional constraints are imposed via a prior geologic model to ensure 'plausibility' of the solution to the inverse problem.[2-6,10-14] Production data misfit is most commonly represented as follows

$$J_p = \sum_{j=1}^{N_w} \sum_{i=1}^{N_{dj}} w_{ij} \left(y_j^{cal}(t_i) - y_j^{obs}(t_i) \right)^2 \tag{10}$$

for $i = 1, \cdots, N_{dj}, \quad j = 1, \cdots, N_w$.

In the above equation, $y_j(t_i)$ denotes the production data for well j at time t_i, N_w and N_{dj} stand for the number of production wells and the number of observed data at each well, respectively and w_{ij} represent the data weights. We refer to the minimization in Eq. 10 as an 'amplitude matching'. It is well known that such minimization leads to a highly non-linear inverse problem.[24] The solution to the inverse problem, in general, will be non-unique, can be unstable and often converges to a local minimum. On the other hand, a travel-time inversion whereby the observed and computed production responses are lined-up at the breakthrough time has quasi-linear properties.[24] As a result, the minimization is more robust and is relatively insensitive to the choice of the initial model.

By defining a generalized travel-time, we effectively accomplish an 'amplitude matching' while preserving most of the benefits of a travel-time inversion. In this approach, we seek an optimal time-shift at each well to minimize the production data misfit at the well. This is illustrated in **Fig. 2a** where the calculated water-cut response is systematically shifted in small time increments towards the observed response, and the data misfit is computed for each time increment. Taking well *j* as an example, the optimal shift will be given by the Δt_j that minimizes the misfit function,

$$J = \sum_{i=1}^{Ndj} \left[y_j^{obs}\left(t_i + \Delta t_j\right) - y_j^{cal}\left(t_i\right) \right]^2 = f(\Delta t_j) \tag{11}$$

Or, alternatively maximizes the coefficient of determination given by the following

$$R^2(\Delta t_j) = 1 - \frac{\sum \left[y_j^{obs}(t_i + \Delta t_j) - y_j^{cal}(t_i) \right]^2}{\sum \left[y_j^{obs}(t_i) - \overline{y_j^{obs}} \right]^2} \tag{12}$$

Thus, we define the generalized travel-time as the 'optimal' time-shift $\Delta\tilde{t}_j$ that maximizes the $R^2(\Delta t_j)$ as shown in **Fig. 2b**. It is important to point out that the computation of the optimal time-shift does not require any additional flow simulations. It is carried out as a post-processing at each well after the calculated production response is derived using a flow simulation. The overall production data misfit can now be expressed in terms of a generalized travel-time misfit at all wells as follows

$$E = \sum_{j=1}^{Nw} (\Delta\tilde{t}_j)^2 \tag{13}$$

Sensitivity of the Generalized Travel-Time. Let **m** represent the vector of reservoir parameters**.** Now, consider a small perturbation in reservoir properties, $\delta\mathbf{m}$, such that it results in a time-shift δt_j for the entire computed production response at well *j*, that is, every data point of well *j* has a common time-shift (**Fig. 6**). We then have the following relationship for the observed times $((t_{1,j},.....,t_{N_{dj},j})$

$$\delta t_j = \delta t_{1,j} = \left[\frac{\partial t_{1,j}}{\partial \mathbf{m}}\right]^T \delta\mathbf{m} \tag{14}$$

$$\delta t_j = \delta t_{N_{dj},j} = \left[\frac{\partial t_{N_{dj},j}}{\partial \mathbf{m}}\right]^T \delta\mathbf{m}$$

Summing Eq. 14 over all the data points, we can arrive at the following simple expression for the sensitivity of the travel-time shift with respect to the reservoir parameter, *m*, which represents a component of the vector **m.**

$$\frac{\partial t_j}{\partial m} = \frac{\sum_{i=1}^{N_{dj}} \left(\partial t_{i,j} / \partial m\right)}{N_{dj}} \tag{15}$$

Also, based on the definition of the generalized travel-time, we have the following

$$\frac{\partial \Delta\tilde{t}_j}{\partial m} = -\frac{\partial t_j}{\partial m} \tag{16}$$

The negative sign in Eq. 16 reflects the sign convention adopted for defining the generalized travel-time shift which is considered negative if the computed response is to the right of the observed data as shown in **Fig. 2a**. For example, the travel-time will decrease if permeability increases; however, the 'travel-time shift' will increase.

Combining Eqs. 14-16, we obtain a rather simple expression for the sensitivity of the generalized travel-time with respect to reservoir parameters as follows

$$\frac{\partial \Delta \tilde{t}_j}{\partial m} = -\frac{\sum_{i=1}^{N_{dj}} \left(\partial t_{i,j} / \partial m \right)}{N_{dj}} \tag{17}$$

It now remains to calculate to the sensitivity of the arrival times at the producing well, $\partial t_{i,j} / \partial m$. These sensitivities can be easily obtained in terms of the sensitivities of the streamline time of flight,[12] and the result is as follows:

$$\frac{\partial t}{\partial m} = \frac{\dfrac{\partial \tau}{\partial m}}{\dfrac{\partial F_w}{\partial S_w}} \tag{18}$$

In the above expression, the fractional flow derivatives are computed at the saturation of the outlet node of the streamline. The time of flight sensitivities can be obtained analytically as in Eq. 9.

There are some important practical issues that are worth mentioning here. First, changing field conditions such as infill drilling and rate changes are accounted for by streamline updating.[12] Second, by utilizing a finite-difference simulators, we are no longer constrained by the limitations of streamline simulation. Third, for wells with no calculated breakthrough response, the application of generalized travel-time concept is not so obvious although the basic idea remains the same. The shift-time is taken as the difference between the observed breakthrough time and the last observation time. Finally, it is better to shift the calculated curve relative to the observed curve if calculated curve has more non-zero water-cut points than the observed curve; and vice-versa.

Data Integration

Our goal is to reconcile high-resolution geologic models to field production history. This typically involves the solution of an underdetermined inverse problem. The mathematical formulation behind such streamline-based inverse problems has been discussed elsewhere.[2,4-5] Both the deterministic and stochastic approaches have been used with equal success.[25] In the deterministic approach pursued here, we start with a prior static model that already incorporates geologic, well log, and seismic data. We then minimize a penalized misfit function consisting of the following three terms,

$$\left\| \Delta \tilde{\mathbf{t}} - \mathbf{S} \delta \mathbf{R} \right\| + \beta_1 \left\| \delta \mathbf{R} \right\| + \beta_2 \left\| \mathbf{L} \delta \mathbf{R} \right\| \tag{19}$$

An alternative formulation based on the Bayesian inverse theory is given by Vega et al.[25] In Eq. 19, $\Delta \tilde{\mathbf{t}}$ is the vector of generalized travel time shift at the wells, **S** is the sensitivity matrix containing the sensitivities of the generalized travel time with respect to the reservoir parameters. Also, $\delta \mathbf{R}$ correspond to the change in the reservoir property and **L** is a second spatial difference operator. The first term ensures that the difference between the observed and calculated production response is minimized. The second term, called a 'norm constraint', penalizes

deviations from the initial model. This helps preserve geologic realism because our initial or prior model already incorporates available geologic and static information related to the reservoir. Finally, the third term, a roughness penalty, simply recognizes the fact that production data are an integrated response and are thus, best suited to resolve large-scale structures rather than small-scale property variations.

The minimum in Eq. 19 can be obtained by an iterative least-squares solution to the augmented linear system

$$\begin{pmatrix} \mathbf{S} \\ \beta_1 \mathbf{I} \\ \beta_2 \mathbf{L} \end{pmatrix} \delta \mathbf{R} = \begin{pmatrix} \Delta \tilde{\mathbf{t}} \\ \mathbf{0} \\ \mathbf{0} \end{pmatrix} \tag{20}$$

The weights β_1 and β_2 determine the relative strengths of the prior model and the roughness term. The selection of these weights can be somewhat subjective although there are guidelines in the literature.[26] In general, the inversion results will be sensitive to the choice of these weights.

Note that one of the major advantages of the generalized travel-time approach is that the size of the sensitivity matrix **S** is dependent only on the number of wells regardless of the number of data points. This leads to considerable savings in computation time. We use an iterative sparse matrix solver, LSQR, for solving this augmented linear system efficiently.[27] The LSQR algorithm is well suited for highly ill-conditioned systems and has been widely used for large-scale tomographic problems in seismology.[28]

Field Applications

In this section, we discuss application of the history matching algorithm to two field examples. The first one is from the Goldsmith San Andreas Unit, a dolomite formation in West Texas. We match 20 years of waterflood production history. The second field example is from a giant middle-eastern reservoir with 16 injectors and 70 producers. A total of 30 years of production history with detailed rate, infill well and re-perforation schedule were matched. Compressibility, gravity effects and aquifer support were included during the finite-difference simulation.

Goldsmith Case. This example includes a CO_2 pilot project area (**Fig. 7)** in the Goldsmith San Andres Unit (GSAU) in west Texas. The pilot area (**Fig. 8)** consists of nine inverted 5-spot patterns covering around 320 acres with average thickness of 100ft and has over 50 years of production history prior to CO_2 project initiation in Dec. 1996. We performed a history matching for 20 years of waterflood prior to the initiation of CO_2 injection. Because of the practical difficulties in establishing correct boundary conditions for the pilot area, extra wells located outside the pilot area were included in this study. The extended study area included 11 water injectors and 31 producers. Among the producers within the study area, 9 wells showed significant water-cut response before the initiation of the CO_2 injection and are used for history matching. The detailed production rates and the well schedule including infill drilling, well conversions and well shut-in can be found elsewhere.[12] The study area is discretized into 58×53×10 mesh or a total of 30,740 grid cells. The porosity field was obtained by a Sequential Gaussian Co-simulation using well and seismic data. These porosities were not altered during history matching. The initial permeability field was generated based on the porosity-permeability

transform (**Fig. 9a**). By altering the permeability during inversion, we effectively altered the porosity-permeability transform which was considered 'soft' information for this carbonate reservoir.

We history matched 20 years of production responses for the 9 producers for the period May 1968 to December 1989. The final permeability field and the resulting permeability multipliers are shown in **Figs. 9b** and **9c**. The permeability multipliers range from 0.05 to 20, a rather wide interval. However, the changes are restricted to small regions determined by the sensitivity calculations. **Fig. 10** shows the water-cut match before and after inversion. Although the initial match was already reasonable for several wells, the matches were further improved by the generalized travel-time inversion. For example, the matches for Well 4, 7, and 9 are significantly improved. **Fig. 11** shows the misfit versus the number of iterations during the inversion. In 9 iterations, the arrival-time misfit is reduced by over 70 percent and the water-cut misfit is reduced by one-third. **Fig. 12** shows misfit of arrival-time at 0.2 fractional water-cut. For this field example with 31 producers, 11 injectors and 20 years of history matching, the computation time requirement was about 100 minutes in a PC (Intel Xeon 3.06 GHz Processor).

A Giant Middle-Eastern Field Example. The reservoir under consideration is located in the middle-east and ranks 22nd largest in the world. It is a carbonate reservoir with a large north-south anticline measuring 25 km by 15 km and contains extra light crude at an average depth of 8000ft. The field has been under waterflood for the last 30 years. A detailed history matching of the water flood production response using streamline models was presented by Qassab et al.[29] Here we repeat the exercise using a commercial finite-difference simulator and the generalized travel-time inversion.

The initial geologic model was created based on well log derived porosity, facies information and 3-D seismic data. From the facies based porosity model, 3-D permeability distributions were generated using appropriate core based porosity-permeability transforms. The fine-scale geologic model contained about 1 million cells. We utilized an upscaled model for production data integration. We performed a vertical upscaling of the geologic model to 13 layers based on the geologic markers**.** Cross-sections of the detailed geologic model and the corresponding upscaled model for both porosity and permeability distributions in the reservoir and the detailed upscaling methods can be found elsewhere.[29] The grid size for the upscaled model is 74×100×13. The initial water saturation in the simulation model was obtained using facies-based J-curves and capillary-gravity equilibrium conditions. Gravity effects were included in the simulation model and had a significant impact on the results, especially on the water-cut responses because of water-slumping. In addition, it was important to include fluid compressibility and aquifer influx to obtain a pressure history consistent with the field observations.

Production data smoothing is an important step during generalized travel-time inversion with field data. The field production history data are frequently erratic with large-scale fluctuations. Very often the time step sizes in simulation are larger than the intervals of observation data. Thus, the fluctuations within short time intervals in the production data are not captured by simulation. We suggest averaging (smoothing) the production data before inversion over pre-specified interval using the simulation time steps as guidelines. This helps the inversion capture the general trend of the production history and not be trapped by small details. Data smoothing also facilitates the calculation of the shift-time during generalized travel-time calculations.

Production Data Integration. Out of the 70 producers in the field (**Fig. 13**), 48 wells had water-cut response. Starting with the upscaled model, the grid block permeabilities were changed via the generalized travel-time inversion to match the water-cut histories at the 48 producers. **Fig. 14** compares the initial permeability field with the final permeability field derived after inversion. From a visual examination, it is difficult to discern any differences. This is partly a consequence of the 'norm' constraint (Eq. 19) during the inversion that attempts to preserve the initial geologic model. Also, the streamline-based sensitivities help target the changes to regions of maximum impact. **Fig. 15** shows the permeability multipliers resulting from history matching and indicates the regions where permeabilities have been altered during inversion. In general, permeabilities increased at the northern higher elevation with higher quality reservoir facies. No permeability enhancements were observed in the lower interval that represents low quality reservoir. These changes are consistent with those observed by Qassab et al.[29] and were found to be geologically realistic. **Fig. 16** shows the misfit reduction during the inversion. In 9 iterations, the arrival-time misfit has been reduced by half and the water-cut misfit has been reduced by almost one quarter. **Fig. 17a** compares the observed and calculated water arrival-times at 0.1 fractional water-cut using the initial static model. After 9 iterations of generalized travel-time inversion, the corresponding arrival-times are shown in **Fig. 17b**. There is a significant reduction in the scatter indicating a close match between the observed and calculated water breakthrough times. The entire history matching took about 9 hours in a PC (Intel Xeon 3.06 GHz Processor).

The water-cut match has significantly improved for most wells. Some examples of these matches are shown in **Fig. 18**. Specifically, the generalized travel-time inversion can match the water-cut history for wells with no calculated initial breakthroughs (Wells A, D, F, L, R, V, and X), wells with high initial water-cut (Wells J, Z, W, K, and Y), and wells with low initial water-cut and late breakthroughs (Wells M, P, G, E, and S). Generalized travel-time inversion improved the match even though the breakthrough-time is already matched (Wells Z and Y). Finally, the match in Well F shows its ability to match non-monotonic production history.

The saturation distribution in the field at the end of the simulation is shown in **Fig. 19**. The water encroachment patterns and the unswept areas indicated by the simulation were found to be consistent with the field surveillance data.[29] The simulation model also shows evidence of water override as observed in field surveillance data.

Statistics After Inversion. We examined the impact of production data integration on the permeability distribution by comparing the statistics of the initial and the final permeability fields. As indicated in **Fig. 20**, the histograms of both the models are almost identical in terms of the median and the upper and the lower quantiles of permeability. In other words, the shape of the distribution has essentially remained unchanged. The mean permeability, however, is slightly higher after history matching. This is primarily because integration of production data has resulted in flow channels and preferential flow paths with higher permeabilities. As a result, the heterogeneity has increased in terms of standard deviation and coefficient of variation.

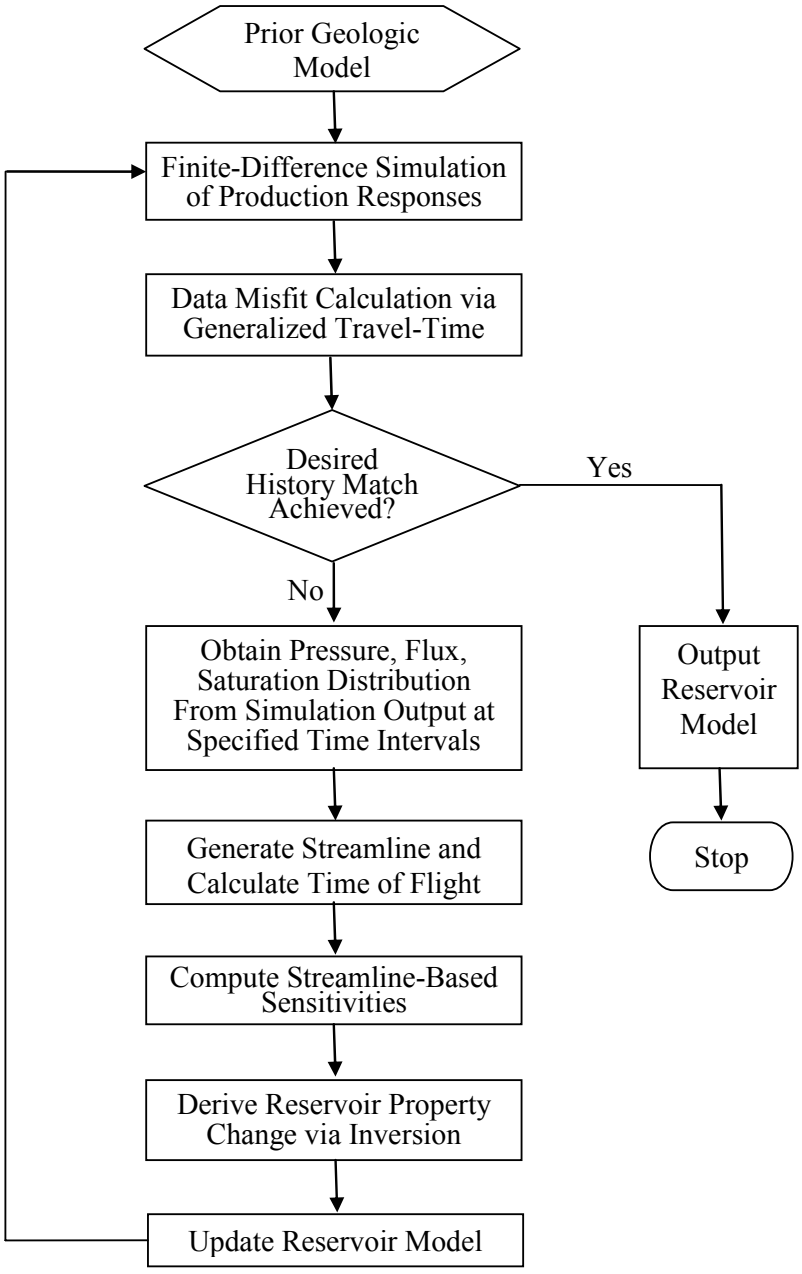

Figure 1- Flowchart for History Matching Finite-Difference Models using Streamline-Derived Sensitivities.

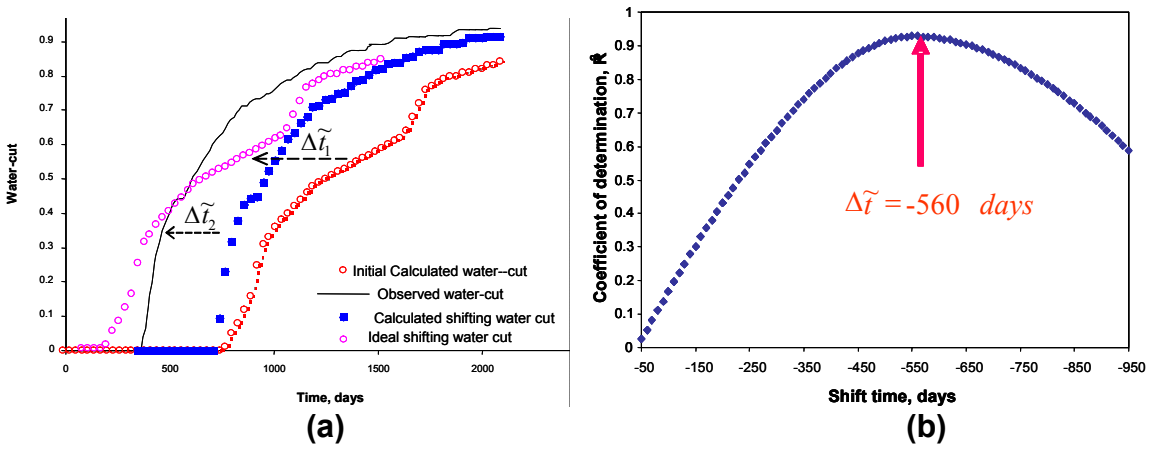

Figure 2- Illustration of generalized travel-time inversion: (a) history-matching by systematically shifting the calculated water-cut to the observed history, (b) best shift-time which maximizes the correlation function

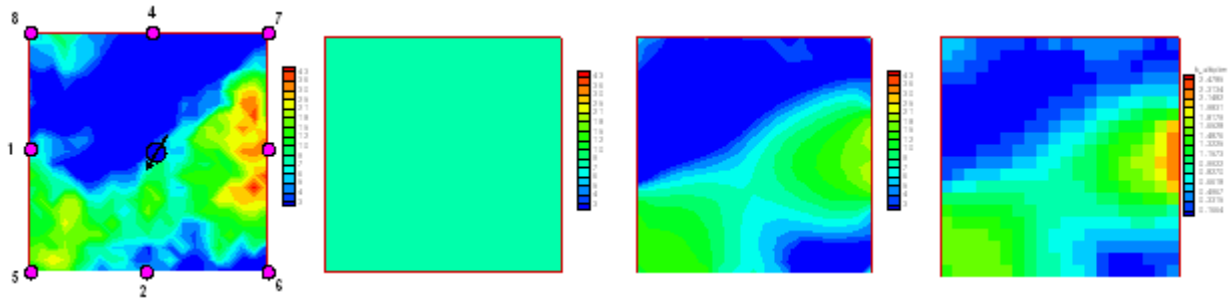

Figure 3- Permeability distribution for the synthetic 9-spot case: (a) reference permeability field, (b) homogeneous initial permeability, (c) final permeability distribution after inversion, and (d) permeability multiplier obtained from history matching.

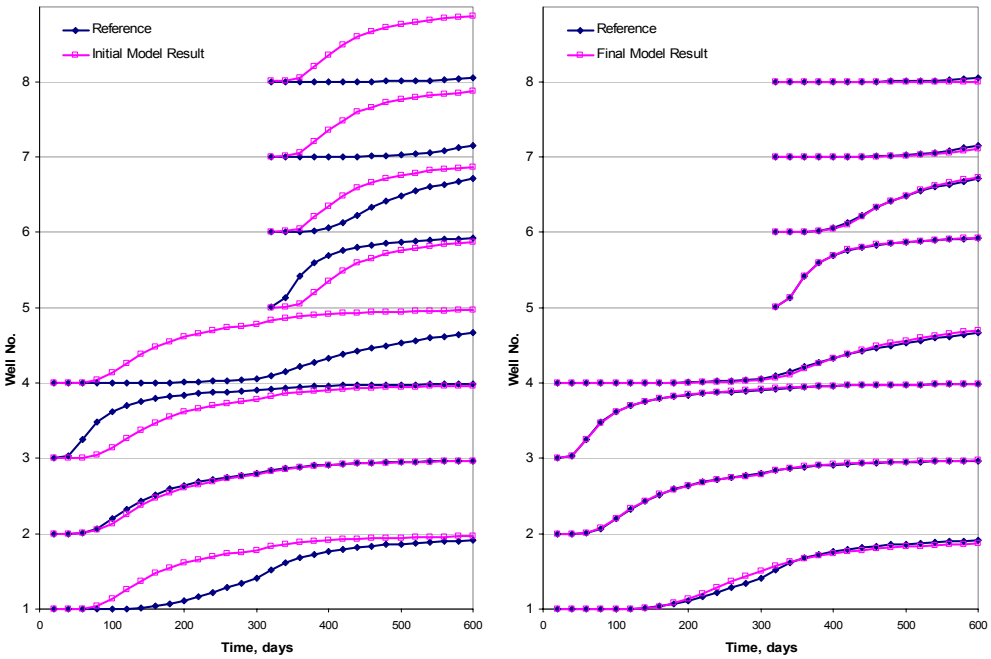

Figure 4- Water-cut match for the synthetic 9-spot case by (a) initial homogeneous permeability model and (b) final inverted permeability model. Red-square stands for model results, and blue-diamond is for reference or observation data.

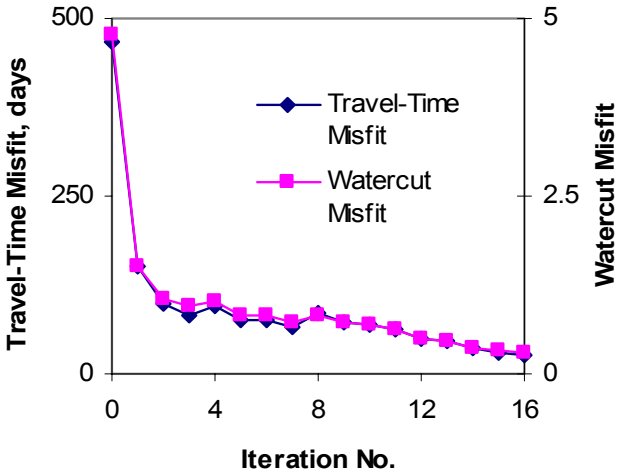

Figure 5- Travel-time and water-cut misfit reduction for the synthetic example.

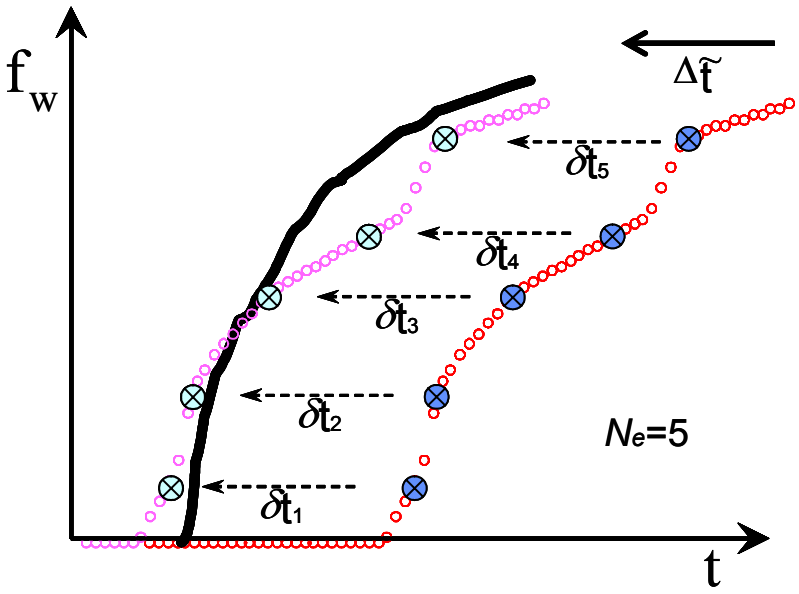

Figure 6- Illustration of generalized travel-time sensitivity computation using the same shift-time for every data points

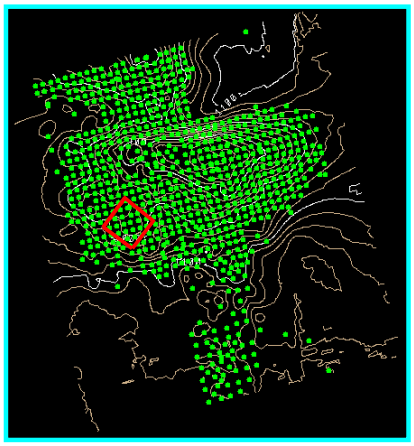

Figure 7- Goldsmith field CO_2 project area.

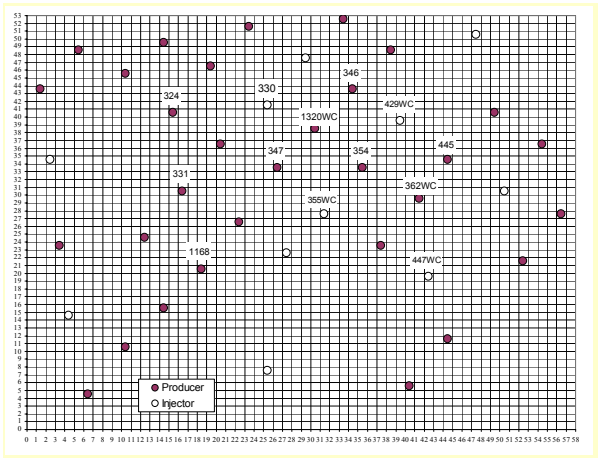

Figure 8- Well configuration of the study area.

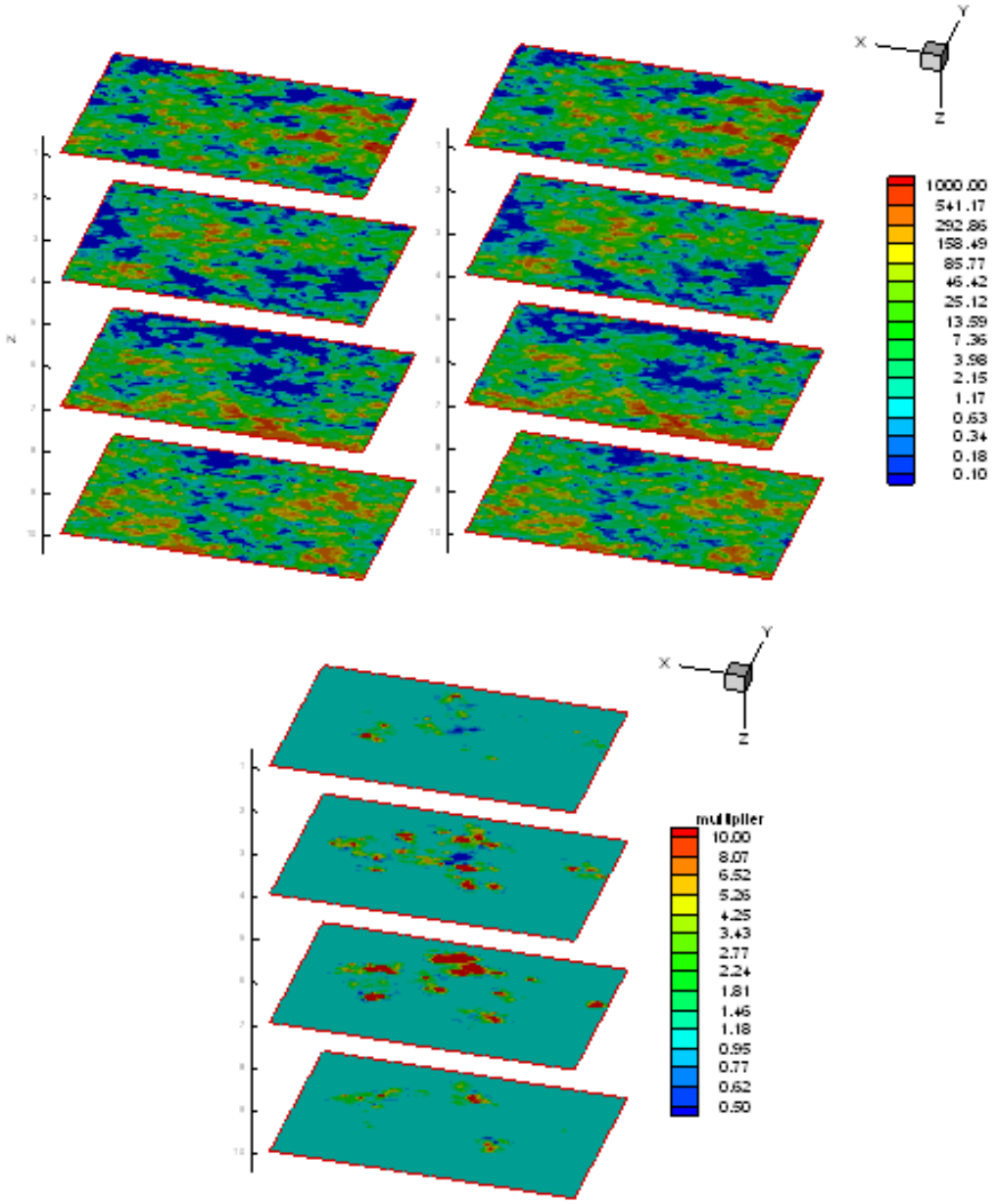

Figure 9 -Permeability distribution for Goldsmith case: (a) initial permeability field generated via a cloud transform based on the porosity-permeability relationship, (b) final permeability field from history matching, and (c) permeability multiplier generated from history matching.

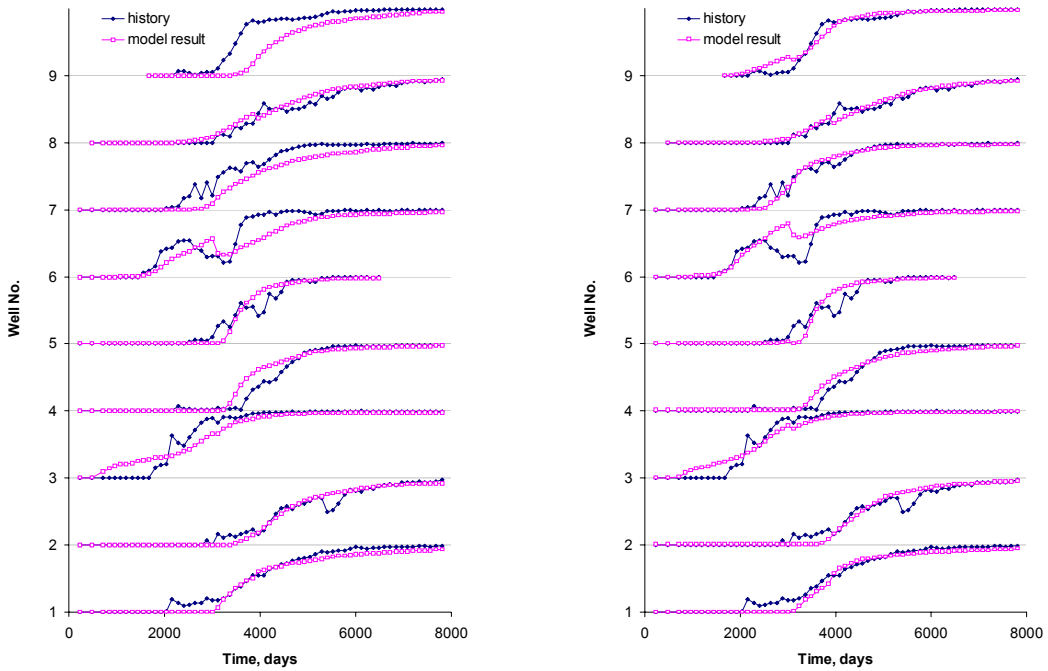

Figure 10 -Water-cut matching for Goldsmith case: (a) initial water-cut match and (b) final water-cut match obtained from history matching.

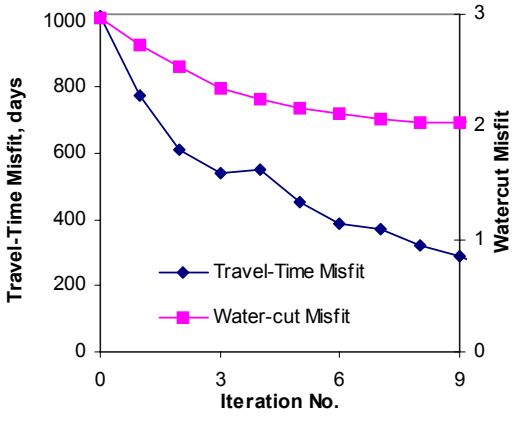

Figure 11- Arrival-time and water-cut misfit reduction, Goldsmith case.

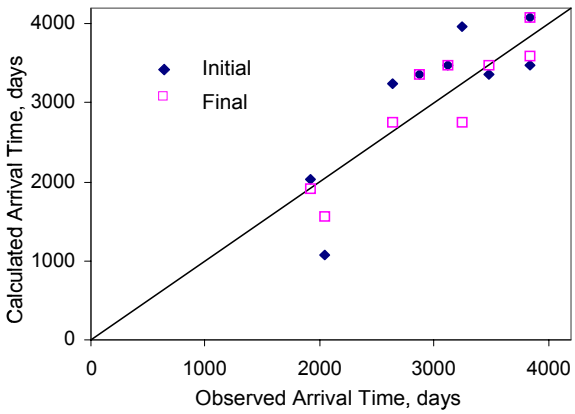

Fig 12- Calculated vs. observed arrival-time for the initial and final model, Goldsmith case.

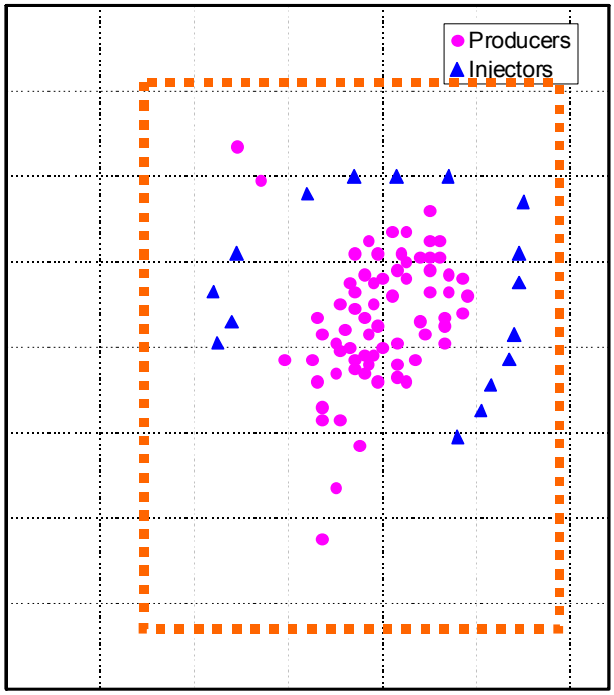

Figure 13- Well location map for the giant middle-eastern case. Dotted lines denote simulation area (from SPE 84079).

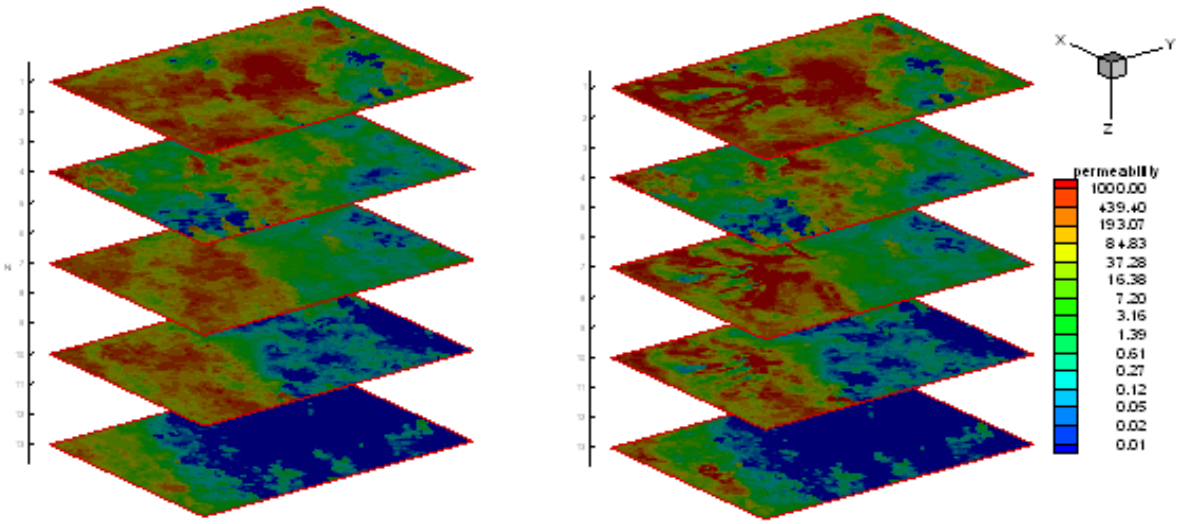

Figure 14- Initial Upscaled permeability field (left) and final upscaled permeability field (right) after production data integration for the middle-eastern case.

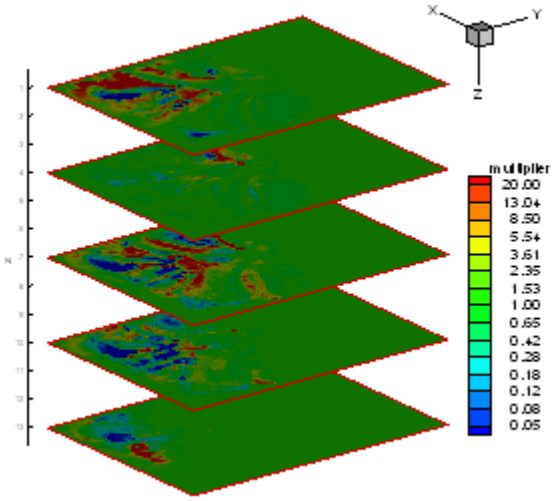

Figure 15- Permeability multiplier obtained from history matching for the middle-eastern case.

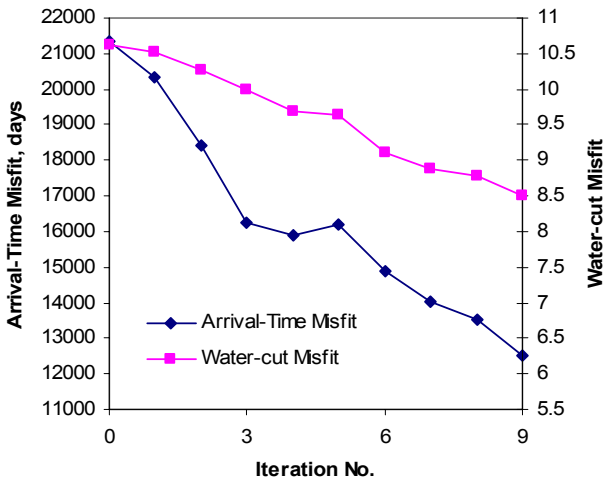

Figure 16- Misfit reduction for the giant middle-eastern case.

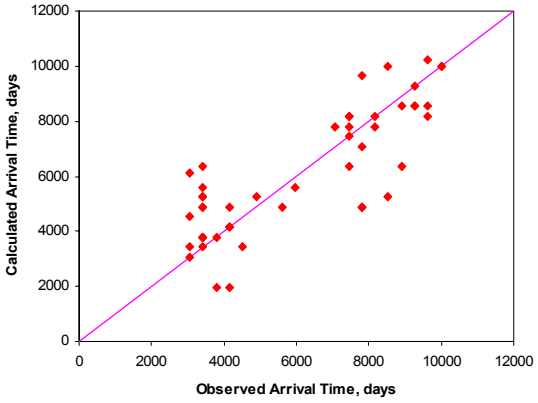

(a)

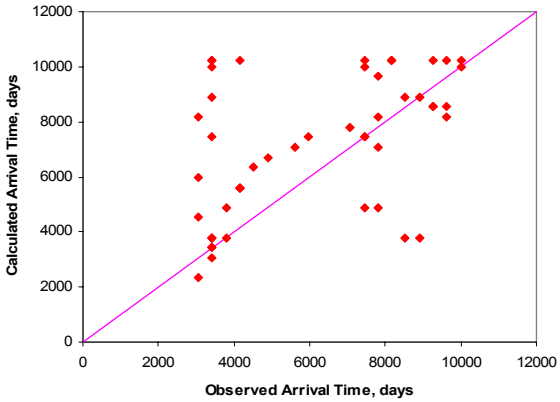

(b)

Figure 17 -(a) Initial arrival-time match and (b) final arrival-time match after 9 iterations for the giant middle-eastern case.

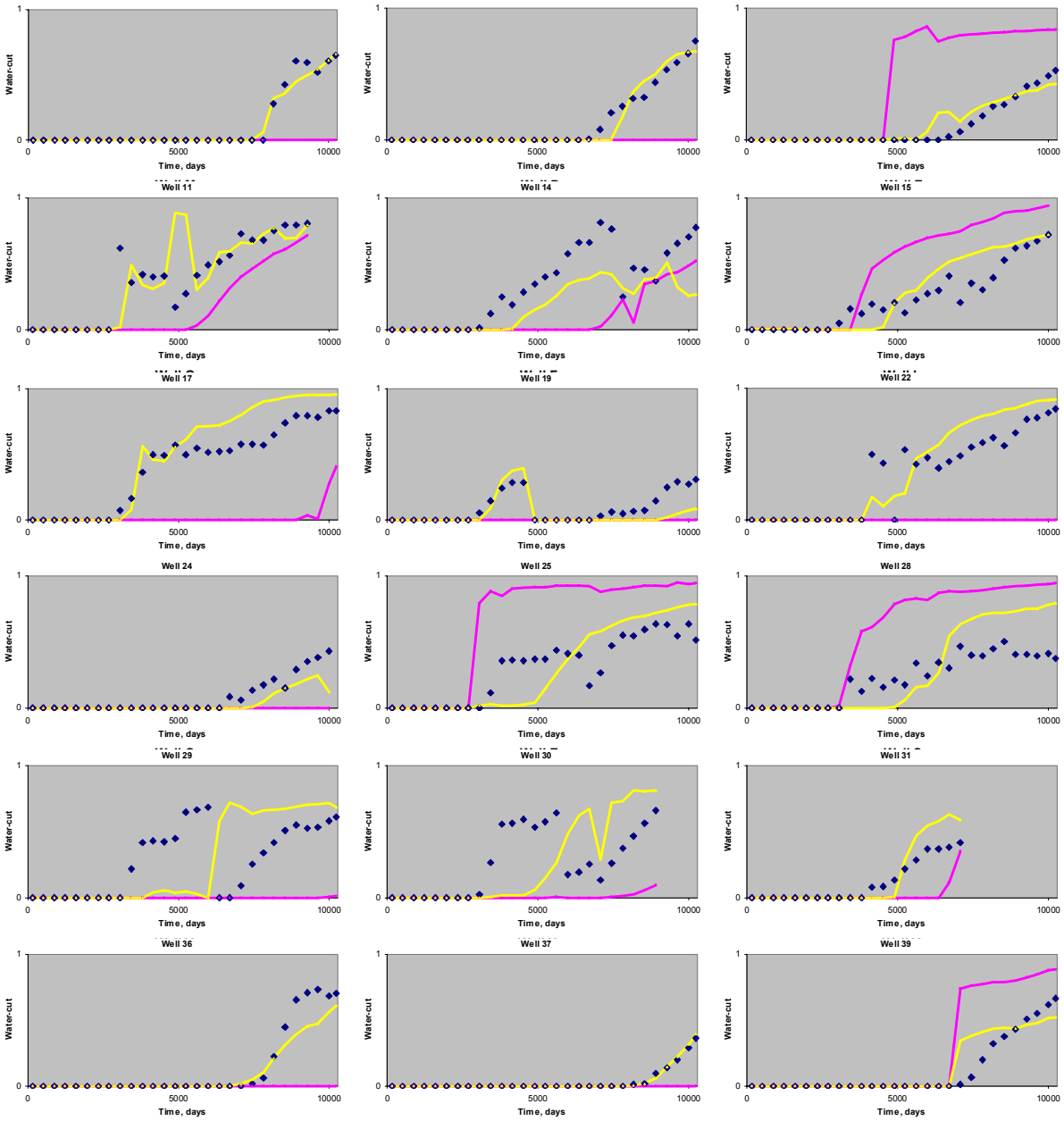

Figure 18- Examples of the water-cut match after history matching for the giant middle-eastern case. Blue-diamond is history, red line is initial model result, and yellow line is the final updated model result. Most of the 48 producers have a much better history matching after inversion.

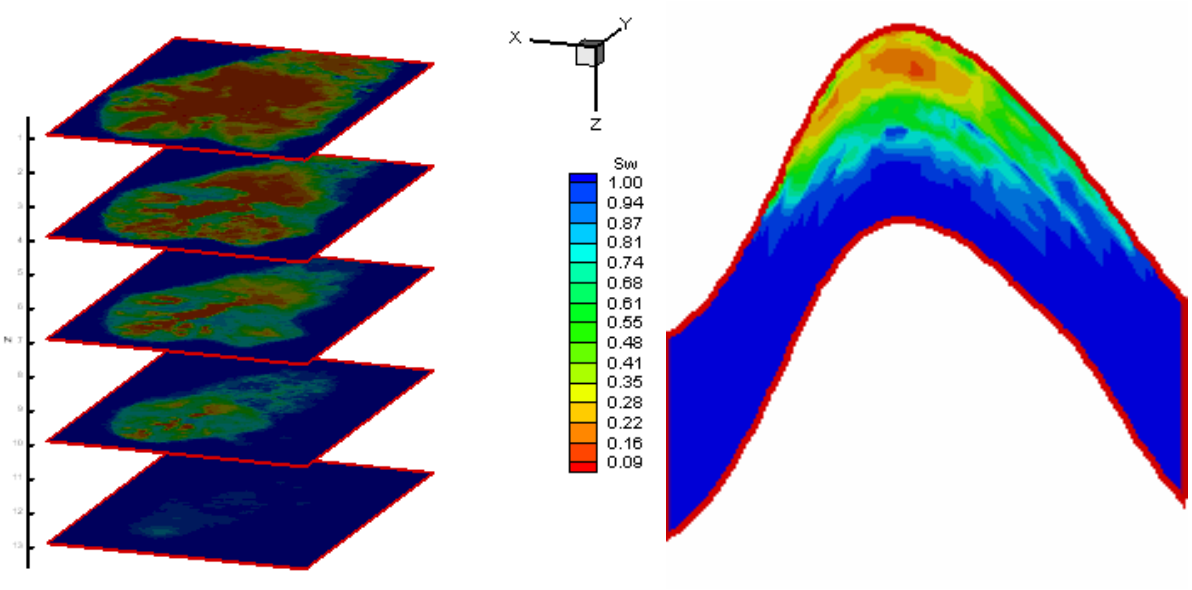

Figure 19- Saturation profile at 10290 days by final updated permeability. Water override is shown from the east-west cross section view.

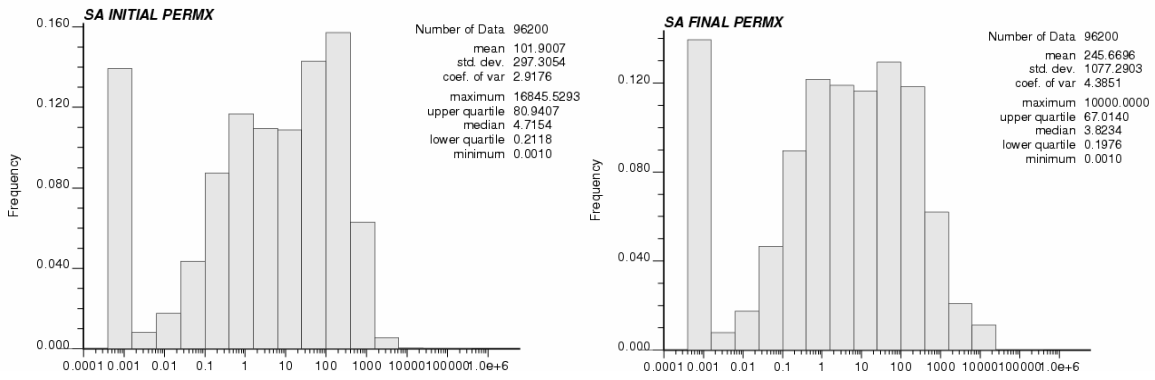

Figure 20- Histogram of the initial permeability (left) and the final updated permeability for the giant middle-eastern case.

RESULTS AND DISCUSSION: PART III

Field-Scale Design Optimization via Analytic Methods and Numerical Simulation

Introduction

Tracer tests have been used in the reservoirs for many years for evaluation of reservoir characteristics such as well communication, flow barriers, preferential flow paths, rate of movement of injected fluids, oil saturations and sweep efficiencies (Zemel, 1995). Partitioning interwell tracer tests have the advantage over single well tracer tests that they can be used to quantify the volume of both mobile and residual oil over the entire reservoir volume swept by the interwell tracers (Tang et al., 1991a, Tang et al., 1991b and Allison, 1998) rather than just the near well region. It is often the unswept oil far from the injection wells that is of most interest to reservoir engineers rather than the values at or even below residual oil saturation near the injection wells. During the past ten years, PITTs have been used extensively to measure the volume of organic liquid contaminants and/or average oil saturation in groundwater as well as in the soil above the water table.

The method of moments was developed for the analysis of both swept pore volume and the average oil saturation within swept pore volumes from PITT data in aquifers (Jin et al., 1995 and Jin et al., 1997). Dwarakanath et al. (1999) estimated the uncertainty in the oil saturation calculated by the method of moments caused by errors in experimental data. Jayanti (2003) studied the impact of heterogeneity on the accuracy of the oil saturation derived from tracer data. In this part of the report, we further develop and apply the method of moments to interpret partitioning interwell tracer data under a variety of oil field conditions.

Derivation of the Method of Moments

The derivation of the method of moments was been generalized to include the calculation of mobile oil saturation (two-phase flow) in three-dimensional, heterogeneous reservoirs including even naturally fractured reservoirs. The swept pore volume is defined as the pore volume of the reservoir contacted by the injected fluid. In general, a tracer is eventually produced at more than one producing well, so the concept must be associated with the volume swept between a particular injection well and a particular production well. Tracers can also be injected in different vertical intervals of the reservoir, so the swept pore volume must also be associated with the injection and production interval. The value of oil saturation must be associated with this swept pore volume to be meaningful. The swept pore volume is also of interest per se since the sweep efficiency is directly proportional to it.

The key equations needed to calculate swept pore volume and oil saturation are given below along with the key steps in the derivation of the method of moments. The mass conservation equations can be integrated under remarkably general conditions to estimate oil saturation and swept pore volume. The assumptions in the derivation of the equation are (1) the partition coefficient of each tracer is constant during the test, which is a very good approximation since very low tracer concentrations are used in practice (2) diffusion at the well boundaries is negligible, which has no practical effect on the results (3) there is no mass transfer of the tracers across the boundaries of the swept volume of interest and (4) the tracers are chemically stable during the test.

The mass conservation equation for tracer i flowing in the reservoir is

$$\frac{\partial \phi C_i}{\partial t} + \nabla \cdot \vec{N}_i = 0 \tag{1}$$

Where

$$C_i = \sum_{j=1}^{n_p} S_j C_{ij} \tag{2}$$

$$\vec{N}_i = \sum_{j=1}^{n_p} \left(C_{ij} \vec{u}_j - \phi S_j \vec{\vec{K}}_{ij} \cdot \nabla C_{ij} \right) \tag{3}$$

For a tracer slug injection over time period $0 \le t \le t_{slug}$

$$\begin{cases} C_{it}\big|_{injector} = C_{iJ}, & 0 \le t \le t_{slug} \\ C_{it}\big|_{injector} = 0, & t \ge t_{slug} \end{cases} \tag{4}$$

Multiplying Eq. (1) by time and integrating over time

$$-\phi m_{0i} + \nabla \cdot \int_0^\infty t \vec{N}_i \, dt = 0 \tag{5}$$

Where

$$m_{0i} = \int_0^\infty C_i \, dt \tag{6}$$

Integrating Eq. (5) over the reservoir volume of interest

$$-\iiint \phi m_{0i} \, dV + \iiint \nabla \cdot \left(\int_0^\infty t \vec{N}_i dt \right) dV = 0 \tag{7}$$

Applying divergence theorem to Eq. (7)

$$-\iiint \phi m_{0i} \, dV + \iint \left(\int_0^\infty t \vec{N}_i \, dt \right) \cdot \vec{n} \, dA = 0 \tag{8}$$

Since mass transfer occurs only at the wells

$$-\iiint \phi m_{0i} \, dV + \left(q m_{1i} \right)\big|_{wells} = 0 \tag{9}$$

Where

$$m_{1i} = \int_0^\infty t\left(\sum_{j=1}^{n_p} f_j C_{ij}\right) dt \tag{10}$$

This equation could be applied to a variety of water, oil and gas combinations. For the specific case of just oil and water, it can be written as follows:

$$\begin{aligned}
&\iiint \phi m_{0i}\, dV \\
&= \iiint \phi \int_0^\infty (S_w C_{iw} + S_o C_{io})\, dt\, dV \\
&= \iiint \phi \int_0^\infty (S_w + K_i S_o) C_{iw}\, dt\, dV \\
&= \iiint \phi \left(\hat{S}_w + K_i \hat{S}_o\right) \int_0^\infty C_{iw}\, dt\, dV \\
&= \iiint \phi \left(\hat{S}_w + K_i \hat{S}_o\right) m_{0iw}\, dV
\end{aligned} \tag{11}$$

Where the partition coefficient is defined as:

$$K_i = \frac{C_{io}}{C_{iw}}$$

And

$$\hat{S}_j = \frac{\int_0^\infty S_j C_{iw}\, dt}{\int_0^\infty C_{iw}\, dt} \tag{12}$$

Equation (9) can be used to show that:

$$-\iiint \phi \left(\hat{S}_w + K_i \hat{S}_o\right) m_{0iw} dV + m_{0iw}\big|_{producer} \overline{V_i} = 0 \tag{13}$$

Where the mean residence volume of tracer i is given as

$$\overline{V_i} = \frac{\int_0^\infty q C_{it} t\, dt}{\int_0^\infty C_{iw}\, dt} - \frac{V_{slug}}{2} \tag{14}$$

Assuming $\hat{S}_j$ is not different between tracers and that m_{0iw} is not a function of space, it follows from Eq. (13) that:

$$-\iiint \phi\left(\hat{S}_w + K_i \hat{S}_o\right) dV + \overline{V}_i = 0 \tag{15}$$

Equation (15) can be used to show that the average oil saturation is given by:

$$\bar{\hat{S}}_o = \frac{\overline{V}_1 - \overline{V}_2}{\overline{V}_2(K_1 - 1) - \overline{V}_1(K_2 - 1)} \tag{16}$$

And the swept pore volume is given by:

$$V_s = \frac{\overline{V}_2(K_1 - 1) - \overline{V}_1(K_2 - 1)}{K_1 - K_2} \tag{17}$$

Since the average oil saturation $\bar{\hat{S}}_o$ is at the mean residence time of the conservative tracer $\bar{t}_1$, the average oil saturation at the end of the PITT is given by subtracting the volume of oil produced after the mean residence time, which is:

$$\overline{S}_o = \frac{V_s \bar{\hat{S}}_o - \int_{\bar{t}_1}^{\infty} q_o \, dt}{V_s} \tag{18}$$

The mean residence volume for each tracer i calculated from Eq. (14) between a particular injection well with injection rate Q and a particular production well n should be calculated using the flow rate q corresponding to the rate in the swept volume of interest. This rate can be calculated by proportioning the mass of tracer produced m_n at the producer n of interest with the total mass of the tracer injected (M) as follows:

$$q = \frac{m_n}{M} Q \tag{19}$$

Where

$$m_n = \int_0^{\infty} q_n C_{it} \, dt \tag{20}$$

$$M = \int_0^{t_{slug}} Q C_{iJ} \, dt = C_{iJ} Q t_{slug} = C_{iJ} V_{slug} \tag{21}$$

Once the mean residence volumes are obtained, the swept pore volume between wells and the average oil saturation in each swept pore volume is performed with the same equations

as that with one injector and one producer. The average oil saturation $\bar{\hat{S}}_o$ calculated from Eq. (16) is the average oil saturation at the mean residence time of the conservative tracer, $\bar{t}_1$, before correction for produced oil. For a reservoir with multiple wells, produced oil can be contributed from multiple injectors and the oil production rate needs to be divided into well pairs so that the moment analysis can be performed for each well pair. The oil production rate is assumed to be proportional to the tracer swept volume. For example, for the case of one producer with streamlines from 4 injectors, the oil production rate corresponding to swept volume 1 is given by:

$$q_o = \frac{V_{s1}}{V_{s1} + V_{s2} + V_{s3} + V_{s4}} Q_o \tag{22}$$

where Q_o is the total oil production rate for this production well and V_{s1} is the swept pore volume of interest. The average oil saturation corrected for produced oil within a particular swept volume is then calculated from Eq. (18) as before.

Simulation Results for Conventional PITTs

In this first example, a slug of tracers in water at residual oil saturation was simulated using the UTCHEM simulator. The 3D simulation domain is a quarter of a five-spot well pattern with dimensions of 660 ft long, 660 ft wide and 50 ft thick (Table 1). A heterogeneous permeability field was stochastically generated using FFT software (Jennings et al., 2000). The permeability field has a log mean permeability of 344 md and a Dykstra-Parsons coefficient of 0.81. The correlation lengths are 100 ft in the horizontal direction and 10 ft in the vertical direction.

Figure 1 shows the permeability and residual oil saturation for a vertical cross-section of the reservoir at J = 1. A residual oil distribution was generated assuming an exponential relation with permeability.14 Regions of high permeability have low oil saturation and vice versa. The average oil saturation in the reservoir is 0.245. The reservoir has a uniform porosity of 0.2. A tracer slug consisting of a conservative tracer and three partitioning tracers with partition coefficients of 0.5, 1.0 and 2.0 was injected for 0.1 pore volumes (PV) followed by water.

Figure 2 shows the tracer concentration curves at the producer. In order to obtain the response curve of a partitioning tracer (the produced concentrations) in a reasonably short time and yet ensure good separation of the conservative and partitioning tracers, the partition coefficients should be within a certain range. The retardation factor for partitioning tracer i relative to the conservative tracer is defined as follows:

$$R_{fi} = 1 + \frac{K_i S_{or}}{1 - S_{or}}$$

Jin (1995) recommended retardation factors between 1.2 and 4.0 for groundwater applications. Times and distances are much longer in the oil field, so retardation factors between 1.2 and 1.5 are more likely to be optimum. The oil saturation calculated from the produced tracer concentrations as a function of time is shown in Fig. 3. The oil saturation was estimated using a conservative tracer and a partitioning tracer with a partition coefficient of 1.0. The oil saturation

calculated from the method of moments gradually approaches the true average value of residual oil saturation used in the simulation and by 800 days is very close to it.
Figure 4 shows the tracer concentration histories for the same case except the tracers were injected continuously rather than as a slug. For a continuous tracer injection, the mean residence volume is the swept pore volume and gradually increases with time. The sweep efficiency as a function of time can be calculated by dividing the swept pore volume by the total pore volume if the partition coefficient is 1.0. Figure 5 illustrates the sweep efficiency calculated using such a tracer. Converting swept pore volumes to sweep efficiency is simple in a confined well pattern such as in this example. For more complicated cases, the total pore volume of interest must first be defined before the swept pore volume can be used to calculate the sweep efficiency.

Table 1: Summary of Reservoir Conditions

Reservoir dimensions	**660 ft x 660 ft x 50 ft**
Number of gridblocks	**22x22x10**
Porosity	**0.2**
Residual oil saturation	**0.25**
Residual water saturation	**0.30**
Water end point relative permeability	**0.15**
Oil end point relative permeability	**0.85**
Corey exponent for water	**1.5**
Corey exponent for oil	**2.0**
Density of oil	**52.88 lb/cu. ft**
Density of water	**62.4 lb/cu. ft**
Viscosity of oil for mobility ratio of 0.5	**1.5 cp**
Viscosity of oil for mobility ratio of 1.2	**5 cp**
Viscosity of oil for mobility ratio of 5.2	**15 cp**
Viscosity of water	**0.7 cp**
Longitudinal dispersivity	**0.3 ft**
Transverse dispersivity	**0.03 ft**

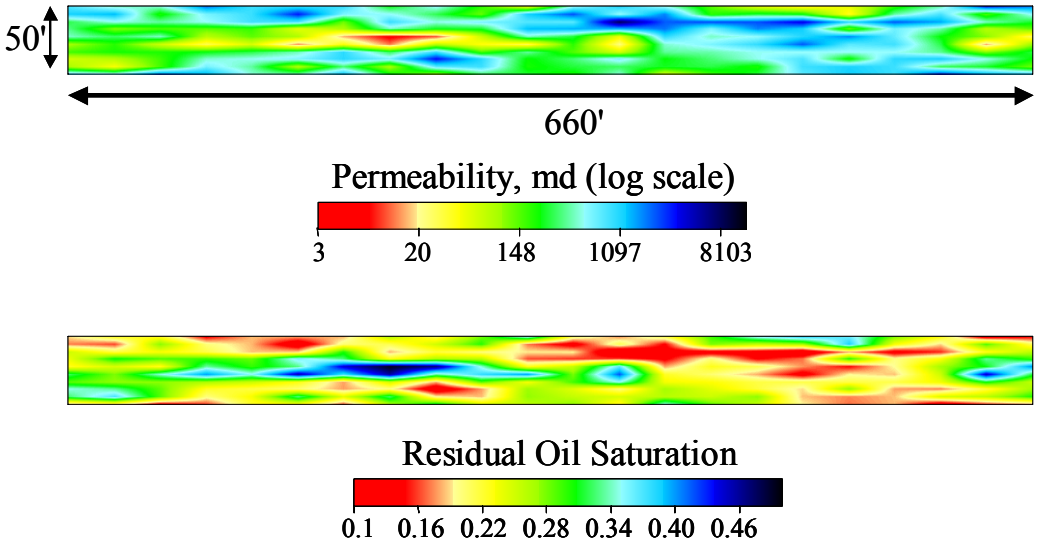

Figure 1- Permeability and oil saturation profiles for the three-dimensional heterogeneous reservoir.

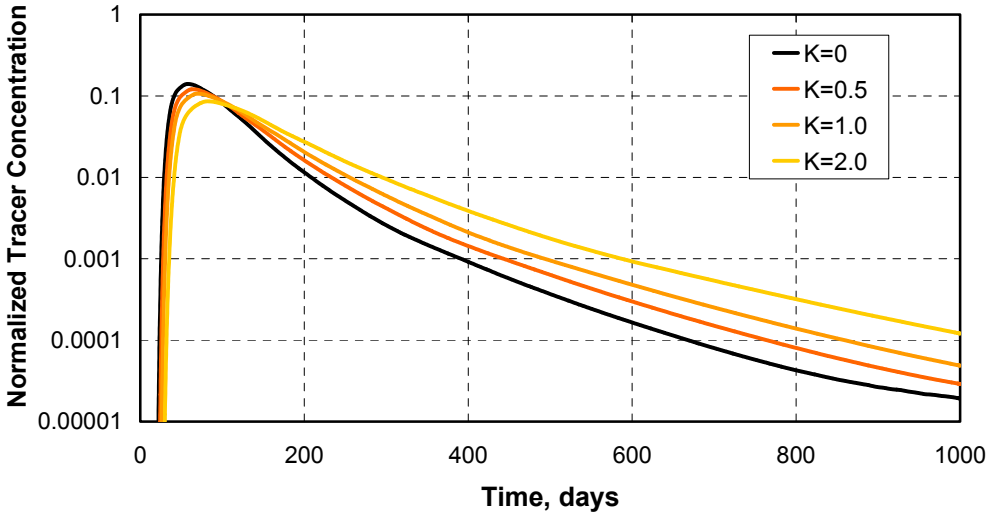

Figure 2- Tracer concentration curves for the three dimensional heterogeneous simulation.

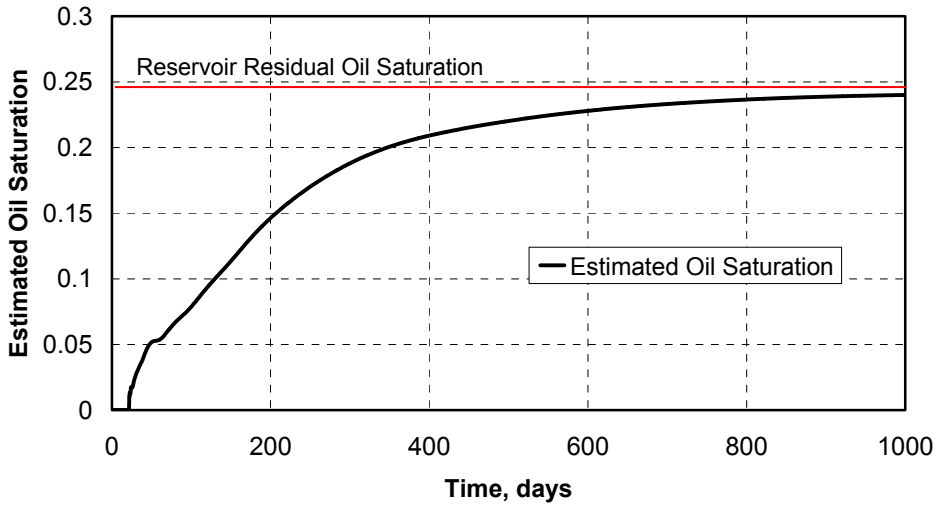

Figure3—Estimated oil saturation using the method of moments.

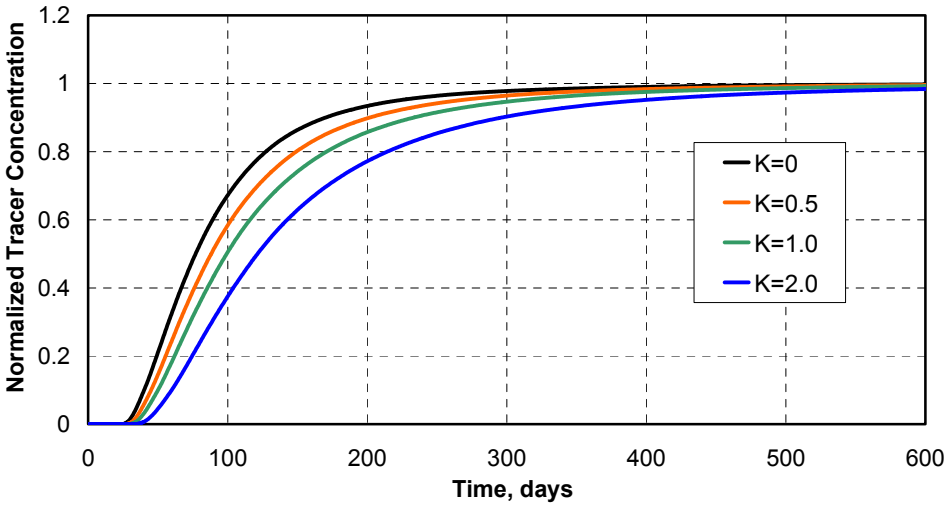

Figure 4- Tracer concentrations for a continuous tracer injection.

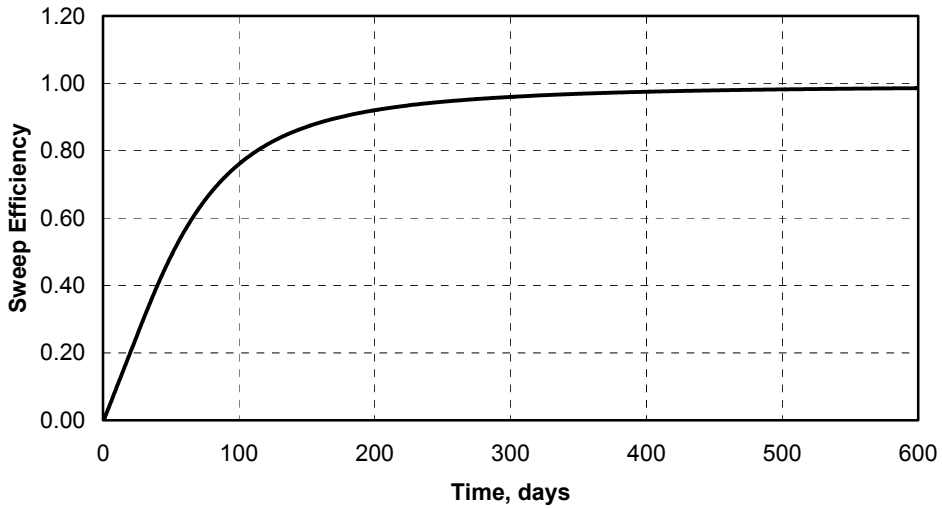

Figure 5- Sweep efficiency calculated using tracer concentrations for a partitioning tracer (K=1) injected continuously.

Oil Saturation as a function of depth

If downhole sensors could be used for real time tracer measurements at different depths in the well during a partitioning interwell tracer test, then such tracer data could be used to generate the vertical distribution of oil saturation in addition to the average oil saturation in the swept volume of the reservoir between well pairs. Sampling at different depths could also be used to provide such data at discrete times. The potential value of obtaining these data is illustrated in the following simulation example.

A slug of tracers in water at residual oil saturation was simulated using the UTCHEM simulator. The 3D simulation domain is a quarter of a five-spot well pattern with dimensions of 660 ft long, 660 ft wide and 50 ft thick (Table 1). A heterogeneous permeability field was stochastically generated using FFT software (Jennings et al., 1997). The permeability field has a log mean permeability of 344 md and a Dykstra-Parsons coefficient of 0.81. The correlation lengths are 100 ft in the horizontal direction and 10 ft in the vertical direction. Figure 1 shows the permeability and residual oil saturation for a vertical cross-section of the reservoir at J = 1. A residual oil saturation distribution was generated assuming an exponential relation with permeability (Sinha, 2003). Regions of high permeability have low oil saturation and vice versa. The average oil saturation in the reservoir is 0.245. The reservoir has a uniform porosity of 0.20.

Tracer concentration data at various depths in the reservoir were used to make the calculations. Figure 2 shows the tracer concentrations at the producer at a depth of 12.5 ft from the top of the reservoir. A sensitivity study was carried out with various values of vertical to horizontal permeability ratio to study its effect on the oil saturation.

Figure 3 shows a comparison between the average oil saturation in the reservoir and the oil saturation estimated from the PITT as a function of depth. The oil saturations estimated from the tracer data are within 0.02 of the true values within each layer of the reservoir and capture the general trend with depth. The accuracy in the results increases with a decrease in vertical to horizontal permeability ratio corresponding to lower cross flow between layers.

Table 2—Summary of Reservoir Conditions

Reservoir dimensions	660 ft x 660 ft x 50 ft
Number of gridblocks	22x22x10
Porosity	0.2
Residual oil saturation	0.25
Residual water saturation	0.30
Water end point relative permeability	0.15
Oil end point relative permeability	0.85
Corey exponent for water	1.5
Corey exponent for oil	2.0
Density of oil	52.88 lb/cu. ft
Density of water	62.4 lb/cu. ft
Viscosity of oil for mobility ratio of 0.5	1.5 cp
Viscosity of oil for mobility ratio of 1.2	5 cp
Viscosity of oil for mobility ratio of 5.2	15 cp
Viscosity of water	0.7 cp
Longitudinal dispersivity	0.3 ft
Transverse dispersivity	0.03 ft

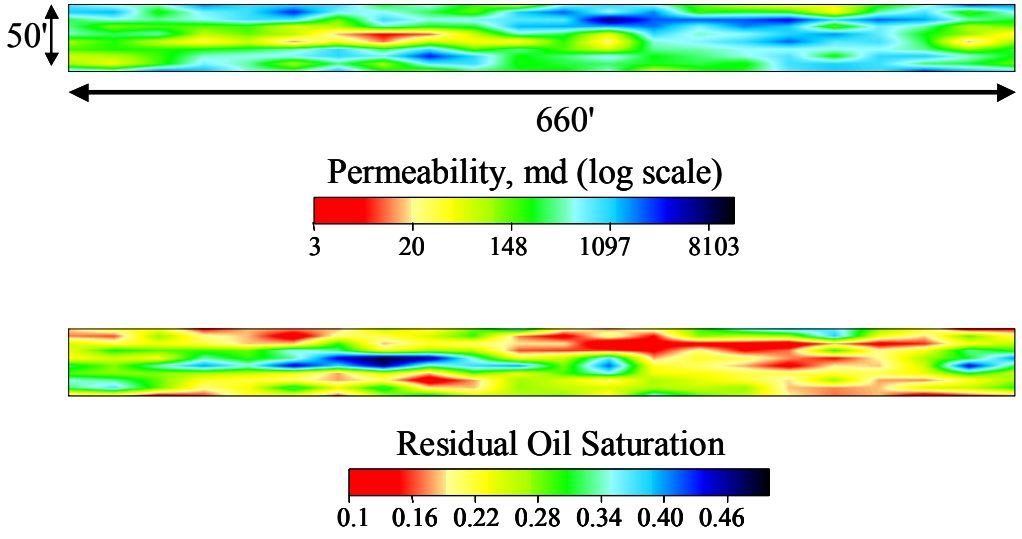

Figure 1- Permeability and oil saturation profiles for the three-dimensional heterogeneous reservoir.

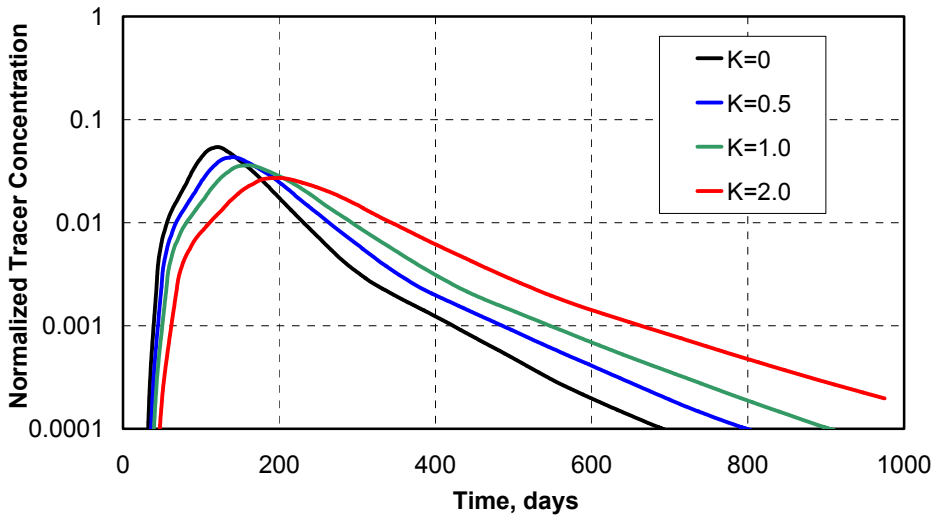

Figure 2- Tracer concentrations at 12.5 ft from the top of the reservoir.

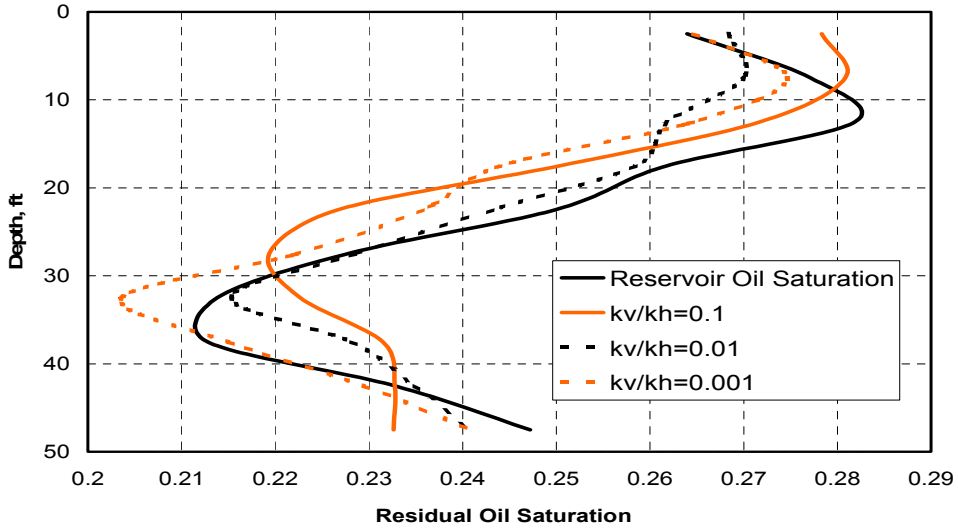

Figure 3- Estimated vertical distribution in oil saturation for various kv/kh ratios.

Simulation of Tracer Tests with Mobile Oil

Although inverse modeling is very useful and much faster computationally than in the past, there is still a lot of advantages in using the simpler method of moments to get average values of oil saturation including its usefulness to condition an inverse calculation or history match with a reservoir simulator. The following examples show that the method of moments can be used to accurately calculate oil saturation even under two-phase flow in the reservoir. Such calculations are very fast and simple compared to inverse modeling.

In this example, the same tracer slug case as before was simulated except the tracers were injected during the waterflood while there was still mobile oil present in the reservoir. In the

previous cases, the residual oil saturation was correlated with permeability so it varied throughout the reservoir. In this example, a uniform residual oil saturation of 0.25 was used.

To simulate tracer tests with different volumes of mobile oil initially in the reservoir, tracer tests were started at different stages of the waterflood. The tracer tests were started after 0.5, 1.0, 1.5, 2.0, 2.5 and 3.0 pore volumes (PV) of water injection. The oil saturation is estimated after 7.0 PV of water injection using the method of moments. In practice, shorter times could be used with some extrapolation of the tracer concentration data (Jin et al., 1995, Jin et al., 1997 and Dwarakanath et al., 1999). A sensitivity study was carried out with waterflood end point mobility ratios of 0.5, 1.2 and 5.2.

Figure 1 shows the oil production rate for the waterflood simulation with an end point mobility ratio of 1.2. Since oil is being produced and partitioning tracers are used, some of the tracer is in the oil as well as in the water. Figures 2 and 3 show the tracer concentration curves for water and oil for a simulation with tracer injection starting at 0.5 PV after the start of the waterflood. Equation (18) was used to calculate the oil saturation using the total tracer concentration rather than the aqueous tracer concentration as in previous examples. The total tracer concentration can be obtained by either directly measuring the tracer concentrations in both the produced water and oil, or by measuring only the concentrations in the water and then calculating the oil concentration from the measured partition coefficient, but this would mean more uncertainty in the estimate.

Figure 4 shows the total tracer concentrations for the same case. Figures 5 to 7 show a comparison between the estimated oil saturation and the oil saturation using total tracer concentrations for mobility ratios of 0.5, 1.2, and 5.2. The maximum difference between the average oil saturation during the PITT and the oil saturation estimated from the PITT is 0.01. Some adjustment in the oil saturation would be needed to estimate the oil saturation at the end of the PITT rather than an average value during the PITT. In these examples, the differences are small. One approach would be to use the PITT estimates to condition a simulation and then predict the oil saturation at other times using the simulator, ideally incorporating other conditioning data at the same time.

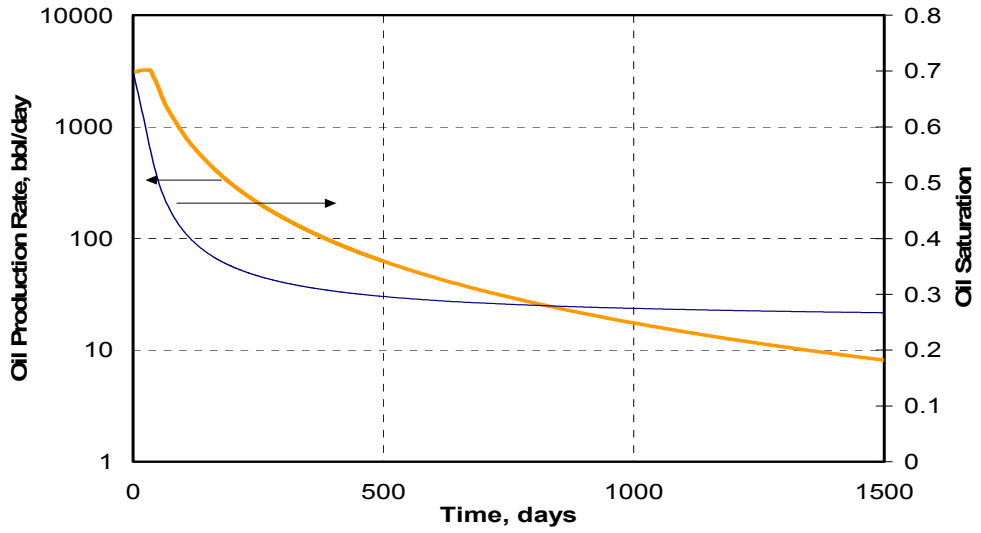

Figure 1- Oil production rate for the simulation with a mobility ratio of 1.2.

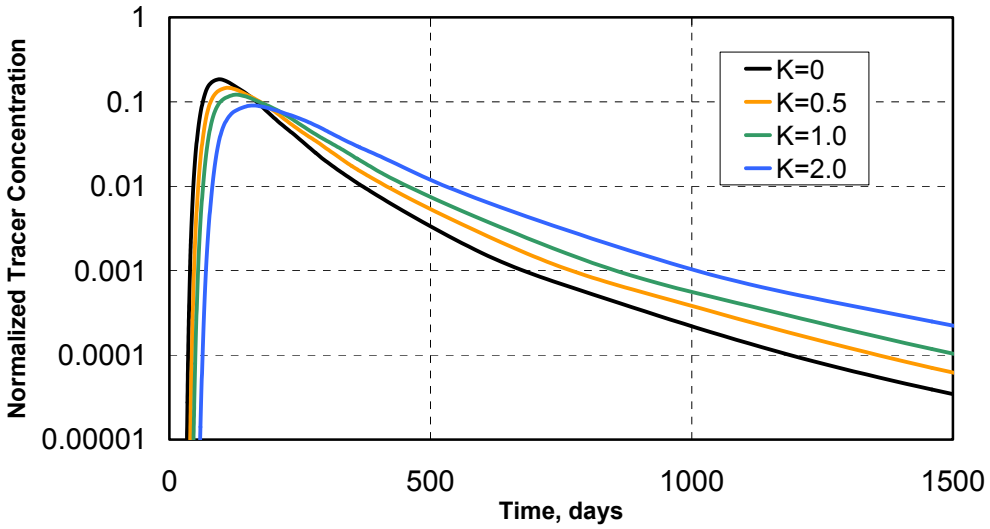

Figure 2- Water phase tracer concentrations for a PITT at 0.5 PV with an end point mobility ratio of 1.2.

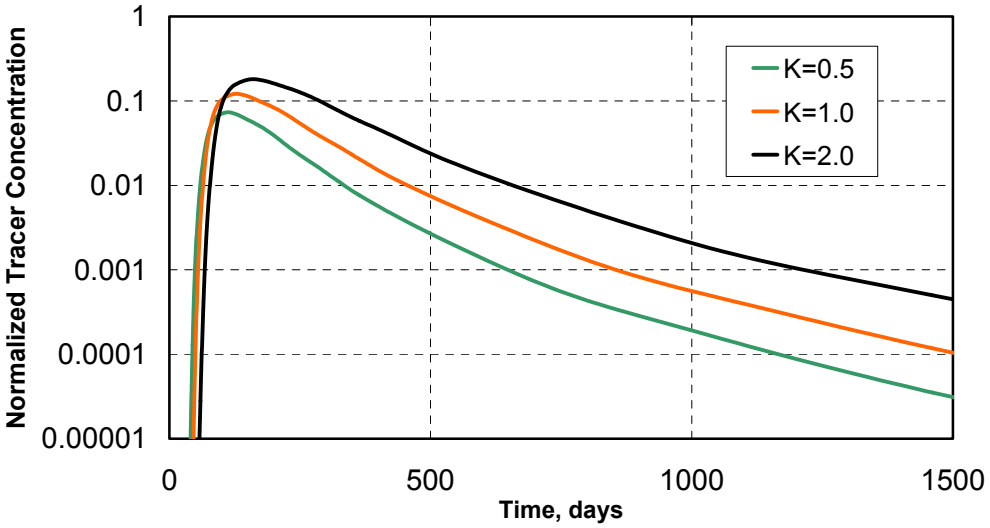

Figure 3- Oil phase tracer concentrations for a PITT at 0.5 PV with an end point mobility ratio of 1.2.

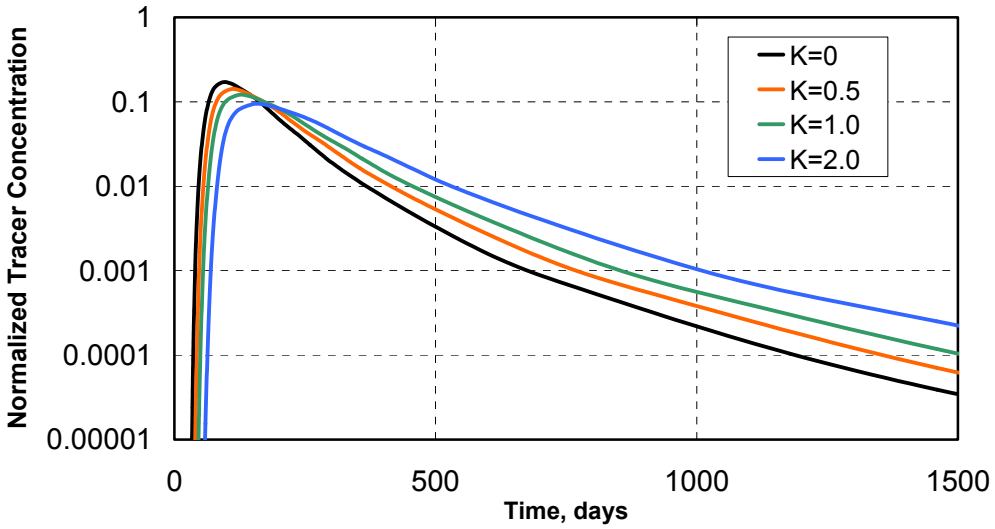

Figure 4- Total tracer concentrations for a PITT at 0.5 PV with an end point mobility ratio of 1.2.

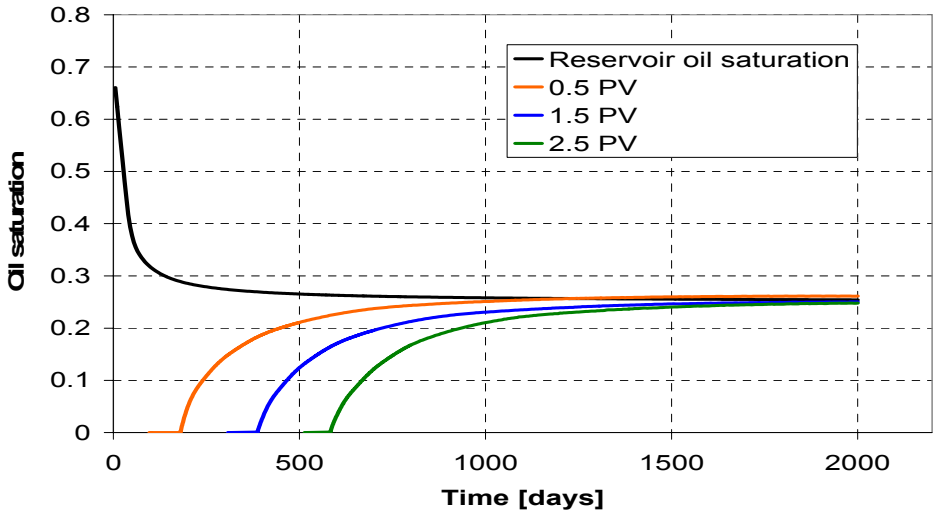

Figure 5- Estimated oil saturation using total tracer concentrations for an end point mobility ratio of 0.5

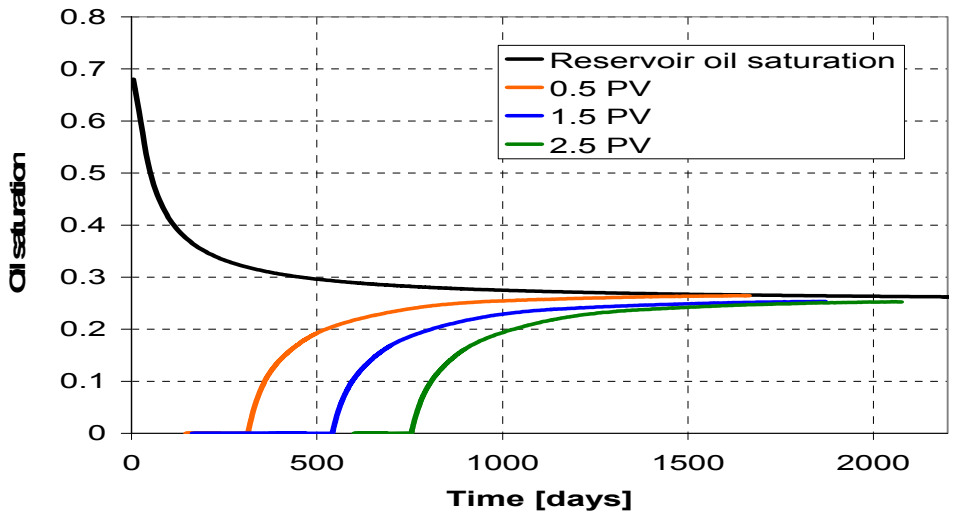

Figure 6- Estimated oil saturation using total tracer concentrations for an end point mobility ratio of 1.2.

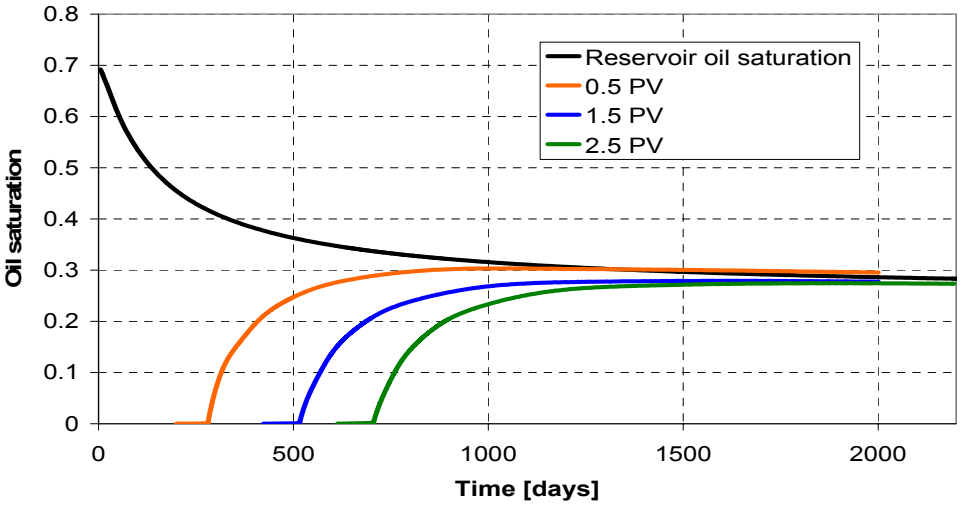

Figure 7- Estimated oil saturation using total tracer concentrations for an end point mobility ratio of 5.2.

In example INVO2-run4, a PITT was simulated in an inverted, confined, 40 acre five-spot well pattern (Table 1). A constant injection rate of 6000 bbl/day was used. The producer was constrained to produce at a constant bottom hole pressure of 2000 psi. A stochastic permeability field with the properties shown in Table 1 was generated using FFT method.

Figure 1 is a plot of the permeability field with a Dystra-Parsons coefficient of 0.81. Figures 2 and 3 show the permeability distribution of the most and the least permeable layers. The reservoir was water flooded for 2000 days before the tracer injection (99% water cut). The oil production rate from the start of tracer injection is shown in Figure 4. Total simulation time

is 6000 days (12 PVs). Four tracers were injected as a slug for 50 days (0.1 PV) with partition coefficients of 0, 0.5, 1, and 2. The results illustrated below were calculated using the partition coefficient of 2.

Tracer concentration plots for each production well are given in Figures 5 to 8. In Figures 5 and 7, tracer breakthrough is quite early and the tracer curves have sharp peaks. This can be explained with the high permeable channels around production wells 1 and 3. Early breakthrough of the tracers in these production wells is clearly seen in Figures 9 and 10, which show the tracer concentration profiles 35 days after the tracer injection in layers 1 and 8.

Figure 20 shows the oil saturation calculated between the injector and each producer using the method of moments. Table 2 shows the difference between these results and the reservoir oil saturation values in each quadrant at the end of the simulation. In the first row of table 2, the residual oil saturation in the reservoir is given as 0.234. This value is calculated by subtracting the amount of oil produced (ECLIPSE output) from the initial oil saturation and is smaller than the input value of 0.25, which implies there is some numerical error in this result.

The difference between the method of moment results and the reservoir values vary between -0.035 and -0.001. The biggest difference is seen in the oil saturation between the injector and producer 1 although the swept pore volume is quite high for this well as it can be seen in Figure 21. This is because of the unrecovered tracer around this well. Figure 22 shows the remaining tracer (partition coefficient K=2) around production well 1. Table 3 shows the swept pore volumes between the injector and each producer. After 6000 days of simulation, 98.4% of the reservoir is swept and oil saturations for each quadrant were estimated with acceptable errors. Figures 23 and 24 have the oil saturation distribution profiles in the 1st and the 2nd layers at the end of the simulation.

Table 1. Reservoir description for Case INVO2-run4

Grid	**44x44x10**
Grid block size, ft	**30x30x5**
Reservoir dimensions, ft	**1320x1320x50**
Area of the reservoir, acres	**40**
Reservoir pore volume, bbl	**3,103,117**
Porosity	**0.2**
Horizontal correlation lengths, ft	**100**
Correlation length in the z direction, ft	**10**
Dykstra-Parsons coefficient	**0.81**
Standard deviation of log permeability	**1.65**
Log mean of permeability, md	**312**
Initial water saturation Swi	**0.3**
Residual water saturation Swr	**0.3**
Residual oil saturation Sor	**0.25**

Table 2. Comparison of Oil Saturations

	Well-1	*Well-2*	*Well-3*	*Well-4*
MOM results for So	0.223	0.247	0.240	0.253
Average So of the reservoir in each quadrant	0.258	0.261	0.254	0.254
Difference	-0.035	-0.013	-0.014	-0.001
Difference %	-3.5%	-1.3%	-1.4%	-0.1%
Sor in the reservoir calculated from ECLIPSE production data	0.234			

Table 3. Swept pore volume

	Well-1	*Well-2*	*Well-3*	*Well-4*
Vswept, bbl	1,052,168	555,314	886,385	558,286
Total Vswept, bbl	3,052,153			
Vswept/Vreservoir	0.339	0.179	0.286	0.180
VsweptTotal/Vreservoir	0984			

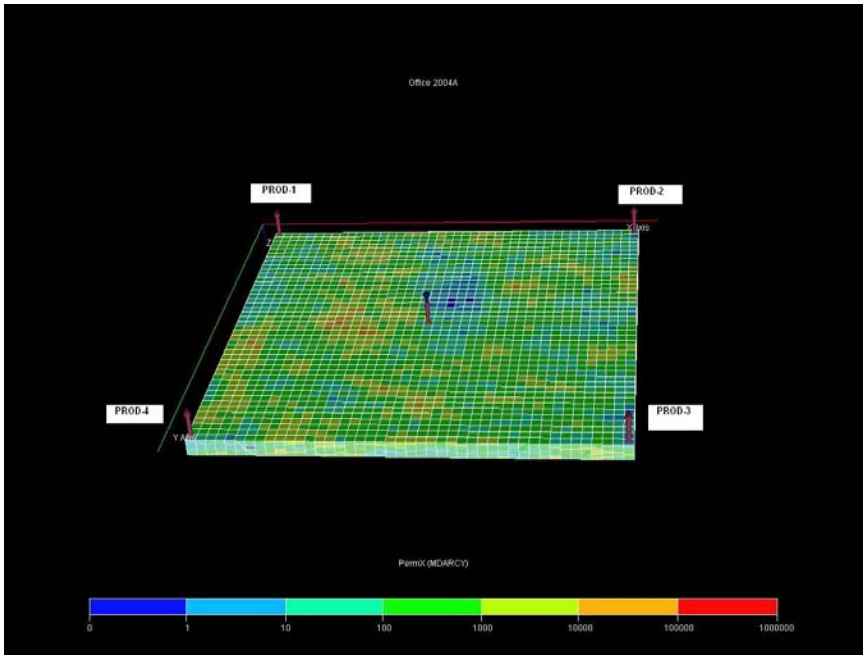

Figure 1- The permeability distribution

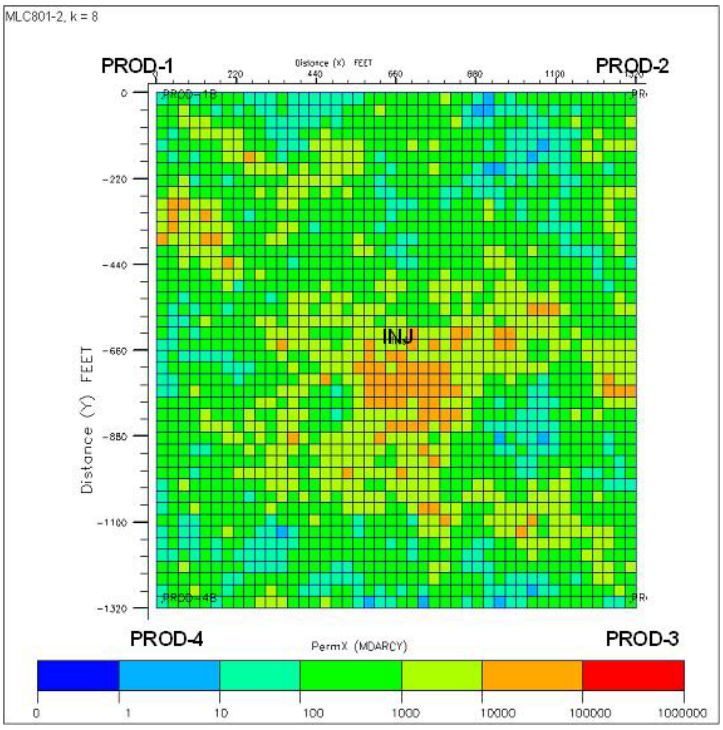

Figure 2- Logarithmic permeability distribution in layer 8 (most permeable layer)

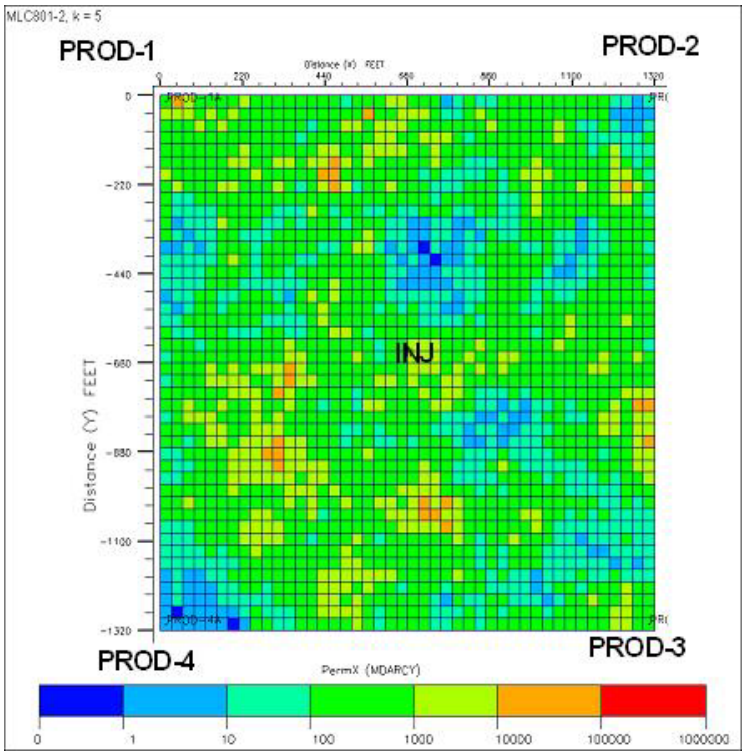

Figure 3- Logarithmic permeability distribution in layer 5 (least permeable layer)

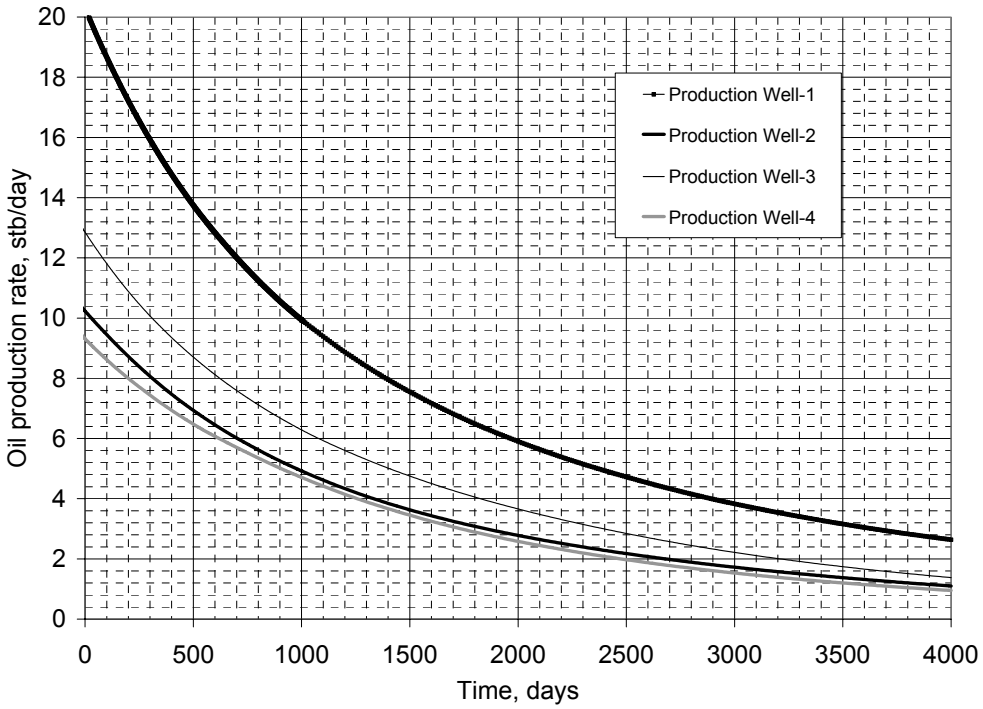

Figure 4- Oil Production rate

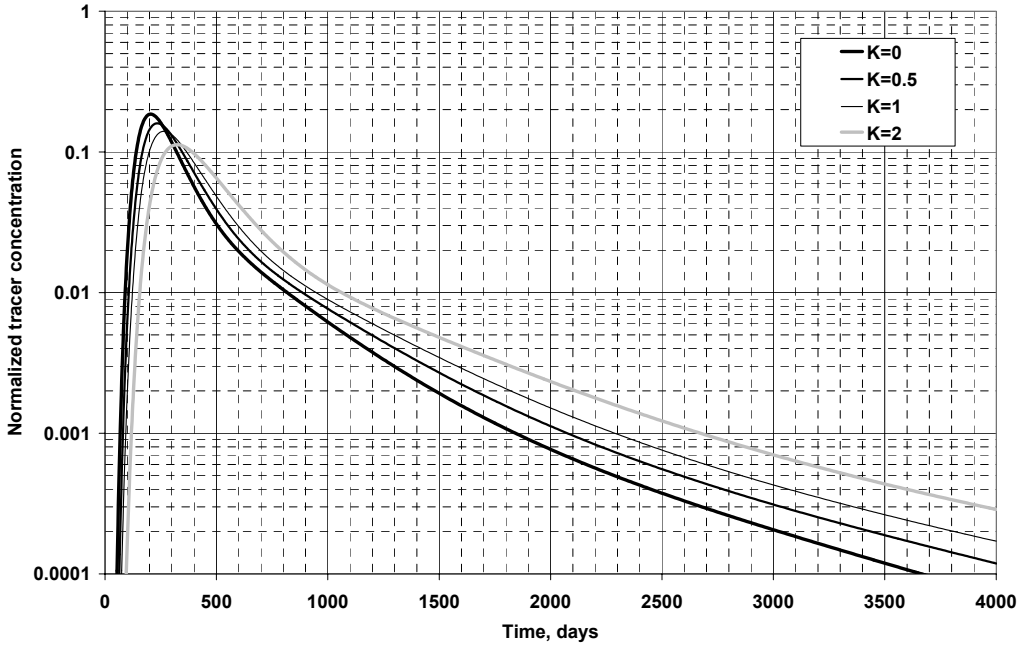

Figure 5- Normalized tracer concentration at production well 1

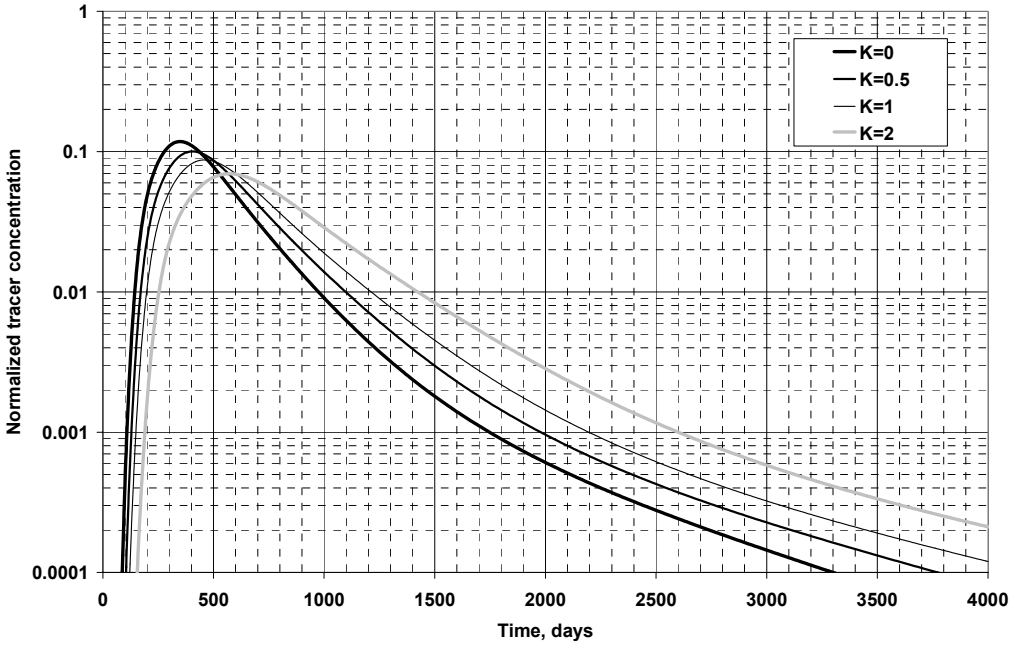

Figure 6- Normalized tracer concentration at production well 2

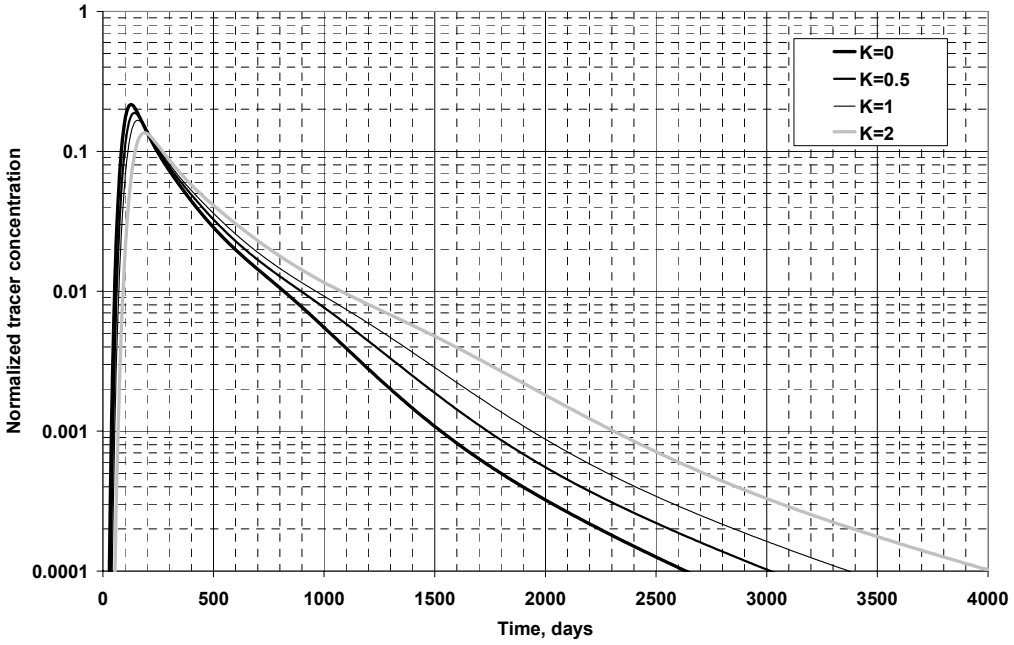

Figure 7- Normalized tracer concentration at production well 3

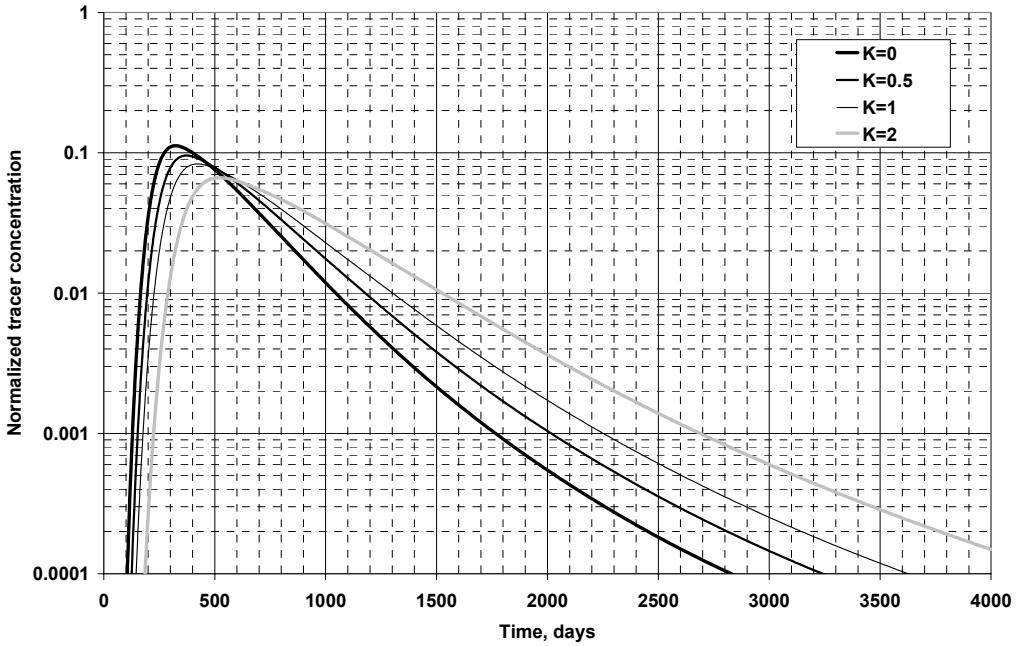

Figure 8- Normalized tracer concentration at production well 4

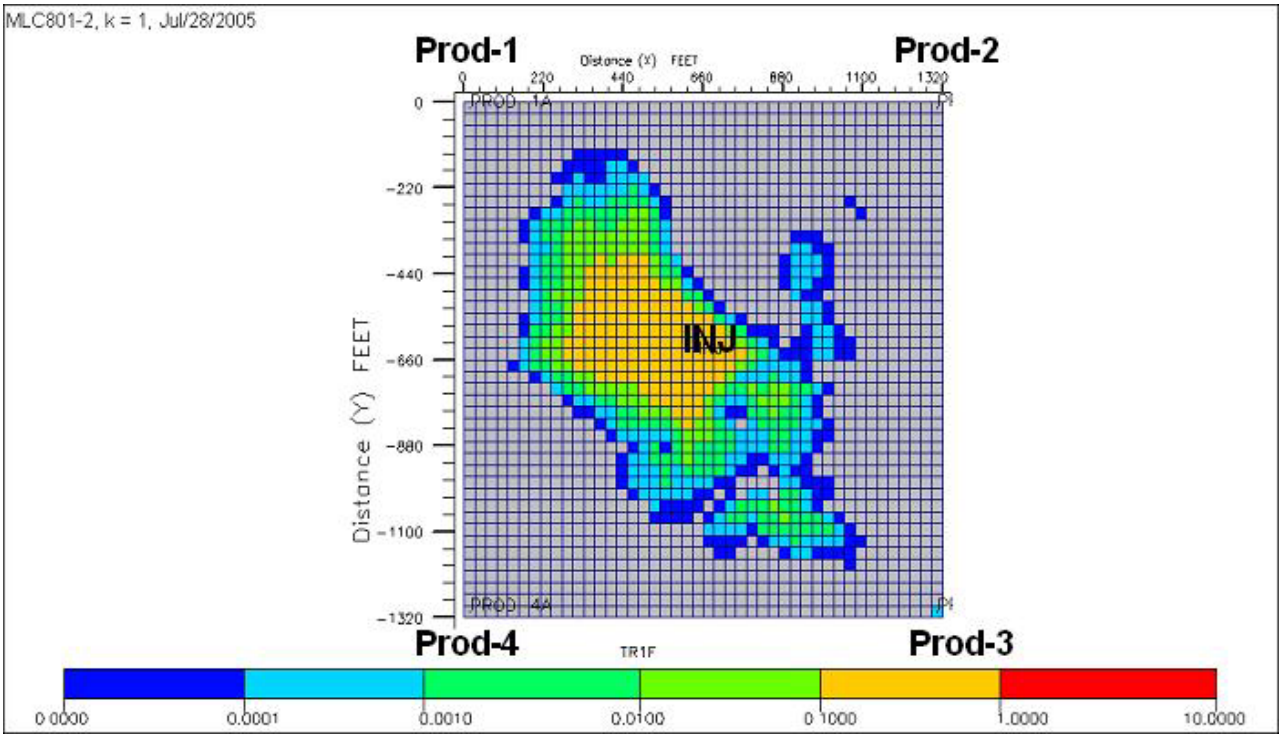

Figure 9- Conservative tracer concentration profile (logarithmic scale) in layer 1 after 35 days of tracer injection

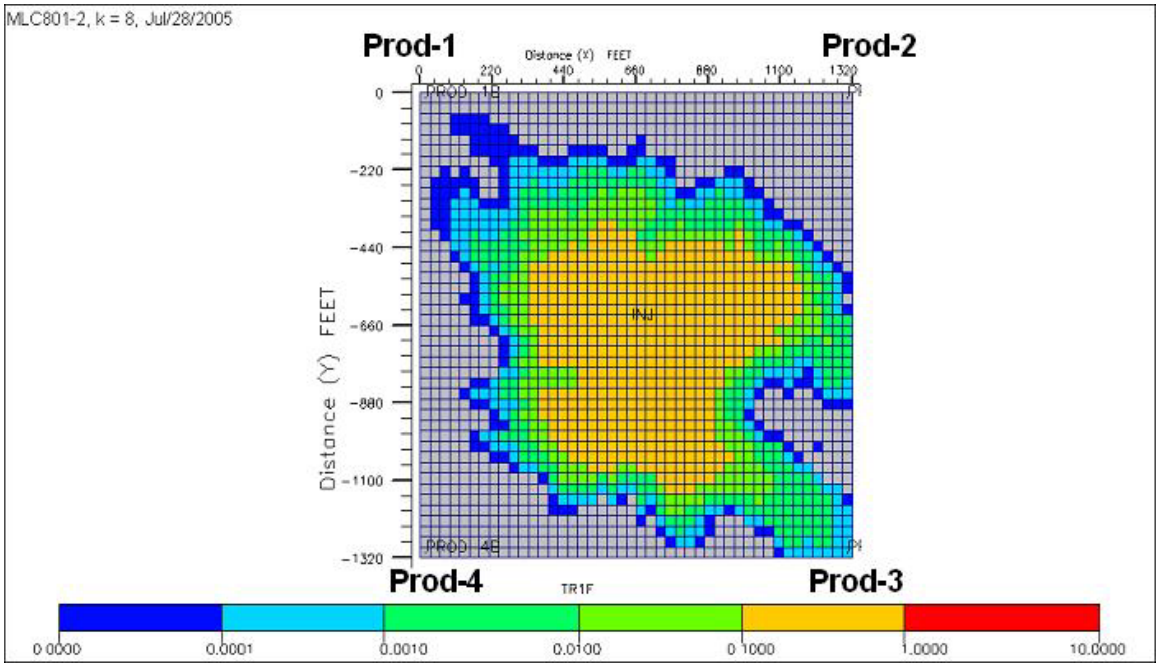

Figure 19- Conservative tracer concentration profile (logarithmic scale) in layer 8 after 35 days of tracer injection

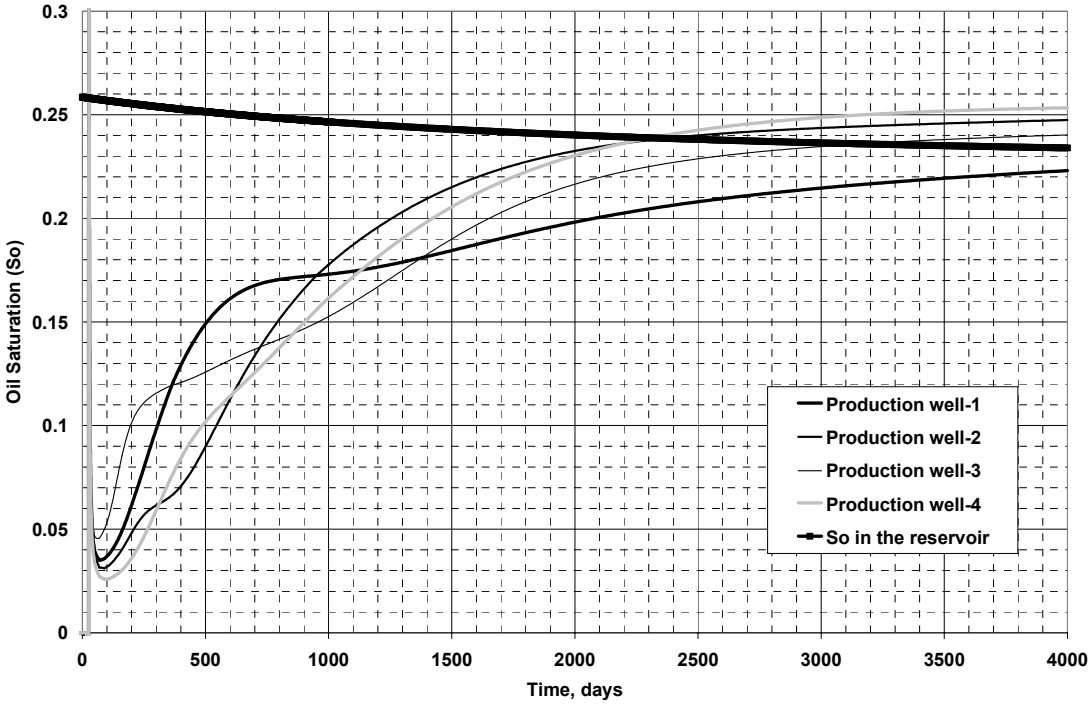

Figure 20- Oil Saturation Calculated from the Method of Moments

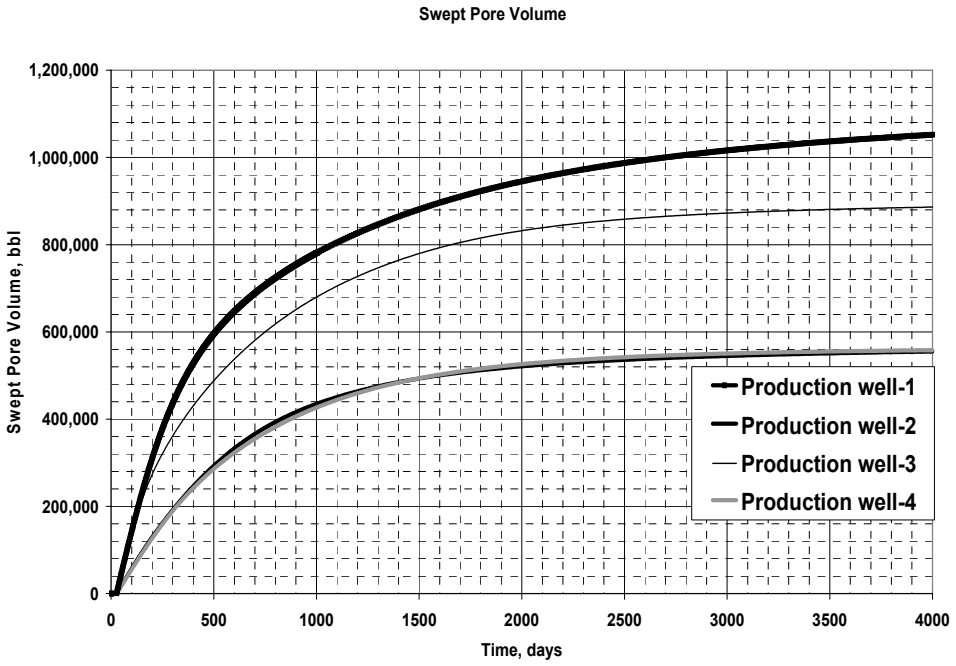

Figure 21- Swept pore volume between the injector and the each production well.

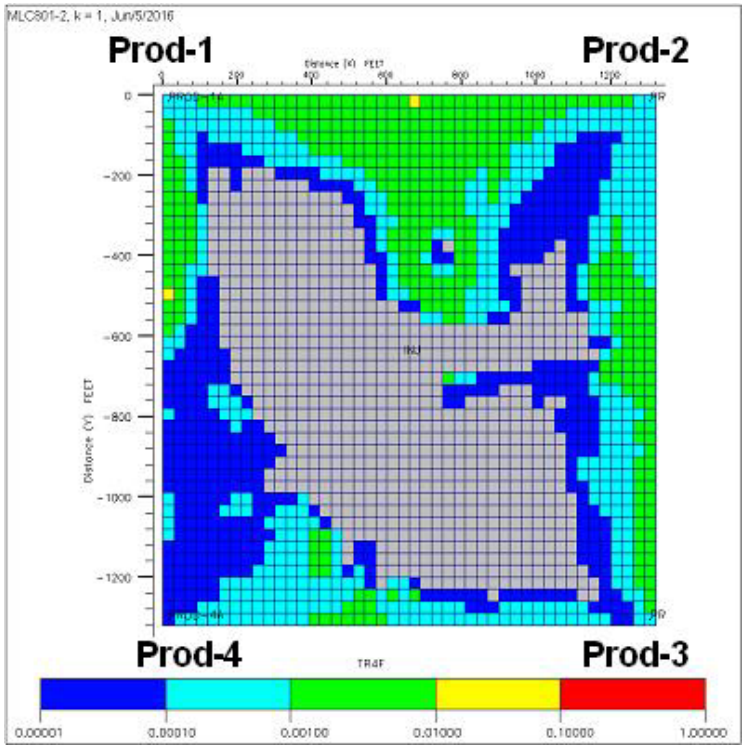

Figure 22- Tracer concentration profile (Partition coefficient=2) in layer 1 at the end of the simulation

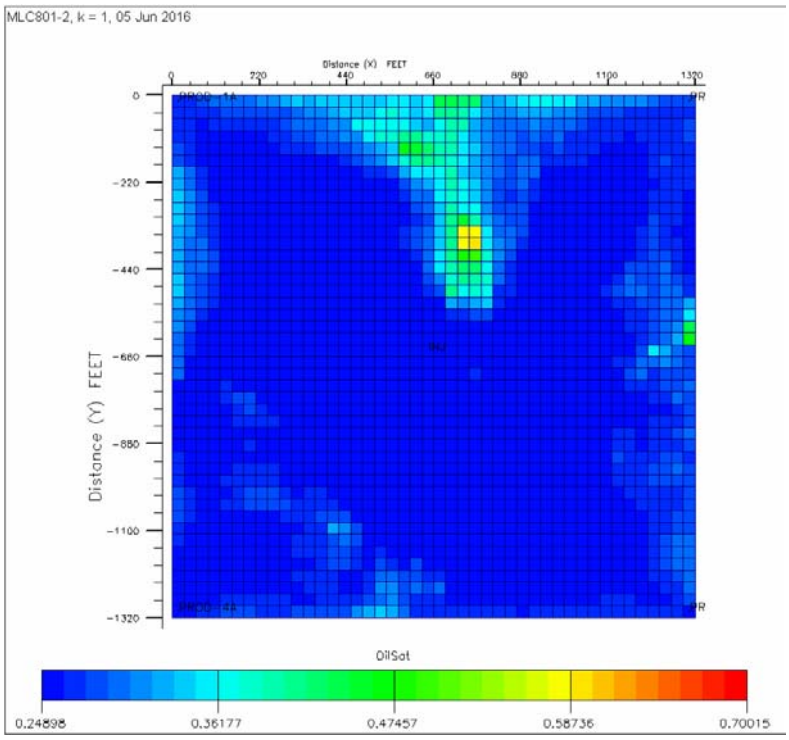

Figure 23- Oil saturation distribution in layer 1 at the end of the simulation

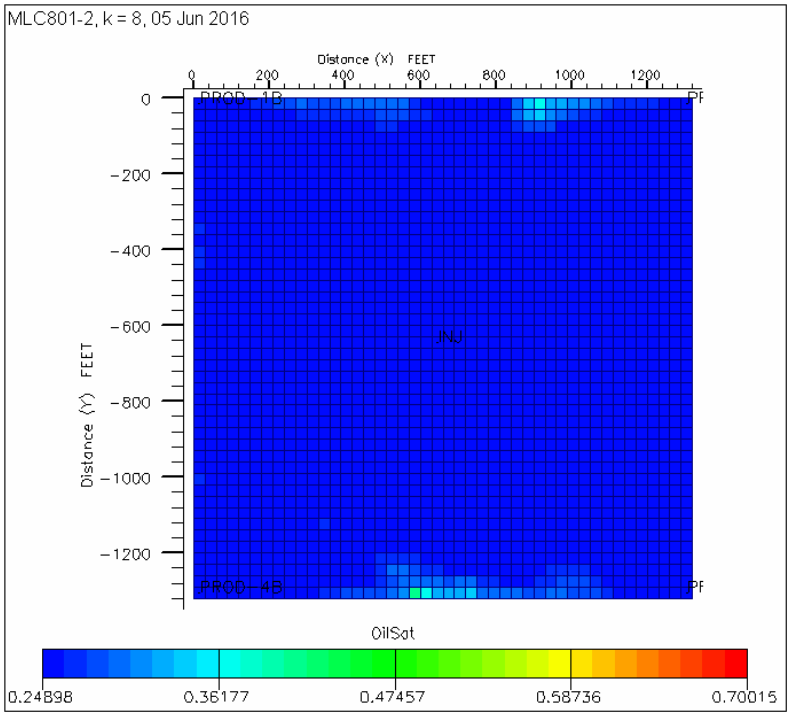

Figure 24- Oil saturation distribution in layer 8 at the end of the simulation

In this example INVO2-run5, all parameters were kept the same as the previous run except the Dykstra-Parsons coefficient was increased to 0.90 to see how this would affect the PITT results. Figures 1 and 2 show the permeability distribution of the most and the least permeable layers. The reservoir was water flooded for 2000 days (99% water cut) before the PITT. A slug with four tracers was injected for 50 days (0.1 PV). The oil saturation distribution at the beginning of the PITT is shown in Figures 3 and 4. Tracer production concentration curves are shown from Figures 5 to 8. Figures 9 and 10 show the tracer concentration profiles for layers 1 and 8 for the tracer with a partition coefficient of 2. Table 1 compares the oil saturations for each swept pore volume. The results are still good even though the reservoir is much more heterogeneous than the first case. Table 2 shows the swept pore volumes and sweep efficiency at the end of the PITT.

Table 1. Comparison of Oil Saturations for Case INV02-run5

So at the end of the tracer inj.	*Well-1*	*Well-2*	*Well-3*	*Well-4*
MOM results	0.230	0.240	0.240	0.237
So of the reservoir in each quadrant	0.254	0.253	0.253	0.255
Difference	-0.024	-0.013	-0.014	-0.018
Difference %	-2.4%	-1.3%	-1.4%	-1.8%
Sor in the reservoir calculated from ECLIPSE production data	0.235			

Table 2. Swept pore volume

	Well-1	*Well-2*	*Well-3*	*Well-4*
Vswept, bbl	589,444	818,921	888,288	735,376
Total Vswept, bbl	3,032,029			
Vswept/Vreservoir	0.190	0.264	0.286	0.237
VsweptTotal	0.977			

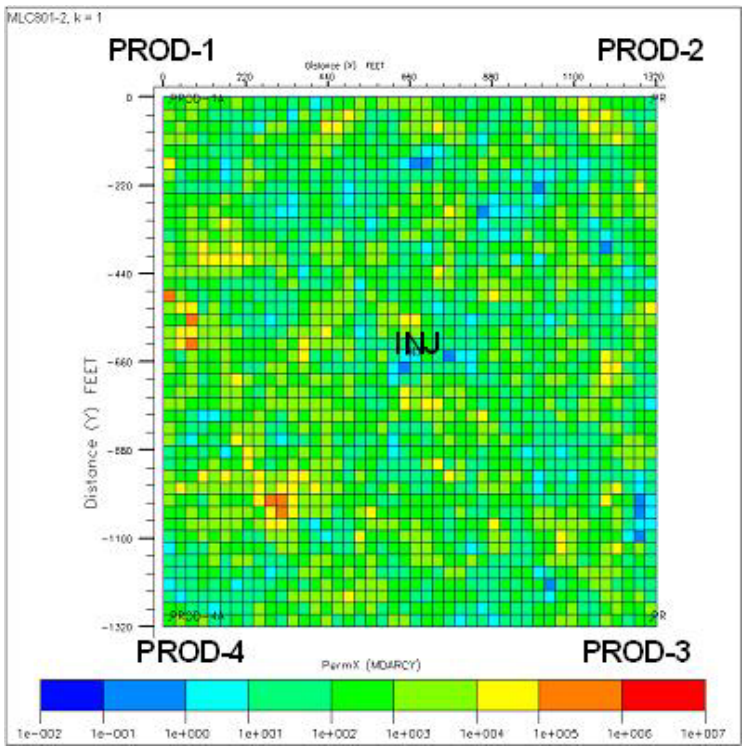

Figure1- Permeability in the least permeable layer 1

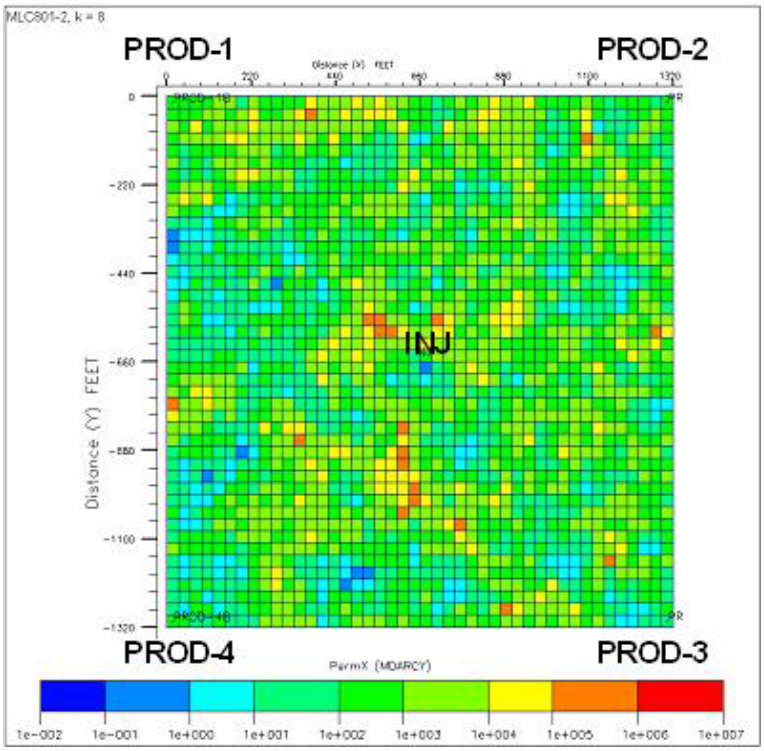

Figure 2- Permeability in the most permeable layer 8

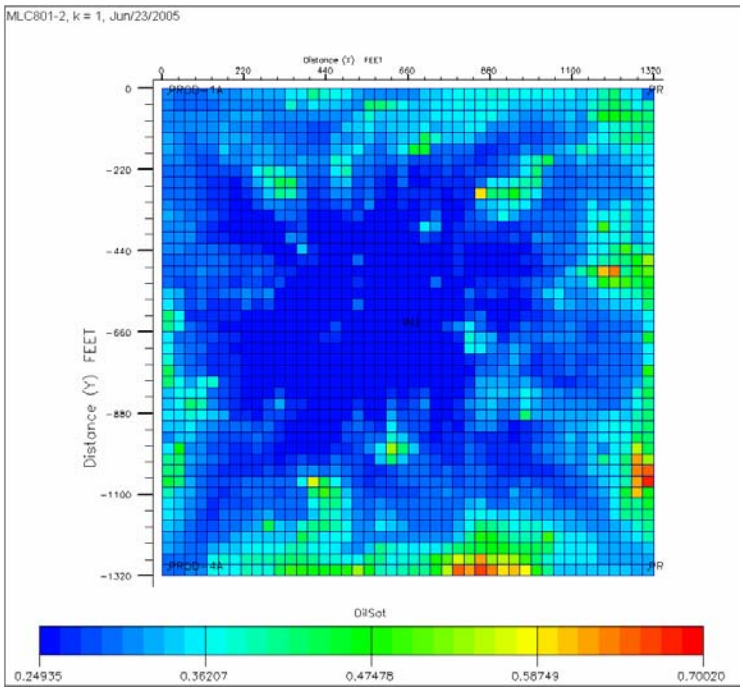

Figure 3- Oil saturation distribution in layer 1 at the beginning of the tracer injection

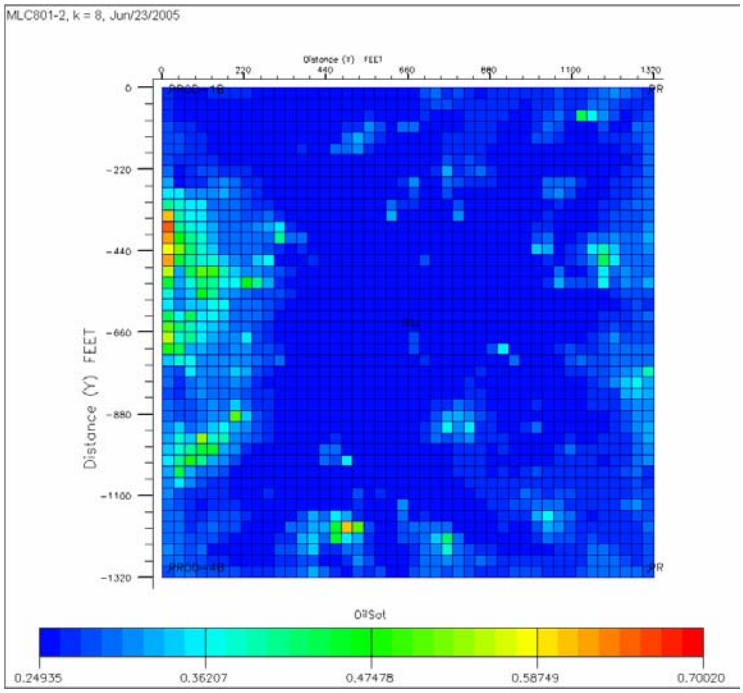

Figure 4- Oil saturation distribution in layer 8 at the beginning of the tracer injection

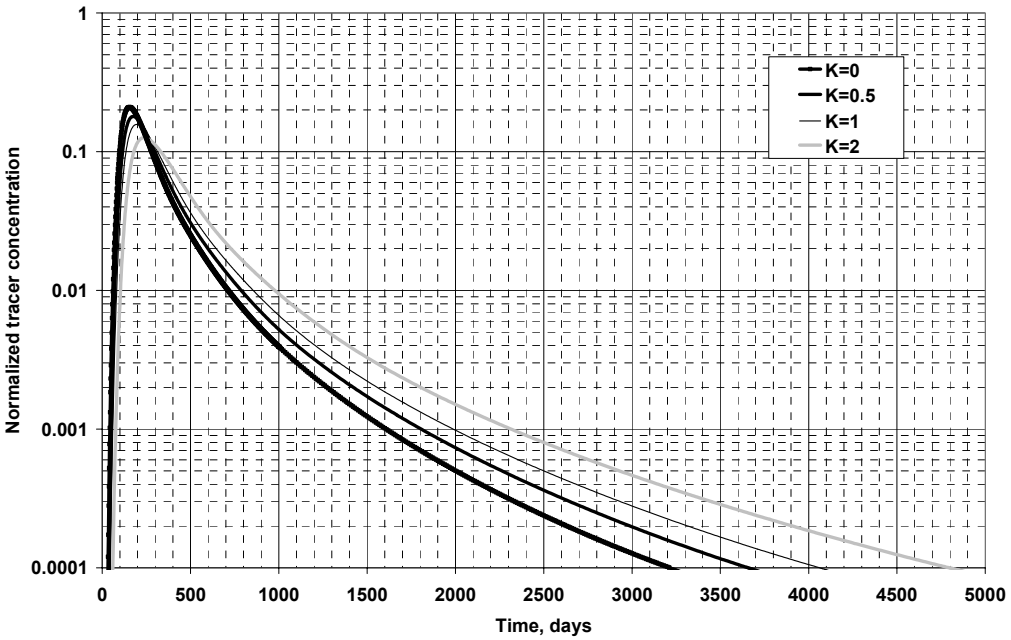

Figure 5- Normalized tracer concentration at production well 1

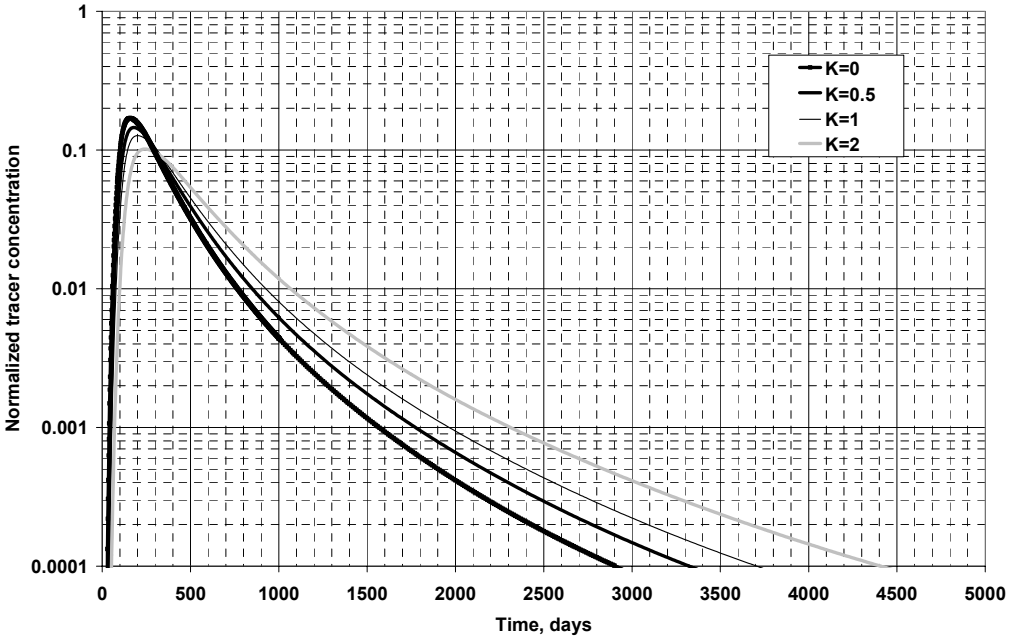

Figure 6- Normalized tracer concentration at production well 2

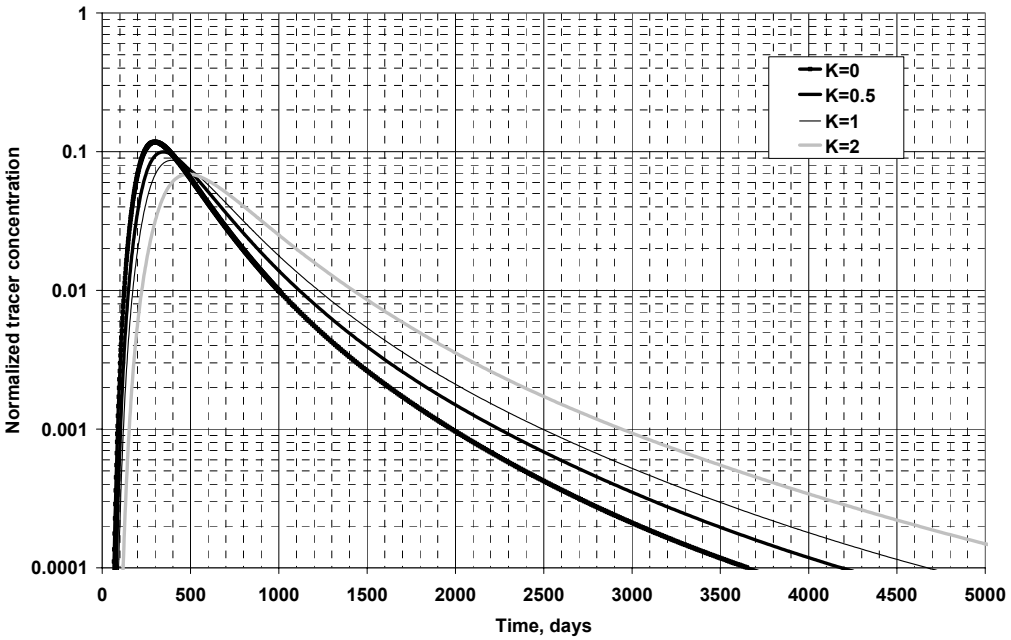

Figure 7- Normalized tracer concentration at production well 3

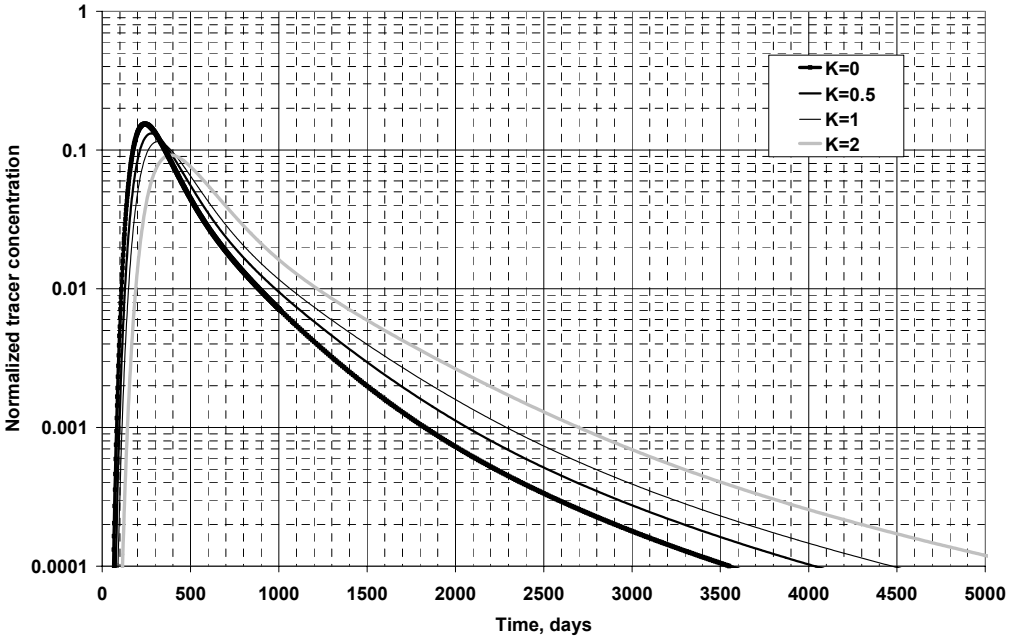

Figure 8- Normalized tracer concentration at production well 4

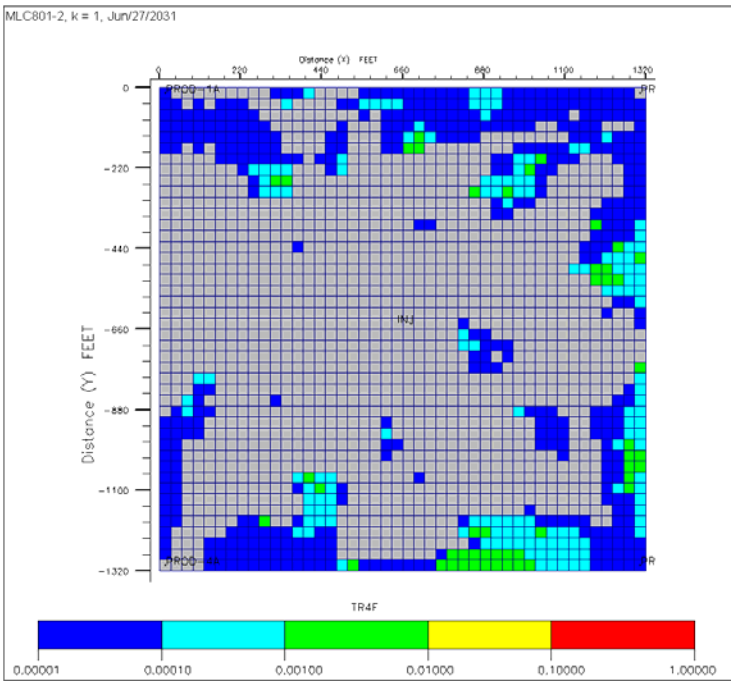

Figure 9- Tracer concentration profile in layer 1 at the end of the PITT

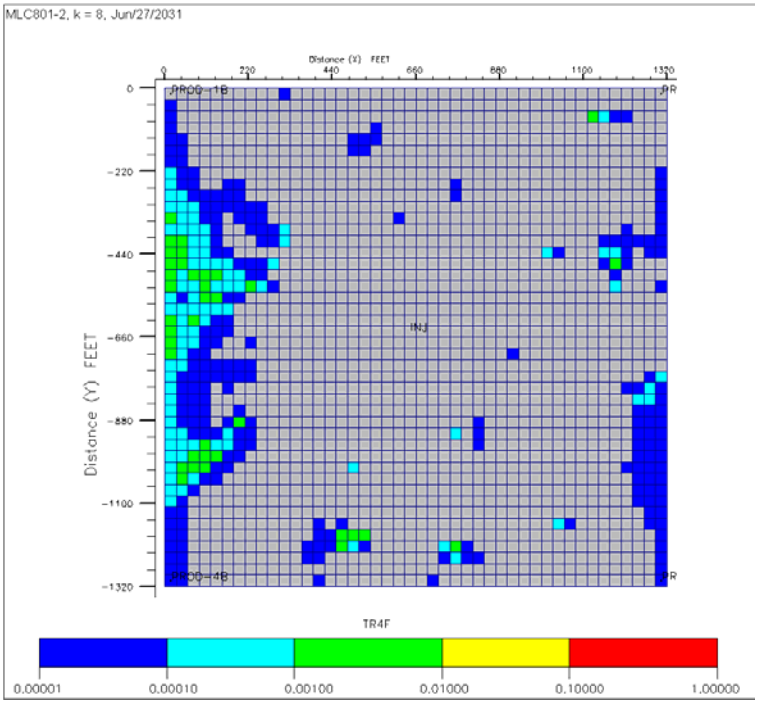

Figure 10- Tracer concentration profile in layer 8 at the end of the PITT

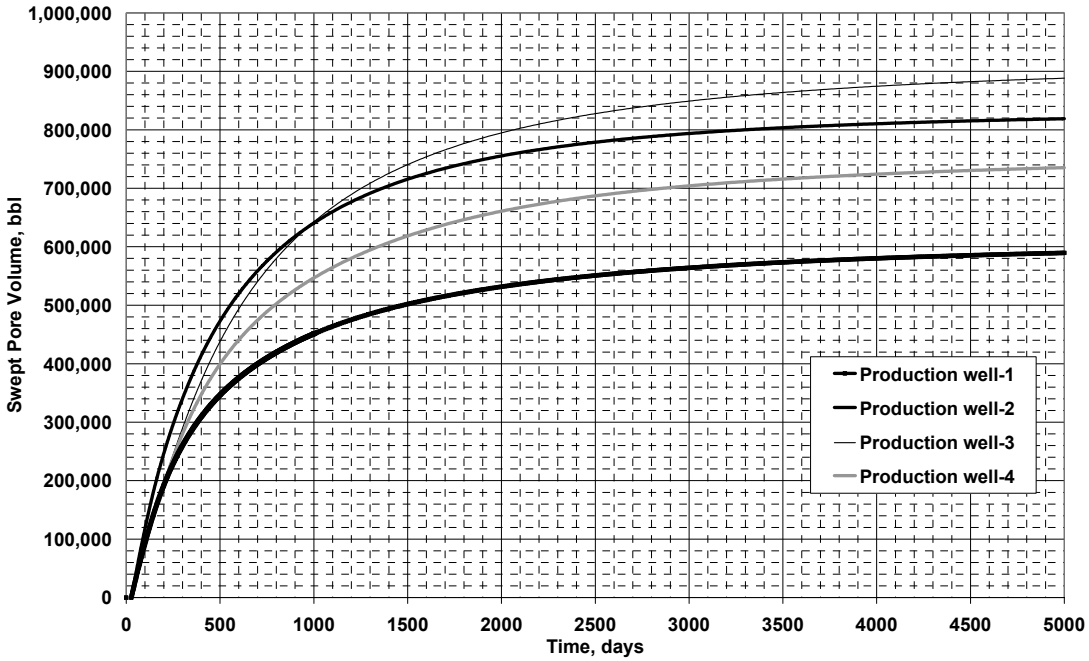

Figure 11- Swept pore volume between the injector and the each production well.

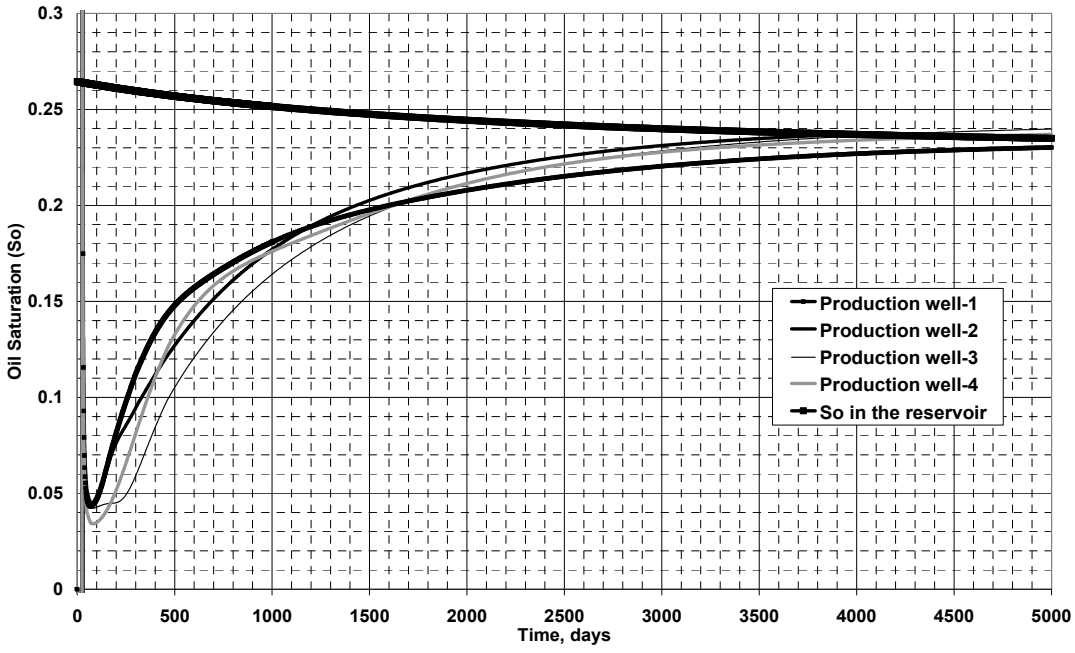

Figure 12- Oil Saturation calculated from the method of moments

In this example INVO2-run7, an unconfined, inverted 20 acre five-spot well pattern was simulated with the same reservoir parameters used in the confined 5-spot well pattern with a Dystra-Parsons coefficient of 0.81. The reservoir was water flooded for 1000 days (99% water cut) and then a tracer slug was injected for 50 days (0.1 PV). Total simulation time was 6000 days. Figures 1 and 2 show the oil saturation in the least and most permeable layers (layers 5 and 8) at the beginning of the tracer injection. Figures 3 and 4 show the conservative tracer concentration in those 2 layers at 50 days. Figures 5 and 6 show the conservative tracer concentration at 6000 days.

Figures 7 to 10 show the tracer concentration history of the partition coefficient of 0, 0.5, 1, and 2 for 4 producers, respectively. Regarding to the tracer breakthrough time, only tracer with partition coefficient of 2 shows the difference from the conservative tracer. The separations in the tails are noticeable among tracers.

Figure 11 shows the swept pore volume and the ratio of volume swept in the reservoir. The swept pore volume is increased even after 5000 days because the tracers sweeping between the outer boundary and they haven't been produced yet. Figure 12 shows the sweep efficiency, combined for all of the producers. The oil saturations in each swept pore volume are shown in Figure 13 and Table 1. The largest error in the estimated oil saturation is for the swept pore volume between the injector and production well 2, which has a very low permeability region. Table 2 summarizes the swept pore volumes.

Table 1: Oil saturation

So at the end of the tracer inj.	*Well-1*	*Well-2*	*Well-3*	*Well-4*
MOM results	0.210	0.202	0.234	0.225
So of the reservoir in each quadrant	0.269	0.276	0.263	0.261
Difference	-0.059	-0.074	-0.028	-0.036
Difference %	-5.9%	-7.4%	-2.8%	-3.6%
Sor in the reservoir calculated from ECLIPSE production data	0.240			

Table 2: Swept pore volumes

	Well-1	*Well-2*	*Well-3*	*Well-4*
Vswept, bbl	780,465	663,622	736,652	674,832
Total Swept Pore Volume	2,855,570			
Vswept/Vreservoir	0.25	0.21	0.24	0.22
VsweptTotal/Vreservoir	0.92			

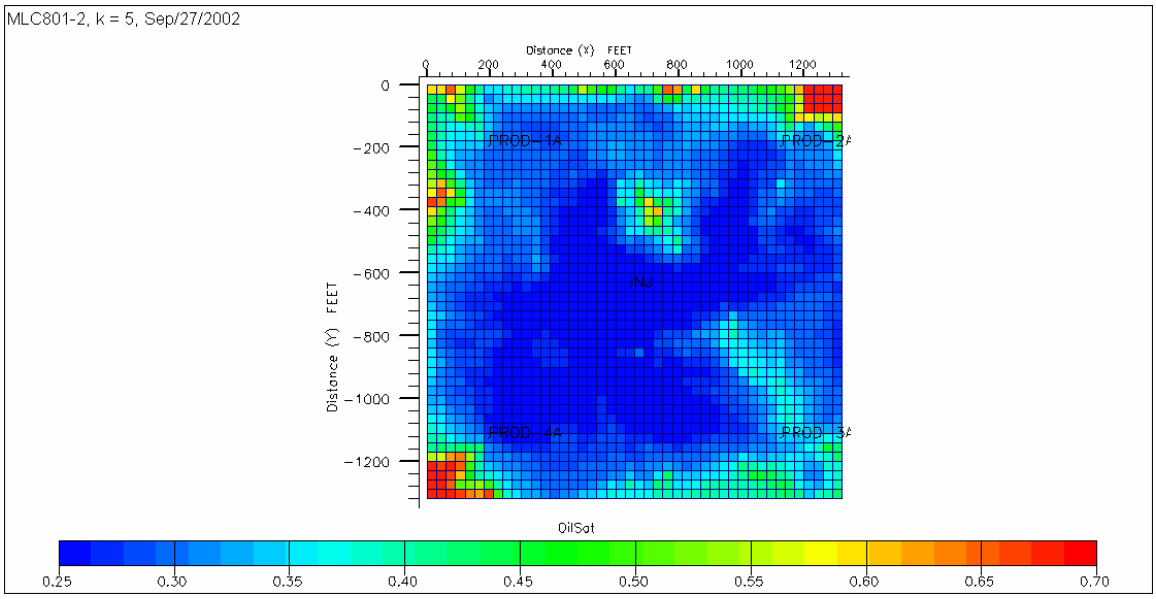

Figure 1- Oil saturation distribution at the start of tracer injection on Layer5 (least permeable layer)

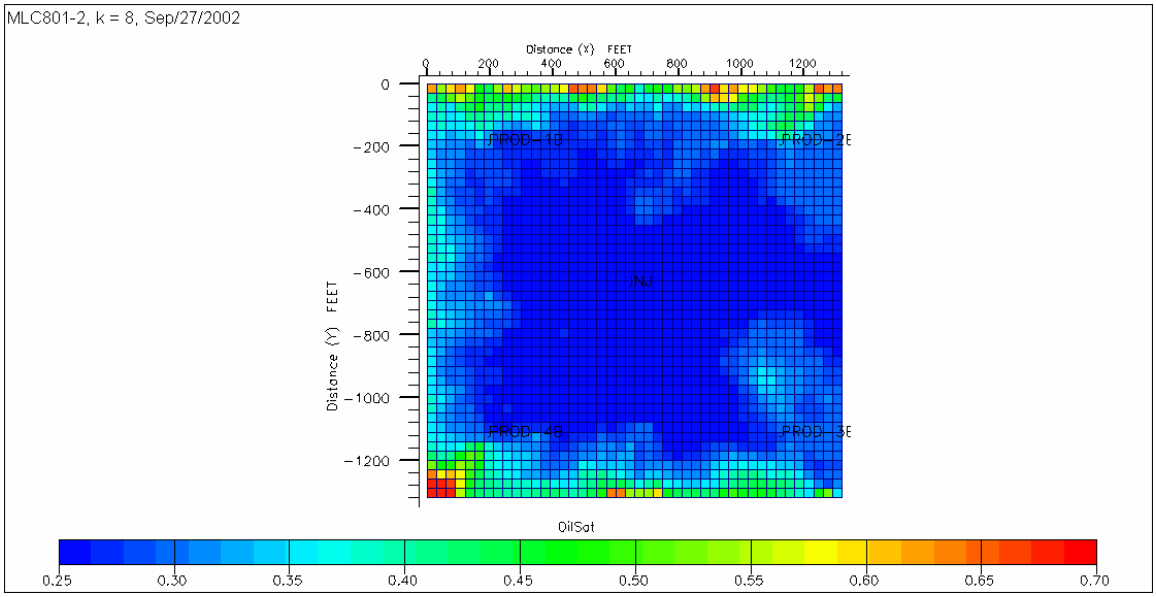

Figure 2- Oil saturation distribution at the start of tracer injection on Layer8 (most permeable layer)

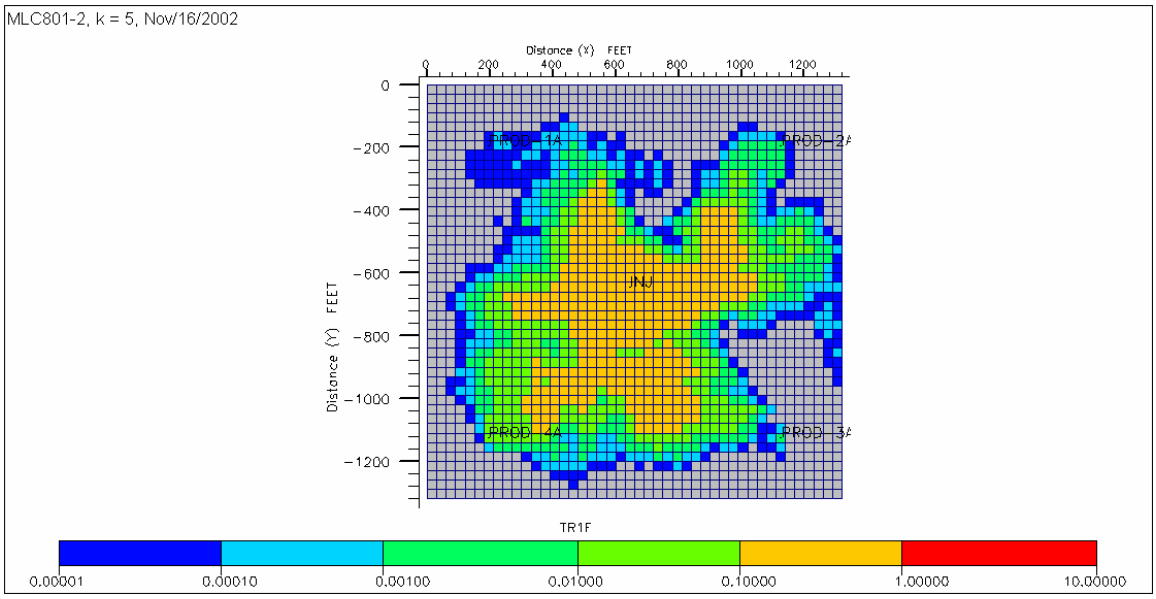

Figure 3- Conservative tracer concentration at 50 days in layer5 (least permeable layer)

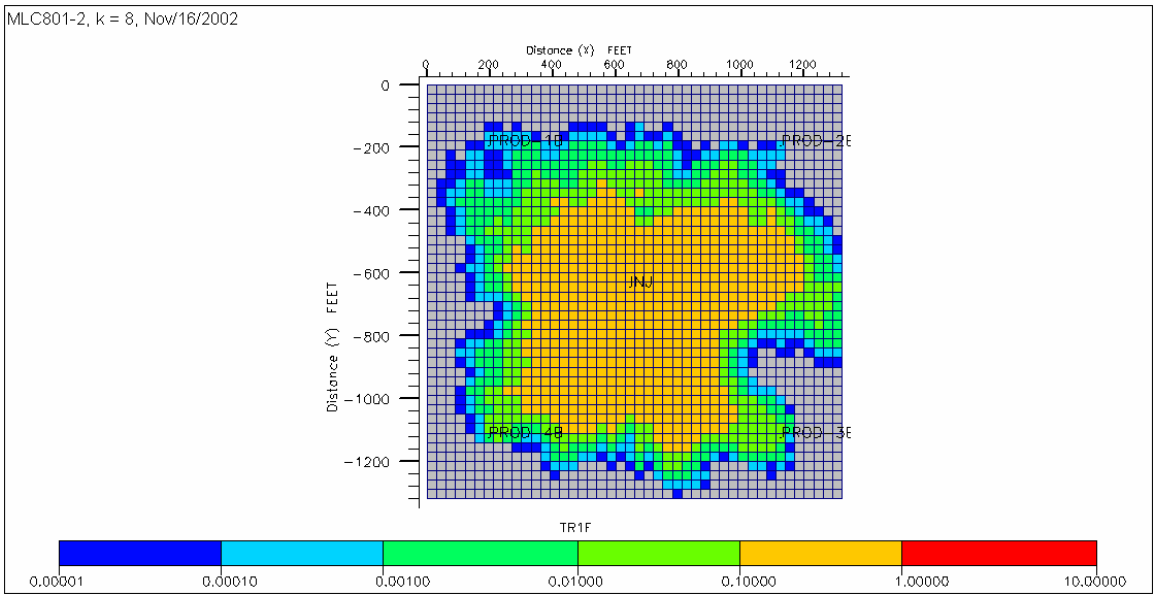

Figure 4- Conservative tracer concentration at 50 days in layer8 (most permeable layer)

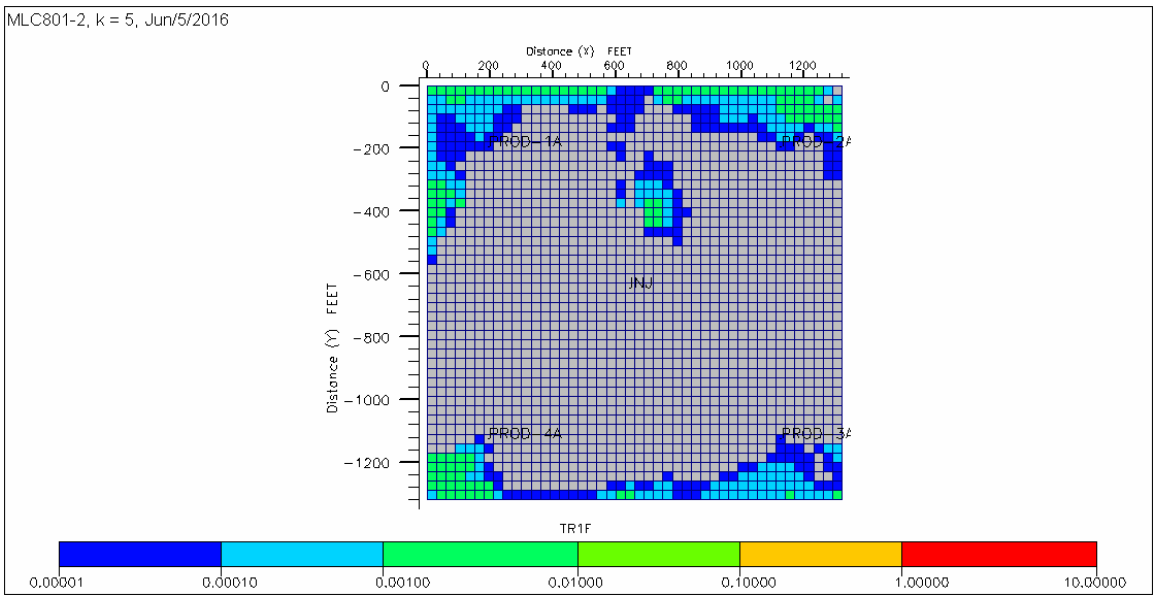

Figure 5- Conservative tracer concentration at 5000 days in layer 5 (least permeable layer)

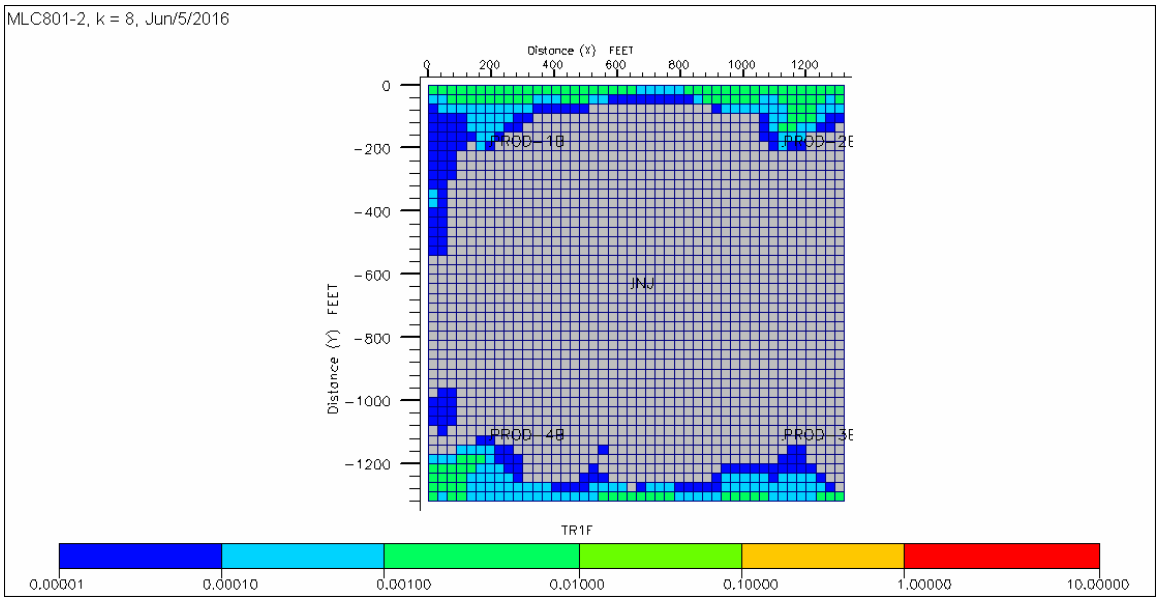

Figure 6- Conservative tracer concentration at 5000 days in layer8 (most permeable layer)

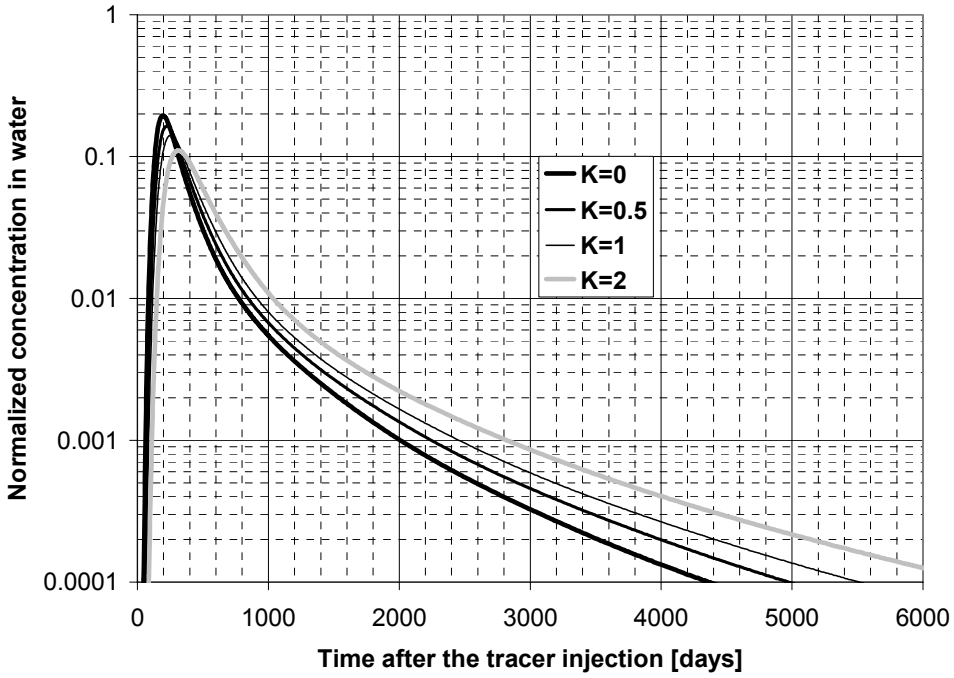

Figure 7- Tracer concentration history at Producer 1

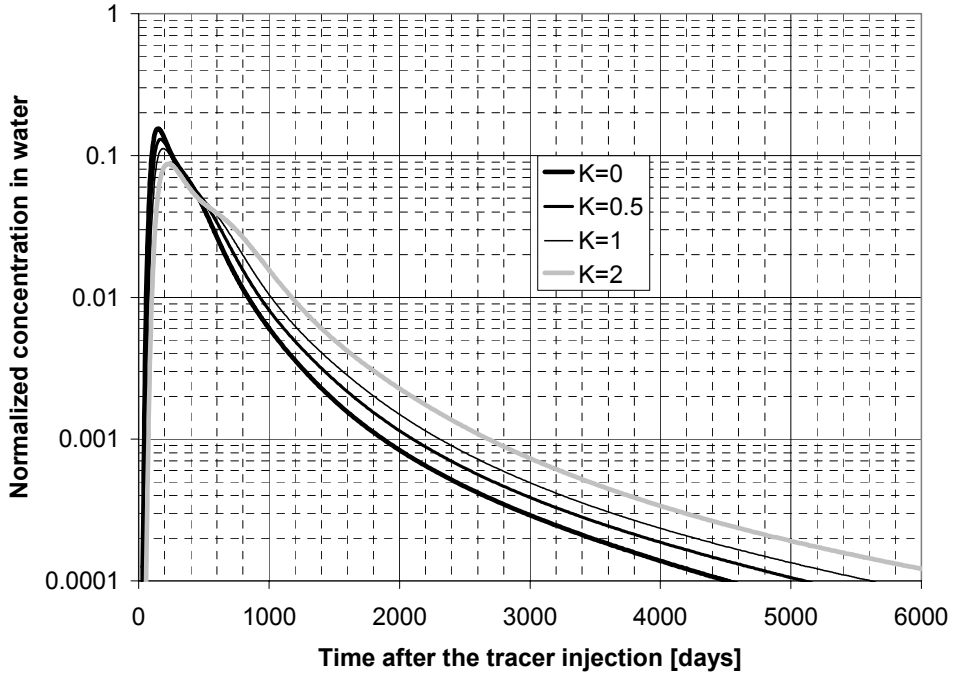

Figure 8- Tracer concentration history at Prod2

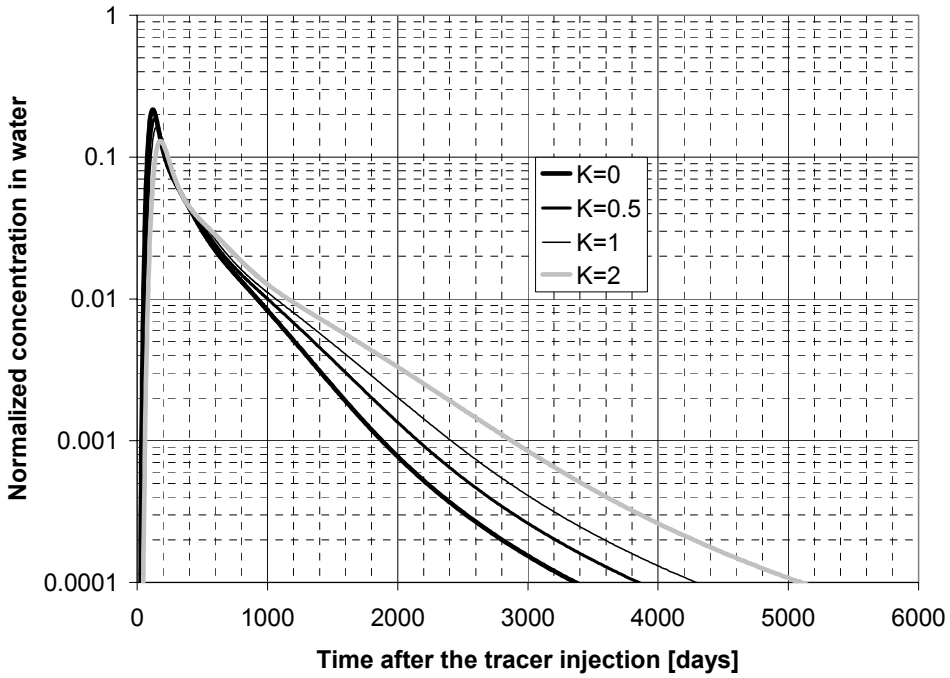

Figure 9- Tracer concentration history at Prod3

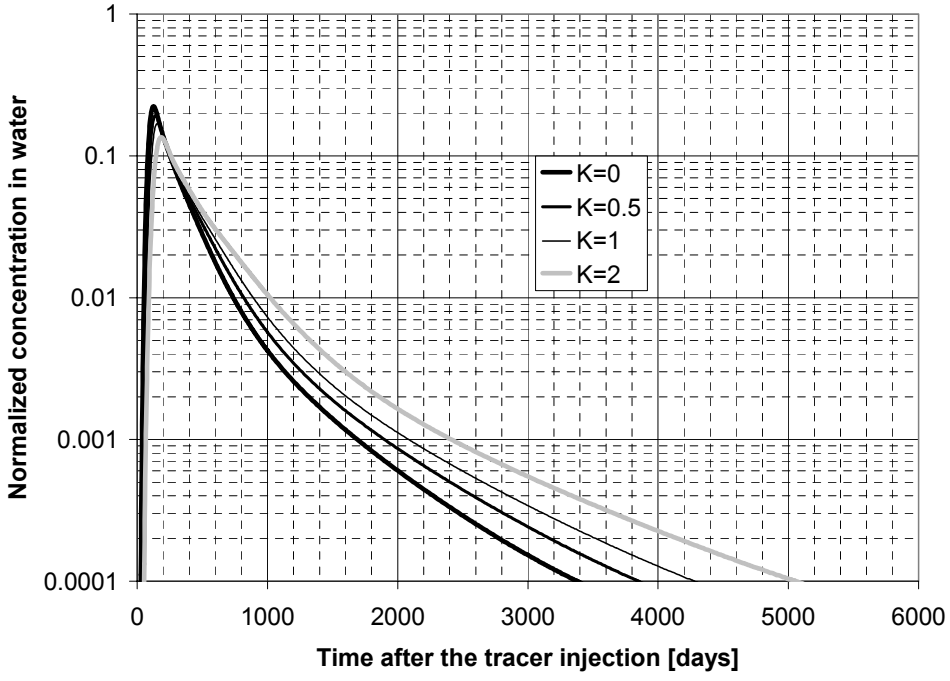

Figure 10- Tracer concentration history at Prod4

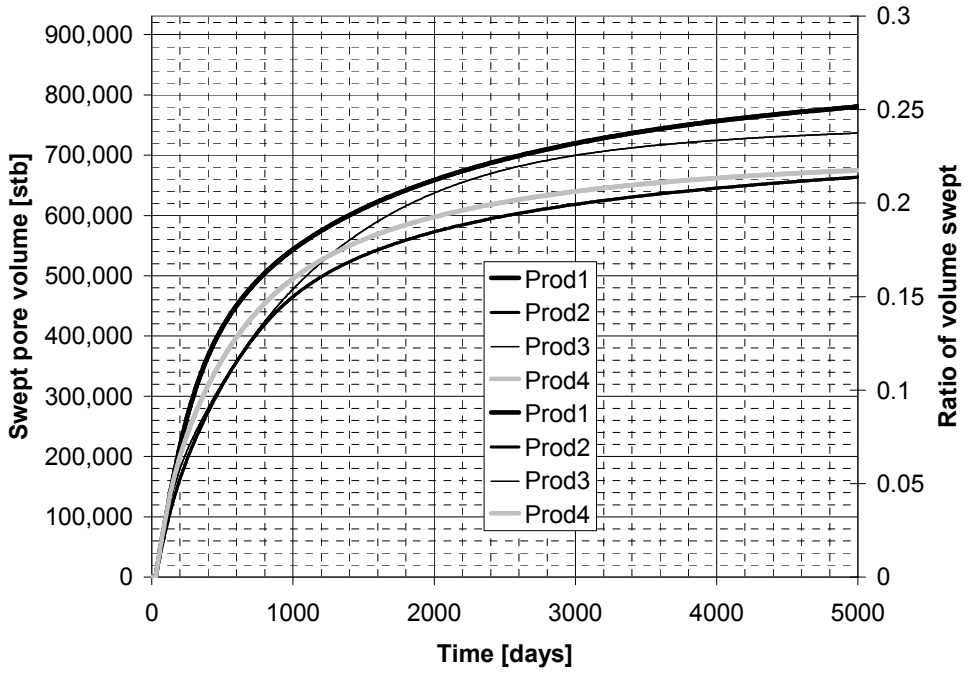

Figure 11- Swept pore volume and the ratio of volume swept

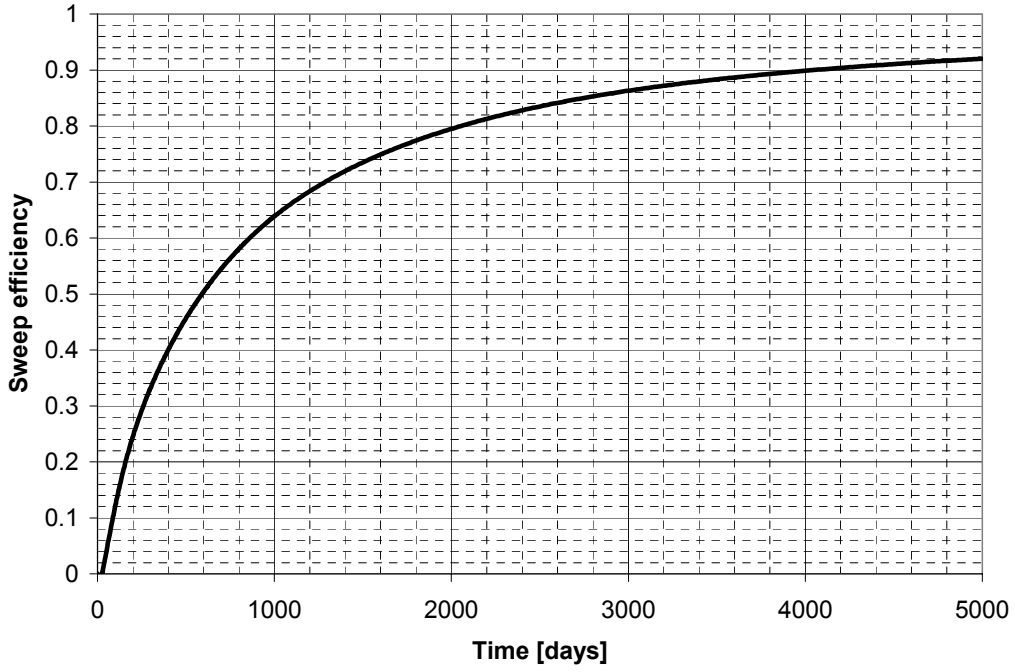

Figure 12- Sweep efficiency in the reservoir

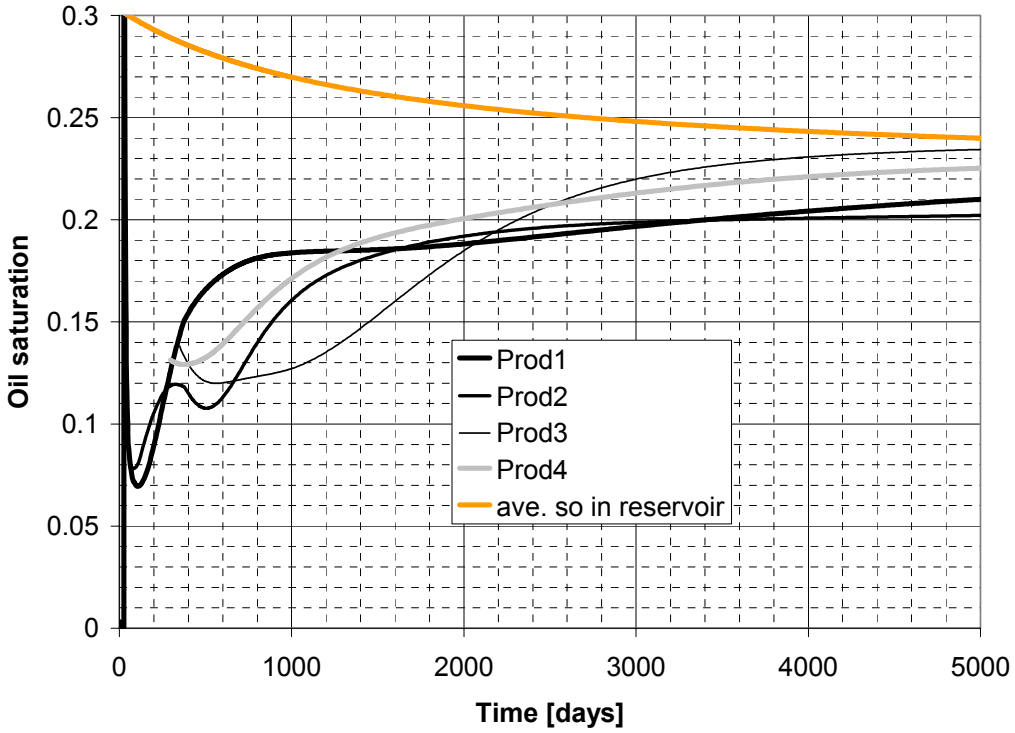

Figure 13- Oil saturation calculated from the method of moments

In this example INVO2-run8, tracer injection began after 250 days of water flooding (0.5 PV and 77% water cut). The purpose of this example was to test the method of moments for a case with more mobile oil to verify that the generalized method as derived in this report can be used to give a good approximation to the oil saturation even if it is far above residual oil saturation.

Figures 1 and 2 show the oil saturation in the reservoir at the beginning of the tracer flood. Figures 3 to 6 show the tracer concentrations for each production well. In Figures 4 to 6, early tracer breakthrough is observed. Figure 8 shows the tracer concentration in layer 5 after 25 days of tracer flooding and also shows the early breakthrough at production wells 2, 3 and 4. Figures 9 and 10 show the tracer concentration in layers 8 and 5 at the end of the simulation. Most of the tracer was recovered except past the four production wells.

Figures 11 and 12 show the swept pore volumes and the oil saturations calculated from the method of moments. Table 1 summarizes the oil saturation values. Table 2 shows the swept pore volumes. Although the tracer injection started at 77% water cut, mobile oil in the reservoir didn't increase the error in the estimated oil saturations compared to the previous example with the PITT starting at 99% water cut.

Table 1. Oil saturations INVO2-run8

So at the end of the simulation	*Well-1*	*Well-2*	*Well-3*	*Well-4*
MOM results for So	0.226	0.197	0.251	0.226
Average So of the reservoir in each quadrant	0.269	0.276	0.263	0.261
Difference	-0.044	-0.079	-0.012	-0.036
Difference %	-4.4%	-7.9%	-1.2%	-3.6%
Sor in the reservoir calculated from ECLIPSE production data	0.24			

Table 2. Swept pore volumes

	Well-1	*Well-2*	*Well-3*	*Well-4*
Vswept, bbl	781,780	659,269	727,266	671,643
Total Vswept, bbl	2,839,958			
Vswept/Vreservoir	0.252	0.212	0.234	0.216
VsweptTotal/Vreservoir	0.915			

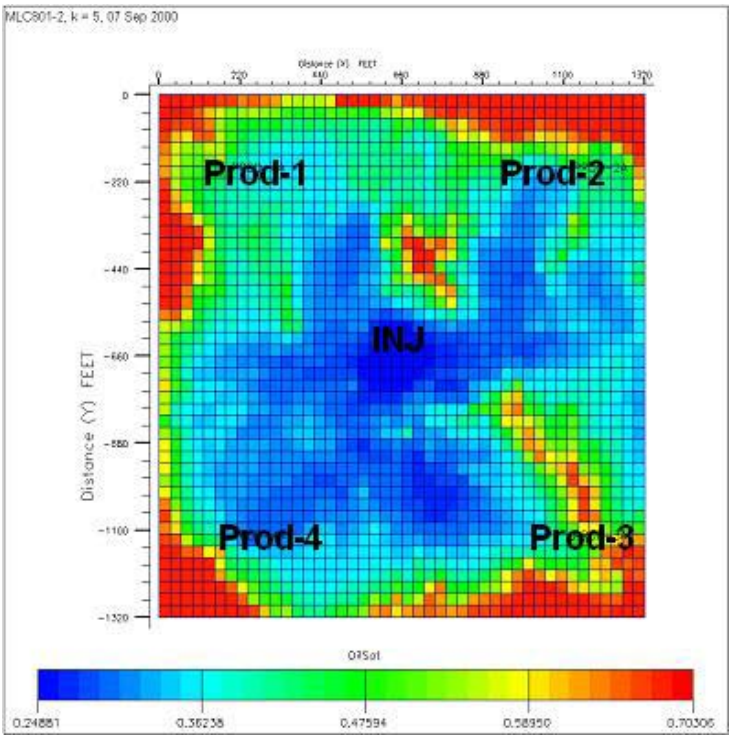

Figure 1- Oil saturation distribution in layer 5 at the beginning of the tracer injection

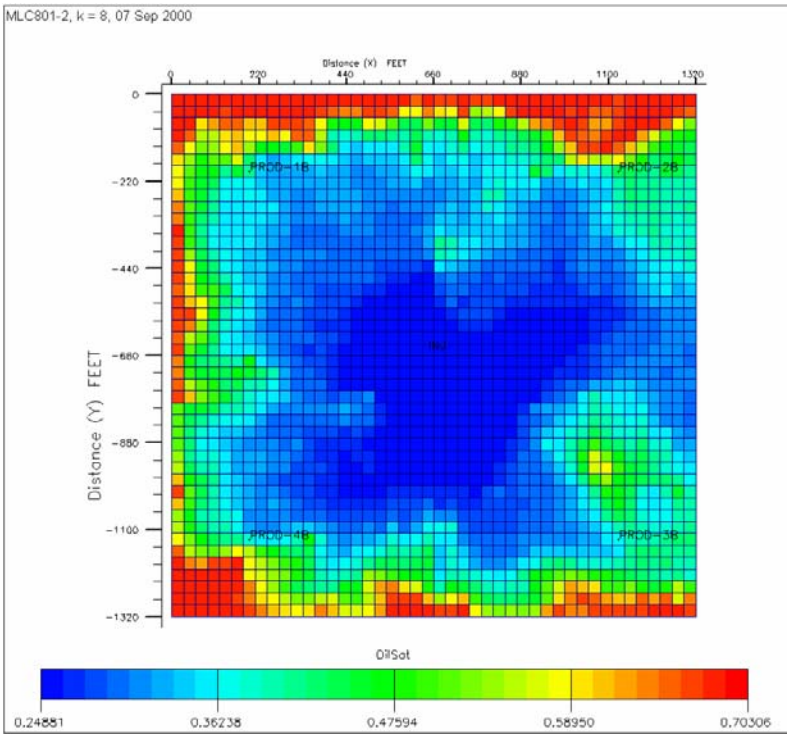

Figure 2- Oil saturation distribution in layer 8 at the beginning of the tracer injection

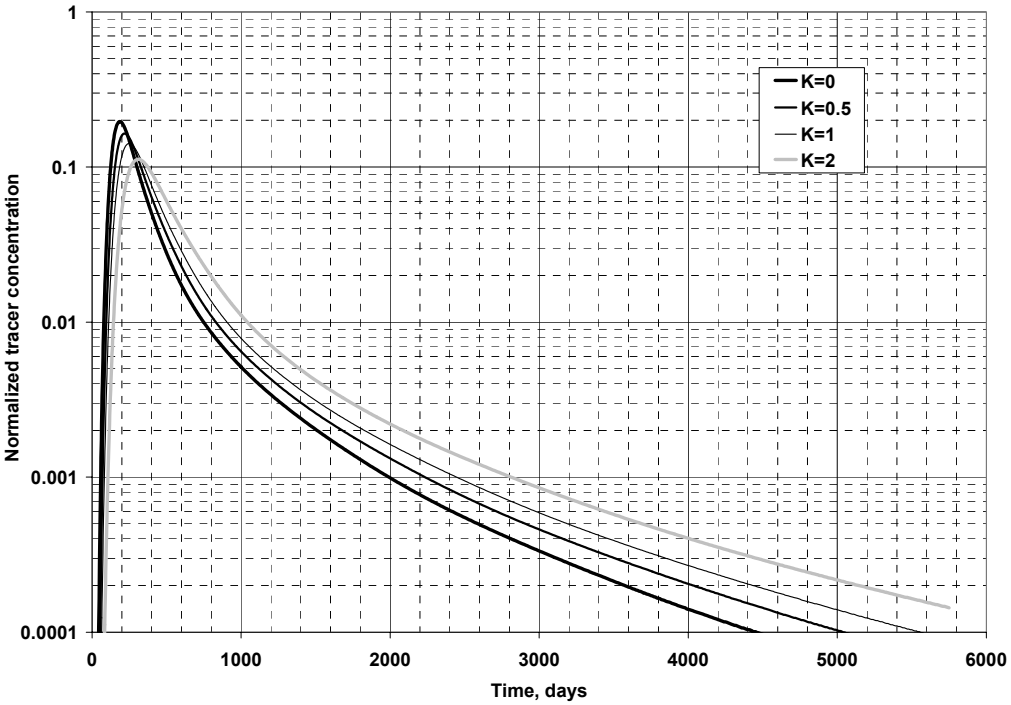

Figure 3- Normalized tracer concentration at production well 1

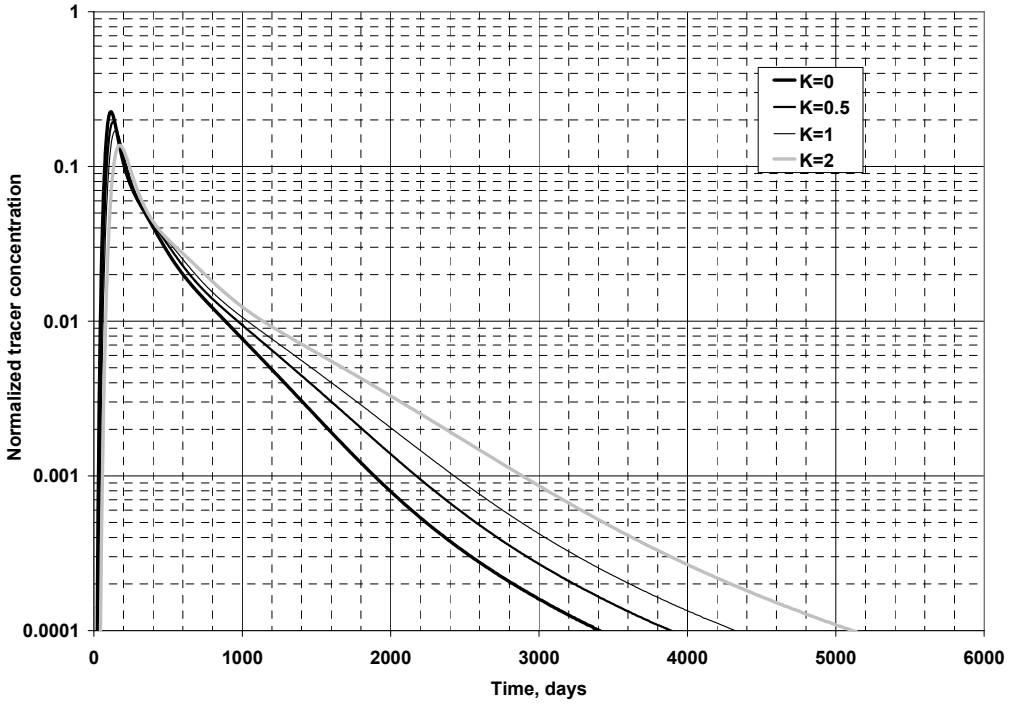

Figure 4- Normalized tracer concentration at production well 2

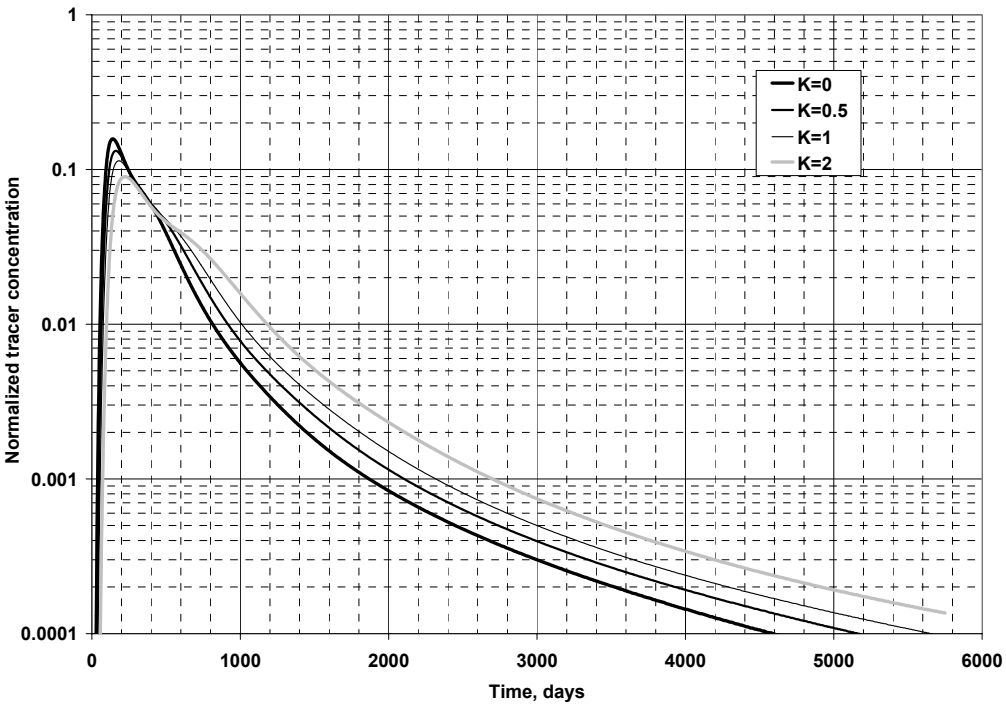

Figure 5- Normalized tracer concentration at production well 3

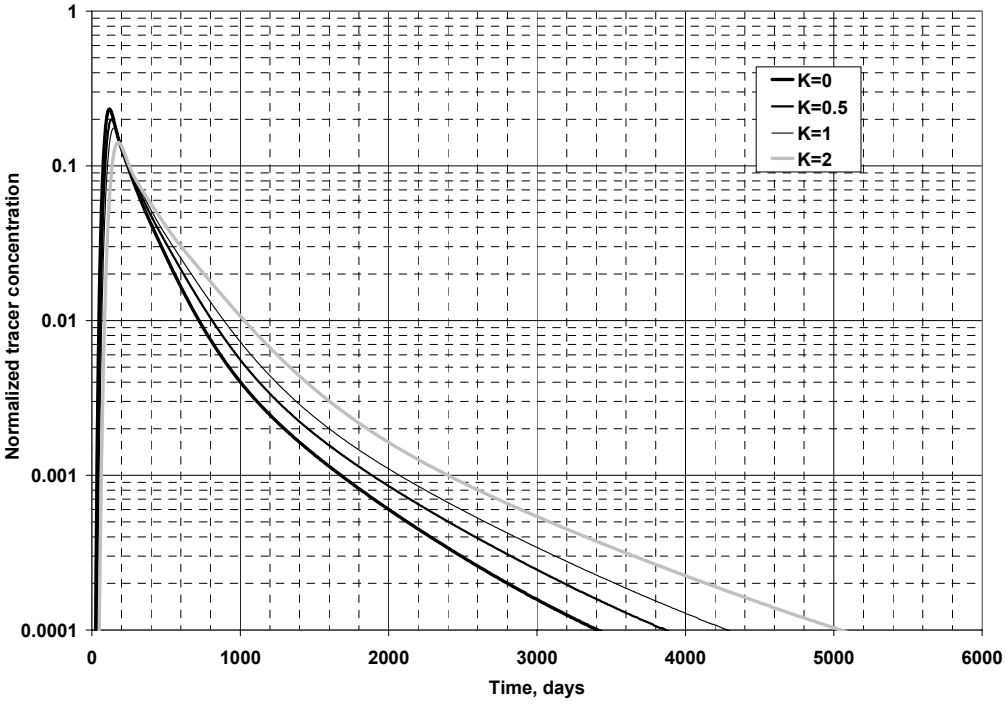

Figure 6- Normalized tracer concentration at production well 4

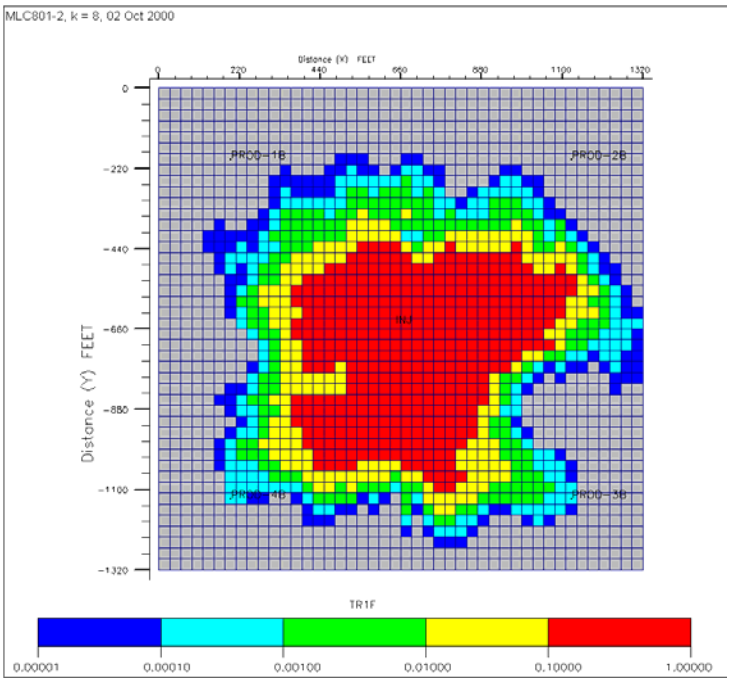

Figure 7- Tracer concentration (partition coefficient 2) profile in logarithmic scale after 25 days of tracer injection in layer 3

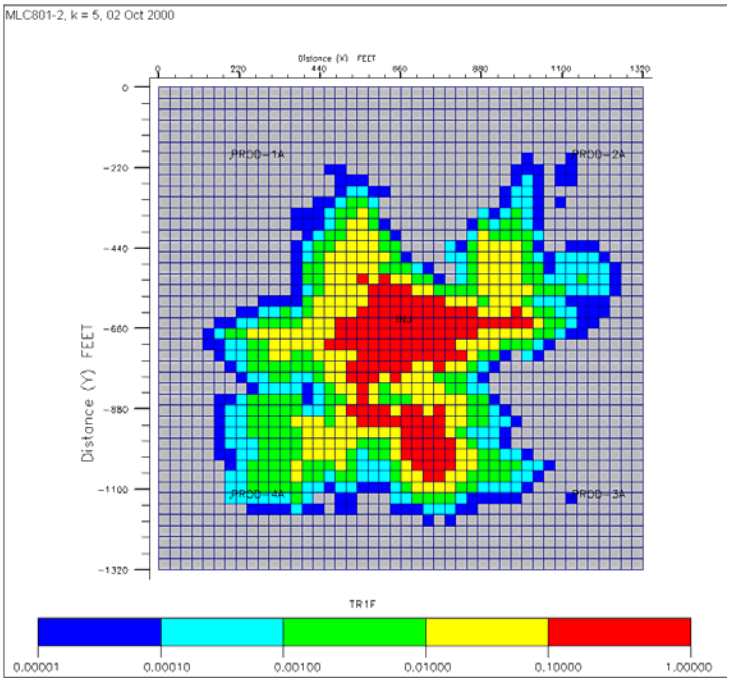

Figure 8- Tracer concentration profile (partition coefficient 2) in layer 5 after 25 days of tracer injection

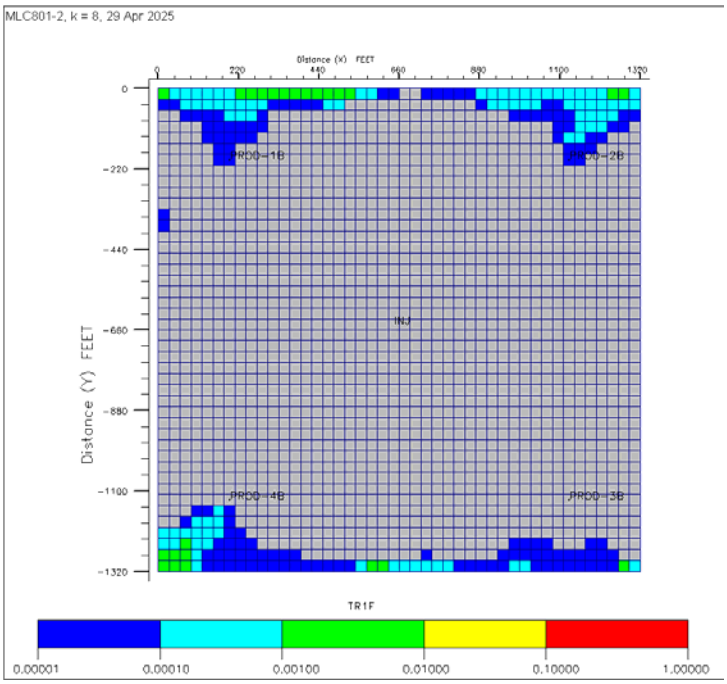

Figure 9- Tracer concentration profile (partition coefficient 2) in layer 8 at the end of the simulation

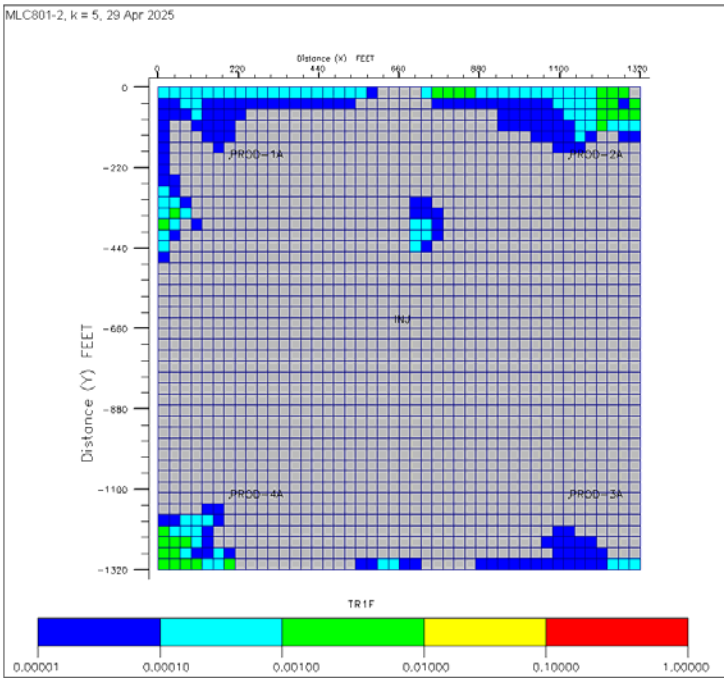

Figure 10- Tracer concentration profile (partition coefficient 2) in layer 5 at the end of the simulation

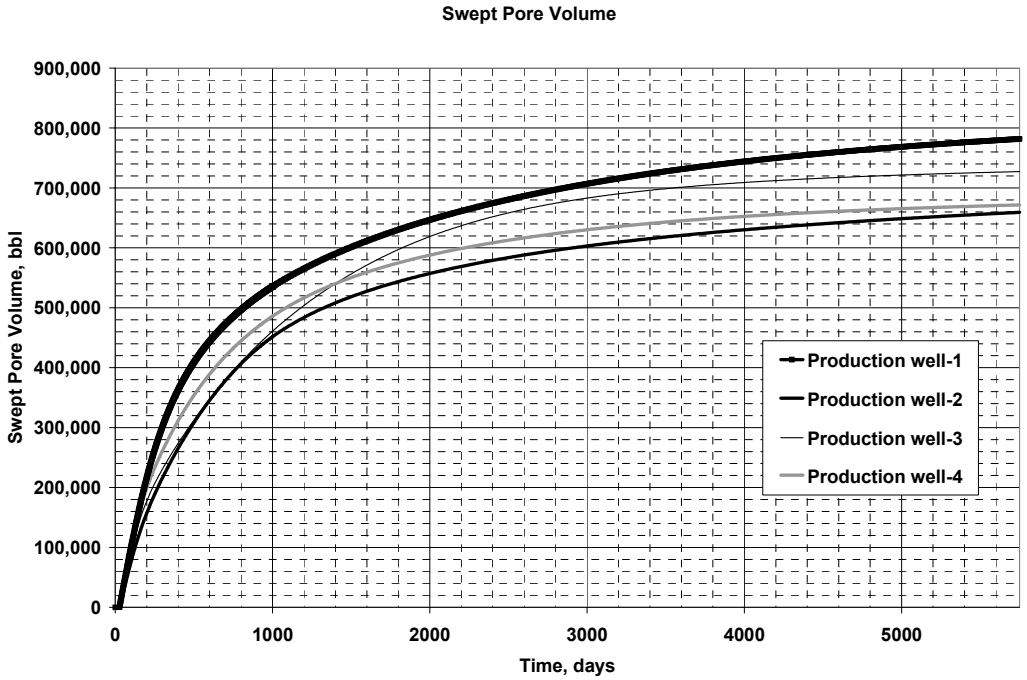

Figure 11- Swept pore volume between the injector and the each production well.

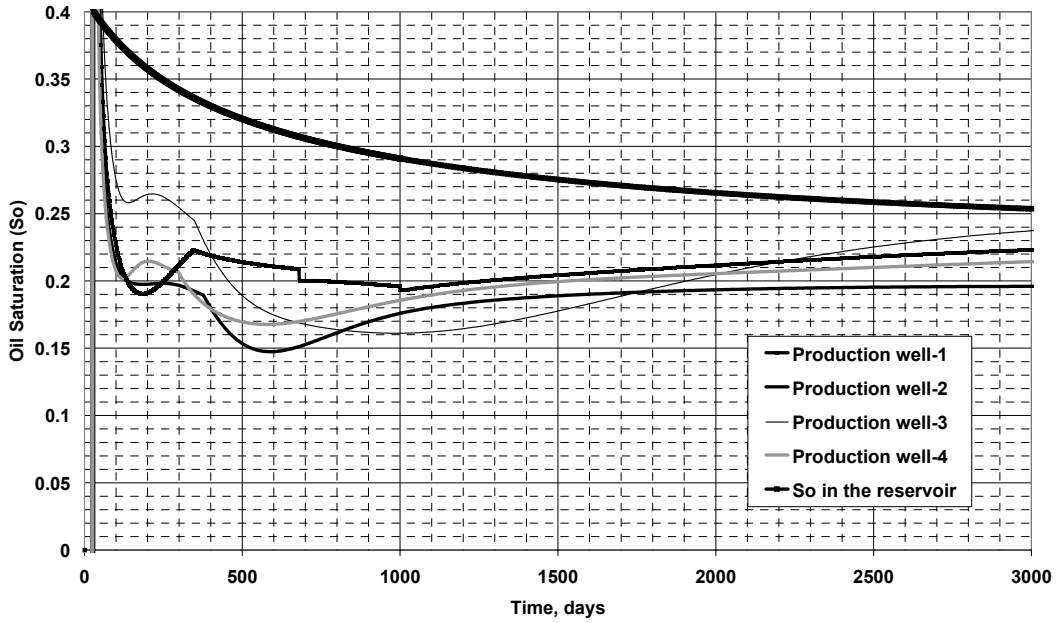

Figure 12- Oil saturation calculated from the method of moments

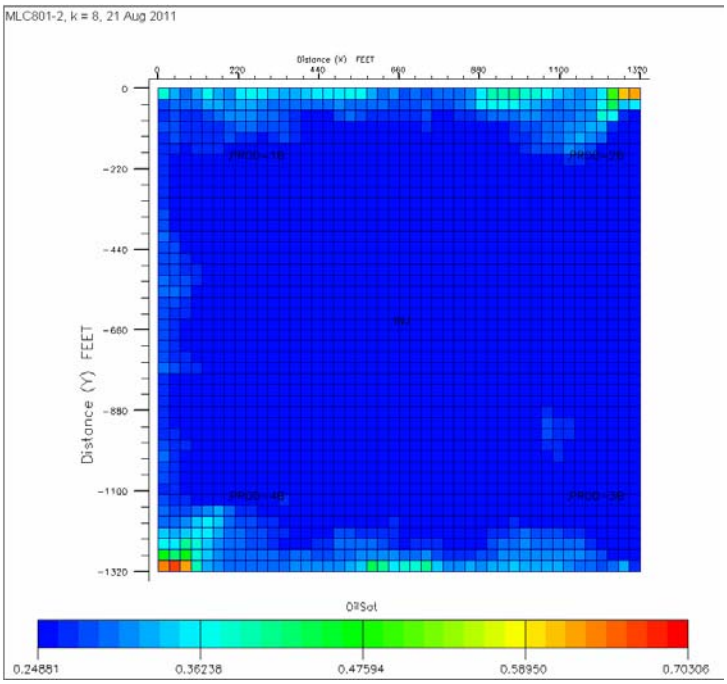

Figure 13- Oil saturation distribution in layer 8 at the end of the simulation

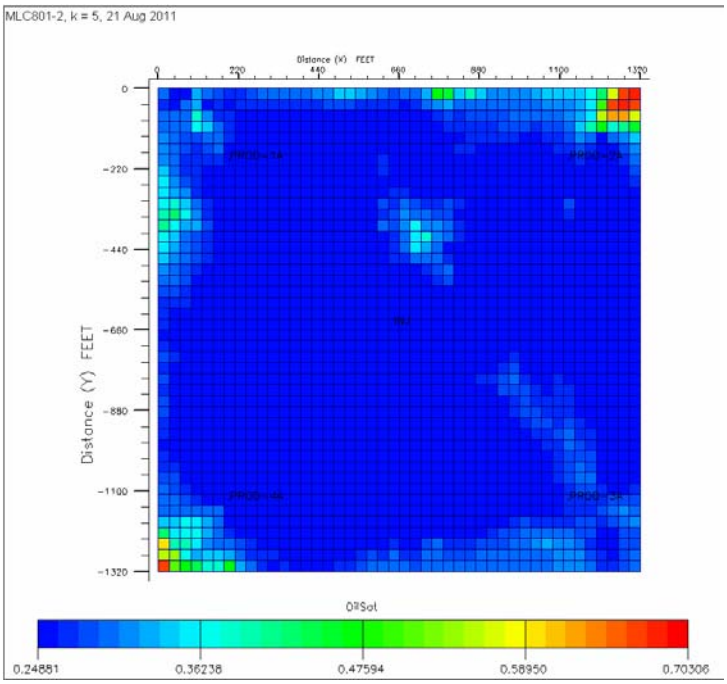

Figure 14- Oil saturation distribution in layer 5 at the end of the simulation

Tracer Tests using Natural Tracers

Crude oil is a mixture of organic components. These components have varying solubilities in water. Partition coefficients and concentrations of aliphatic acids and alkyl phenols present in crude oil are in publications (Reinsel et al., 1994 and Taylor et al., 1997). We have investigated the possibility of using some of the more soluble components as natural tracers to estimate oil saturation and swept pore volumes. The goal is to achieve a low cost alternative to a conventional PITT.

The same heterogeneous permeability field used for the previous simulations has been used to illustrate the production of natural tracers. The initial oil saturation is 0.70. The oil is modeled as five components of different water solubilities. Data for the modeled components was obtained from publications (Reinsel et al., 1994 and Taylor et al., 1997). Table 1 shows the oil components and their initial concentrations. One pore volume of water is injected in 388 days.

Figure 1 shows the concentrations in the produced brine for the components in the crude oil that partition into the brine during a simulated waterflood. As the components are stripped out of the oil phase, their concentrations in both the oil and the water phases decrease with time. The decrease in concentration depends upon the partition coefficient of the component at reservoir conditions. Lower partition coefficients correspond to higher solubility in water and hence a faster decrease in produced concentrations. Figure 14 shows the normalized concentration for phenol. The concentrations are normalized by the initial aqueous phase concentration C_{iwI} assuming local equilibrium between the crude oil and the water. The normalized concentration is defined as follows:

$$C_{niw} = \frac{C_{iwI} - C_{iw}}{C_{iwI}}$$

The normalized tracer curves look similar to tracer curves in a continuous tracer injection. Figure 2 also shows a comparison between a natural tracer and a continuous injection of partitioning tracers. Therefore, the simulation of a continuous tracer with the same partition coefficient gives the same result as simulating a dissolved component i.e. a natural tracer. Although UTCHEM can be used either way, many simulators do not include an option for the dissolution of components of the crude oil into the brine, so they could not be used to model natural tracers directly. But they might be able to model such tracers indirectly in this way.

The measured concentrations of any two partitioning components can be used to estimate oil saturation and swept pore volumes rather than the conventional use of the conservative tracer and one or more partitioning tracers. This is critical to this application because there is no conservative tracer available for the case of natural tracers. Actually, some anionic components of the brine such as the chloride anion are conservative, but not likely to be synchronized with the dissolved components and therefore not useful for calculating oil saturation. Figure 3 shows the estimated initial oil saturations using the various components. Since the initial concentration of the components in the water phase is needed, the choice of oil components will depend upon when the concentration measurements are initiated. For example, if measurement of organic component concentrations were started after 500 days of water injection, the obvious choice of components would be o-cresol and 2,4 -dimethyl phenol. Figure 4 shows a comparison between the estimated swept pore volume and the reservoir pore volume. Since the initial oil saturation and swept pore volumes have been estimated, the oil saturation at the end of a waterflood can be

calculated. Figure 5 shows the estimated oil saturation at the end of a waterflood. The estimated oil saturations and pore volumes match the reservoir values closely.

Naturally Fractured Reservoirs

PITTs in naturally fractured reservoirs will typically take longer and the tracer concentrations will be lower than for single porosity reservoirs due to matrix transfer.14 Therefore, the possibility of using natural tracers in fractured reservoirs has been researched as an alternative to injected tracers since it would cost less than injecting tracers. Natural tracers were simulated for a waterflood in a quarter of a five-spot well pattern with dimensions of 111.5 ft long by 111.5 ft wide by 17 ft thick. The reservoir has a fracture spacing of 3 ft in both the horizontal and vertical directions, which is typical of carbonate beds of equivalent thickness (Nelson, 1985). We modeled the fractures explicitly as distinct gridblocks with the properties of the fracture rather than use the traditional dual porosity approach. The matrix has a porosity of 0.10. The fracture occupies 0.1 % of the total reservoir pore volume. The permeabilities of the fracture and matrix are 1000 and 1 md, respectively. One pore volume of water is injected in 1 year. The oil was modeled as four soluble components initially in equilibrium with the water. This simulation was performed using ECLIPSE.

Figure 6 shows the produced component concentrations. Figure 7 shows the oil saturations calculated from the produced tracers. One of the obvious differences compared to a single porosity simulation is the longer time required to estimate the oil saturation due to the lower rate of decline in the concentrations at the producers. However, the estimates of the oil saturation are ultimately as accurate as for the single porosity cases. At earlier times, the estimated oil saturations are low compared to the matrix values, but even this information could be useful. It might be possible to use inverse modeling to greatly shorten the time required to give useful estimates of the remaining oil saturation.

Table 1—Component Concentrations and Partition Coefficients for the Natural Tracer Simulation

Component	*Initial Concentration in Oil, mg/l*	*Partition Coefficient*
acetic acid	1.0	0.009
butyric acid	1.0	0.084
phenol	1.5	1.3
o-cresol	7.5	5.2
2,4-dimethyl phenol	8.5	15

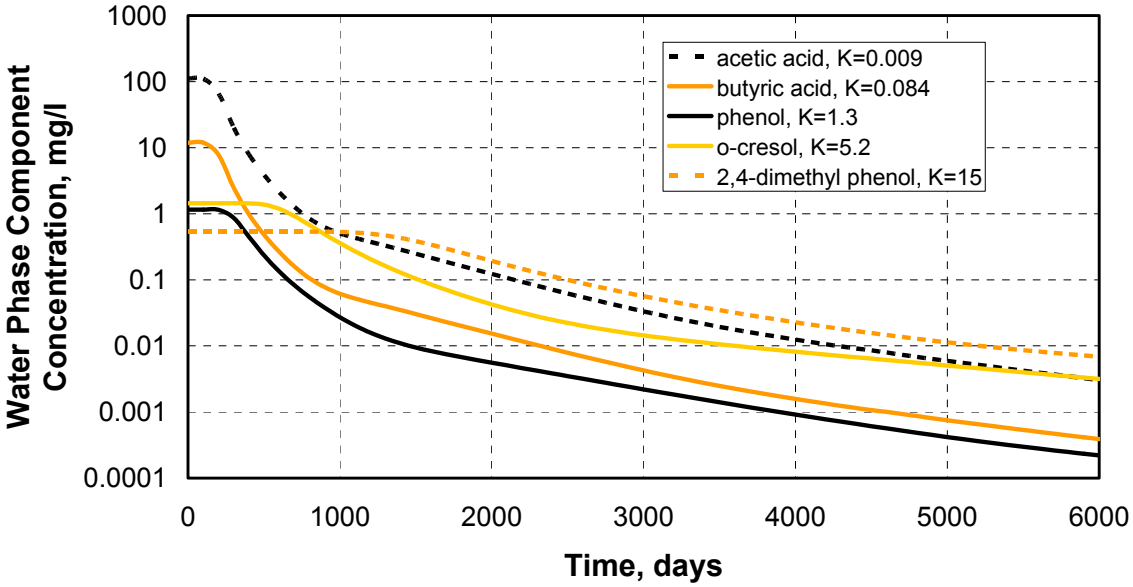

Figure 1- Component concentrations in the water phase.

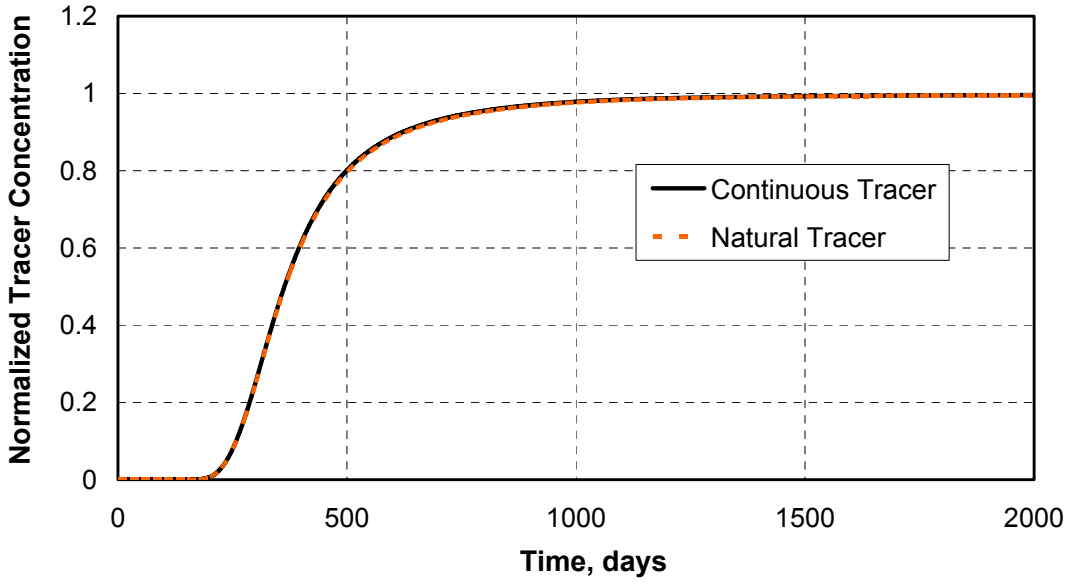

Figure 2- Comparison between natural and continuous tracer injection.

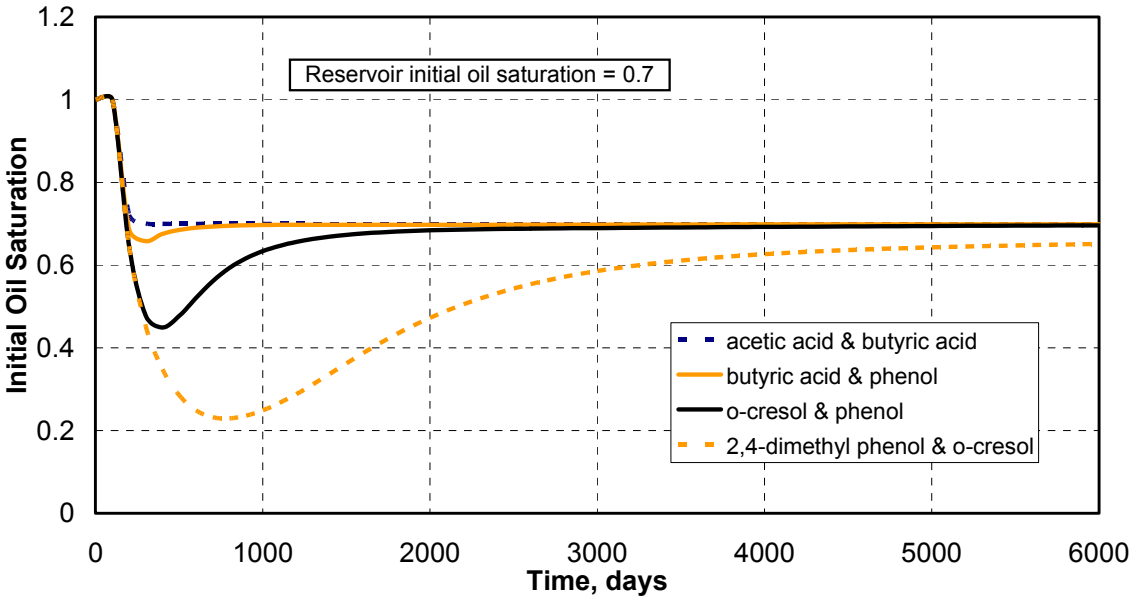

Figure 3- Estimated initial oil saturation using various components for the natural tracer test.

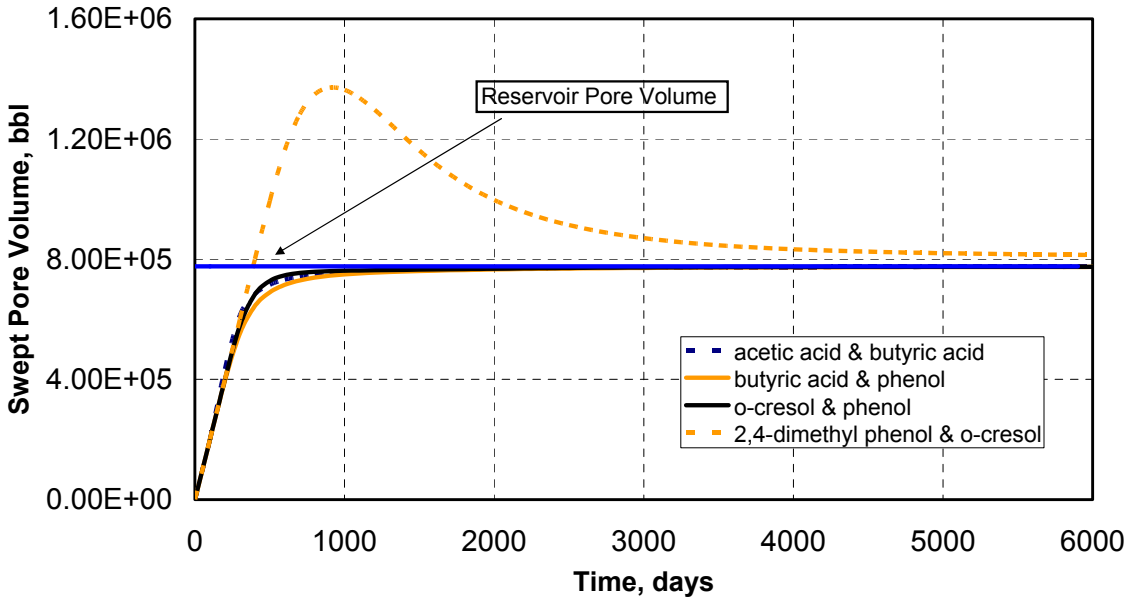

Figure 4- Estimated swept pore volume using various components for the natural tracer test.

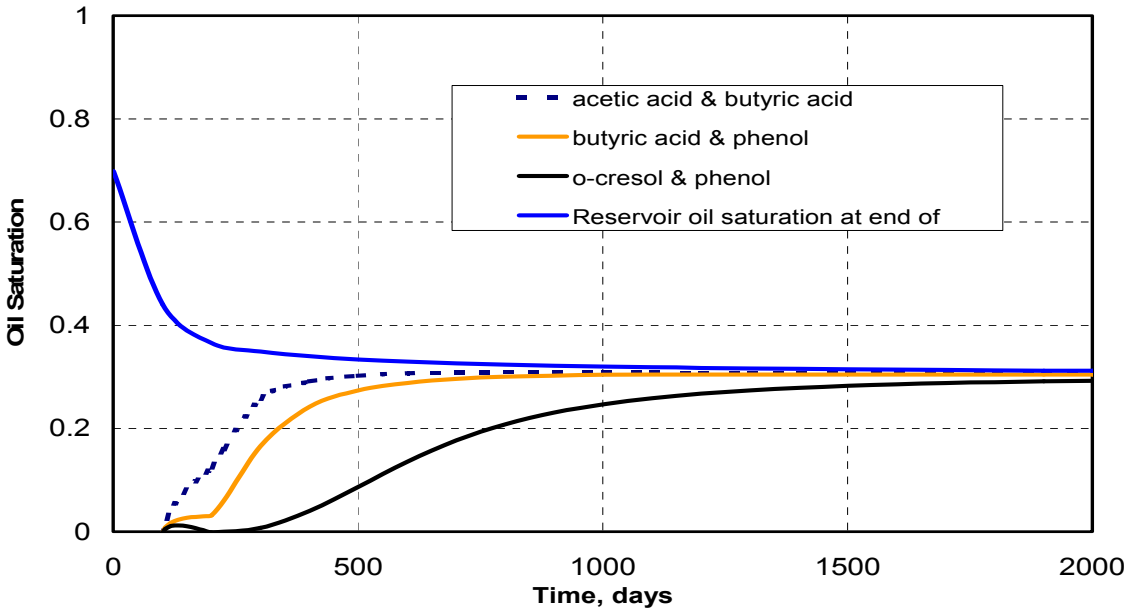

Figure 5- Estimated oil saturation at end of waterflood for the natural tracer test.

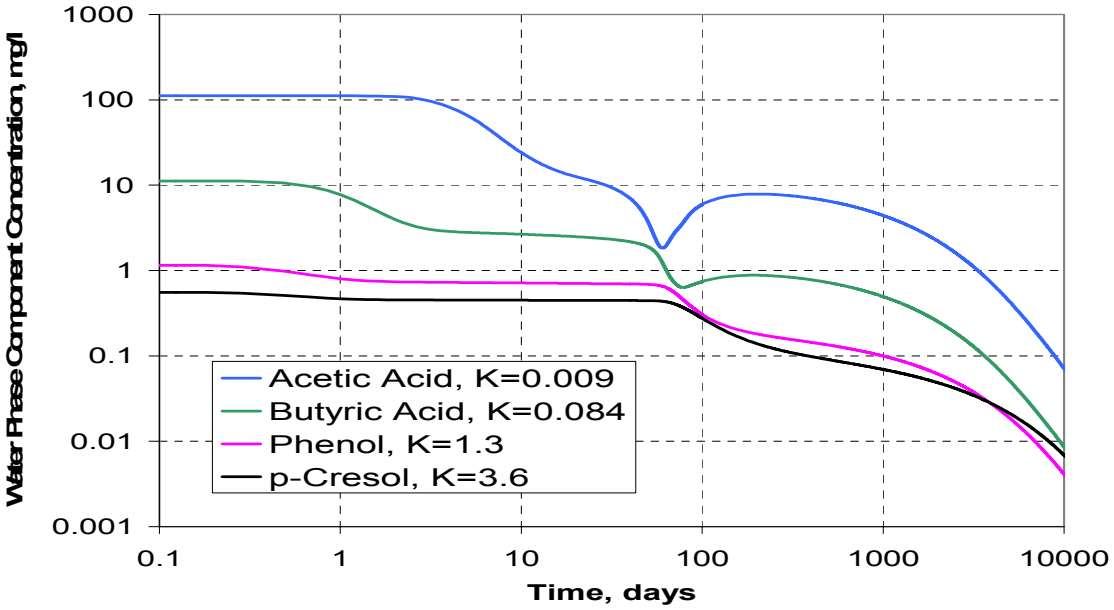

Figure 6- Component concentrations for the fractured reservoir.

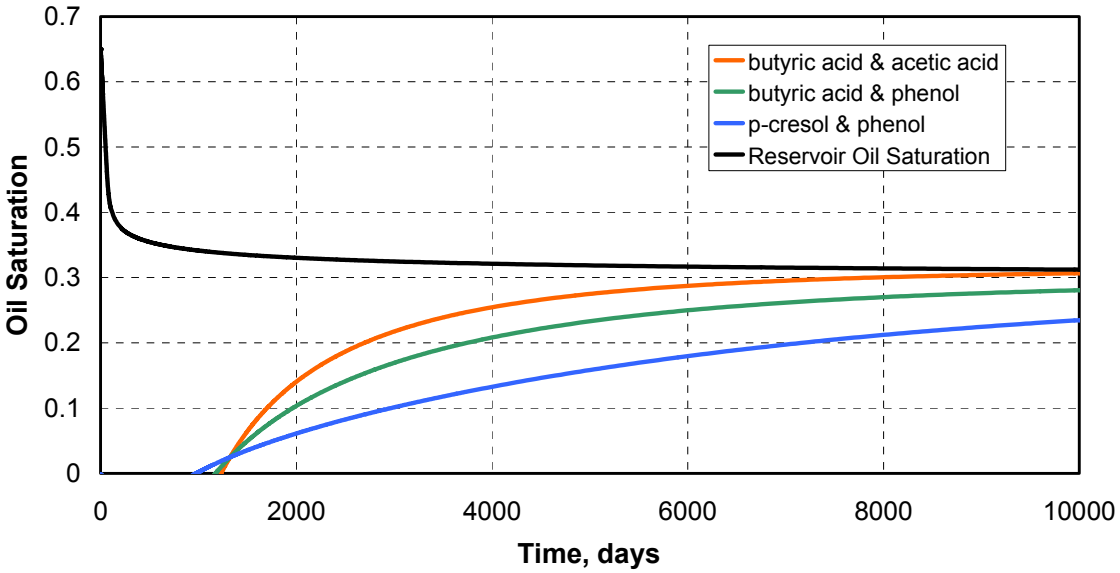

Figure 7- Estimated oil saturations for the fractured reservoir.

Summary and Conclusions

This report discusses several alternative ways of using partitioning interwell tracer tests (PITTs) in oil fields for the calculation of oil saturation, swept pore volume and sweep efficiency, and assesses the accuracy of such tests under a variety of reservoir conditions. The method of moments is used for the interpretation of PITTs in heterogeneous reservoirs with spatially variable residual oil saturation and extends the method to cases with mobile oil saturation. The feasibility of using partitioning tracers to estimate oil saturation at different depths in the reservoir was investigated assuming that the tracer concentrations could be measured with downhole chemical sensors or any other suitable method. The possibility of using natural organic tracers (dissolved components of the crude oil) as a low-cost alternative to injected tracers was also simulated and the method of moments was used to interpret the results for both single porosity and dual porosity reservoirs. All of these applications point to a much greater potential for the PITT technology than is commonly recognized or practiced in the oil field. The results clearly demonstrate that the method of moments is a very simple, fast and robust method to estimate oil saturation and swept pore volumes from either injected or natural partitioning tracer data.

CONCLUSIONS

Part-I

We have presented a general dual porosity dual permeability formulation for streamline simulation of water injection in naturally fractured reservoirs. Our approach accounts for the matrix-facture interactions via transfer functions and reduces to the dual porosity streamline formulation proposed by Di Donato et al.[2] when flow in the matrix is neglected. The proposed approach can be easily implemented within the framework of the conventional single porosity streamline simulators while retaining most of its computational advantages over finite difference models. Some specific conclusions arising from this work can be summarized as follows:

- Streamline simulation can be easily generalized for naturally fractured reservoirs using a dual media approach. As in finite-difference simulation, the matrix and fracture systems are treated as two separate continua interlinked via a transfer function.
- The dual permeability formulation requires streamline generation for both the matrix and the fracture systems. The streamline saturation equations have been presented in the time of flight coordinate that decouples the saturation calculations from the underlying grid. The matrix-fracture transfer function appears simply as a source term in these equations.
- An operator splitting approach is presented to efficiently solve the saturation equation for the dual porosity dual permeability systems. The procedure involves a 'convective step' along streamlines followed by a 'corrective step' on the grid to account for the matrix-fracture interaction.
- We have modeled the matrix-fracture interactions using the conventional transfer function and also an empirical transfer function. For the empirical transfer function, the streamline saturation calculations have been validated using an analytic solution.
- We have compared our streamline-based formulation with ECLIPSE for both dual porosity single permeability (DPSP) and dual-porosity dual-permeability (DPDP) models. In all cases, an excellent agreement is obtained both in terms of water-cut histories and water saturation profiles. Streamline results are shown to be less impacted by numerical dispersion and thus preserves saturation fronts better compared to ECLIPSE.
- A comparison of the scaling of the CPU time with respect to the number of grid blocks shows that the streamline simulator is likely to offer significant computational advantage over finite difference models for large-scale field applications.

Part-II

We have proposed a novel approach to history matching finite-difference models that combines the advantage of the streamline models with the versatility of finite-difference simulation. Streamline-based sensitivity calculations are shown to be adequate for finite-difference simulation with more comprehensive physical mechanisms. We have demonstrated the power and utility of our approach using both synthetic and field examples.
Some specific conclusions from this study can be summarized as follows:

1. A fast history matching approach for finite-difference models is proposed. The new approach combines the versatility of finite-difference simulation with the efficiency of streamline simulation. Use of finite-difference simulation allows us to account for detailed physics including compressibility and gravity effects and also cross-streamline mechanisms.
2. A key aspect of our proposed method is the use of streamline-based sensitivity during history matching finite-difference models. Although these sensitivities are approximate, they seem to be adequate for most purposes and do not significantly impact the quality of the match or the efficiency of the approach.
3. The generalized travel-time inversion for history matching is extremely robust because of its quasi-linear properties. It is computationally efficient, converges rapidly and is designed to preserve geologic realism during history matching. It also eliminates much of the time-consuming trial-and-error associated with manual history matching.
4. We have demonstrated the power and utility of our proposed approach using both synthetic and field examples. A full field application from a giant middle-eastern field with over 80 wells and 30 years of production history convincingly establishes the practical feasibility of the approach. The entire history matching for this field took 9 hours in a PC indicating the potential for cost savings in terms of time and manpower.

Part-III

1. An analytical derivation based on the method of moments has been presented to calculate oil saturations and swept pore volumes using produced tracer concentrations. The general derivation is applicable for three-dimensional heterogeneous reservoirs with mobile oil in the reservoir. The estimated results were quite accurate when compared to the true reservoir values.
2. (Simulations indicate that partitioning interwell tracer tests can be used to accurately estimate the vertical distribution of oil saturation in a reservoir, provided a means such as downhole sensors is available for measuring the tracer concentrations as a function of time and depth in the reservoir. The method of moments is a simple and accurate way to calculate the average oil saturation for each layer in the reservoir.
3. The method of moments has been validated for calculating oil saturation in reservoirs with mobile oil. The procedure is the same as for applications at residual oil saturation except total tracer concentrations are used rather than aqueous phase concentrations. The difference between the average oil saturation during the tracer test and the estimated values was less than 0.01 for all cases simulated.
4. The possibility of using some of the more soluble oil components as tracers for the estimation of oil saturation was investigated. Natural tracers may in some cases provide a low-cost alternative for injected tracers and extend the practical use of the concept of partitioning tracers. In this study, some of the soluble oil components that might be used as natural tracers have been identified based upon their partitioning into water. Oil saturations calculated from the generalized method of moments were in excellent agreement with the actual values even with mobile oil. This method is also not limited to residual oil saturation.
5. The theoretical use of natural tracers was also extended to naturally fractured reservoirs. The values calculated from the generalized method of moments was also in good agreement with the actual values from the simulation in this case, but much longer

waterflood times are required to give good estimates of the oil saturation compared to single porosity reservoirs. However, if natural tracers could be measured over long time periods, this method would give useful results without injecting tracers and other methods such as inverse modeling might greatly shorten the time required to get useful estimates of the remaining oil saturation.

REFERENCES

Part-I

1. Al-Huthali, A.H.: "Streamline-Based Simulation of Water Injection in Naturally Fractured Reservoirs," MS thesis, Texas A&M U., College Station, TX (August 2003).
2. Di Donato, G., Huang, W., and Blunt, M.J.: " Streamline-Based Dual Porosity Simulation of Fractured Reservoirs," paper SPE 84036 presented at the 2003 Annual Technical Conference and Exhibition, Denver, CO, 5-8 October.
3. Bratvedt, F., Bratvedt, K. Buchholz, C. F, Gimes, T., Holden, H., Holden, L. and Risebro, N. H.: "FRONTLINE and FRONTSIM. Two Full Scale, Two-Phase, Black oil Reservoir Simulators Based on Front Tracking," Surv. Math. Ind., 3, 185 (1993).
4. Crane, M. J. and Blunt, M. J., "Streamline-based Simulation of Solute Transport," *Water Resour. Res.*, 35(10), 3061-3078, 1999.
5. Datta-Gupta, A., "Streamline Simulation: A Technology Update," SPE Distinguished Author Series, *Journal of Petroleum Technology*, 68-73 (December 2000).
6. King, M.J. and Datta-Gupta, A.: "Streamline Simulation: A Current Perspective," *In Situ* (1998) **22**, No.1, 91.
7. King, M.J. and Mansfield, M. "Flow Simulation Through Geologic Models," SPE 38877 in Proceedings of the SPE Annual Technical Conference, San Antonio, TX, October 5-8, 1997.
8. Vasco, D.W., Yoon, S., and Datta-Gupta, A.: "Integrating Dynamic Data Into High-Resolution Reservoir Models Using Streamline-Based Analytic Sensitivity Coefficients," paper SPE 49002 presented at the 1998 SPE Annual Technical Conference and Exhibition, New Orleans, LA, 27-30 September.
9. Kazemi, H. *et al.*: "Numerical Simulation of Water-Oil Flow in Naturally Fractured Reservoirs," *SPEJ* (December 1976) 317-26: *Trans.*, AIME **261**.
10. Dean, R.H. and Lo, L.L.: "Simulations of Naturally Fractured Reservoirs," *SPERE* (May 1988) 638-48.
11. Saidi, A.M.: "Simulation of Naturally Fractured Reservoirs," paper SPE 12270 presented at the 1983 SPE Symposium on Reservoir Simulation, San Francisco, California, 15-18 November.
12. Thomas, L. K., Dixon, T.N., and Pierson, R.G.: "Fractured Reservoir Simulation," *SPEJ* (February 1983) 42-54.
13. Sonier, F., Souillard, P., Blaskovich, F.T.: "Numerical Simulation of Naturally Fractured Reservoirs", SPE paper 15627 presented at the 1986 SPE Annual Technical Conference and Exhibition, New Orleans, 5-8 October.
14. Litvak, B.L.: "Simulation and Characterization of Naturally Fractured Reservoirs", Proceedings of the 1985 Reservoir Characterization Technical Conference, Dallas, April 29-May 1.

Part-II

1. Bissel, R.C.: "Calculating Optimal Parameter for History Matching," *Proc*. 4th European Conference on the Mathematics of Oil Recovery, Topic E: History Match and Recovery Optimization, 1994.
2. Vasco, D.W., Yoon, S., and Datta-Gupta, A.: "Integrating Dynamic Data Into High-Resolution Reservoir Models Using Streamline-Based Analytic Sensitivity Coefficients," *SPE Journal* (December 1999) 389.
3. Oliver, D. S.: "Incorporation of Transient Pressure Data into Reservoir Characterization," *In Situ* 18 (3), 243-275 1994.
4. Datta-Gupta, A. *et al.*: "Streamlines, Ray Tracing and Production Tomography: Generalization to Compressible Flow," *Petroleum Geoscience* (May 2001), 75.
5. Yoon, S., Malallah, A.H., Datta-Gupta, A. and Vasco, D.W..: "A Multiscale Approach to Production Data Integration Using Streamline Models," *SPE Journal*, 6(2), 182-192, June (2001).
6. Landa, J.L., Kamal, M.M., Jenkins, C.D., and Horne, R.N.: Reservoir Characterization Constrained to Well Test Data: A Field Example," paper SPE 36511, Presented the 1996 SPE Annual Technical Conference and Exhibition, Denver 6-9 October.
7. Milliken, W.J. *et al.*: "Application of 3-D Streamline Simulation to Assist History Matching," paper SPE 63155 presented at the 2000 SPE Annual Technical Conference and Exhibition, Dallas, 1-4 October.
8. Wang, Y. and Kovscek, A.R.: "A Streamline Approach to History Matching Production Data," paper SPE 59370 presented at the 2000 SPE/DOE Symposium on Improved Oil Recovery, Tulsa, 3-5 April.
9. Wu, Z. and Datta-Gupta, A.: "Rapid History Matching Using a Generalized Travel Time Inversion Method," *SPE Journal*, 7(2), 113-122, June (2002)..
10. Reynolds, A. C., He, N., and Oliver, D.S.: "Reducing Uncertainty in Geostatistical Description with Well Testing Pressure Data," in *Proc*., 1997 International Reservoir Characterization Conference, Houston, 2-4 March.
11. Landa, J.L. and Horne, R.N.: "A Procedure to Integrate Well Test Data, Reservoir Performance History and 4-D Seismic Information into a Reservoir Description," paper SPE 38653 presented at the 1997 SPE Annual Technical Conference and Exhibition, San Antonio, TX, Oct. 5-8.
12. He, Z., Datta-Gupta, A., and Yoon, S.: "Streamline-Based Production Data Integration with Gravity and Changing Field Conditions*," SPE Journal*, 7(4), 423-436, December (2002).
13. King, M.J. and Datta-Gupta, A.: "Streamline Simulation: A Current Perspective," *In Situ* (1998) **22**, No. 1, 91.
14. Wen, X. *et al.*: "High Resolution Reservoir Models Integrating Multiple-Well Production Data," paper SPE 38728 presented at the 1997 SPE Annual Technical Conference and Exhibition, San Antonio, Texas, 5-8 October.
15. Oliver, D. S., Reynolds, A. C., Bi, Zhuoxin and Abacioglu, Y., "Integration of Production data Into Reservoir Models," Petroleum Geoscience, (7), S65-S73, 2001..
16. Yeh, W. W-G: "Review of Parameter Identification Procedures in Groundwater Hydrology: The Inverse Problem," *Water Resources Research* (1986) **22**, No. 2, 95.
17. Anterion, F., Eymard, R. and Karcher, B. : "Use of Parameter Gradients for Reservoir

History matching," paper SPE 18433 presented at the 1989 SPE Symposium on Reservoir Simulation, Houston, February 6-8.

18. Bissel, R.C. *et al.*: "Reservoir History Matching Using the Method of Gradients," paper SPE 24265 presented at the 1992 SPE European Petroleum Computer Conference, Stavanger, 25-27 May.
19. Sun, N-Z and Yeh, W. W.-G.: "Coupled Inverse Problems in Groundwater Modeling, I, Sensitivity Analysis and Parameter Identification," *Water Resources Research* (1990) **26**, 2507.
20. Schlumberger GeoQuest: ECLIPSE Reference Manual 2003A.
21. Provost, M.: "The Streamline Method for Unstructured Grids," M.S. Thesis, Stanford University, Palo Alto, June 2000.
22. Sabir, K. : "Velocity Models, Material Balance and Solution Convergence in Streamline-Based Simulation," M.S. Thesis, Texas A&M University, College Station, Texas, December 2002.
23. Datta-Gupta, A. and King, M.J.: "A Semianalytic Approach to Tracer Flow Modeling in Heterogeneous Permeable Media," *Advances in Water Resources* (1995) **18**, No. 1, 9.
24. Cheng, H., Datta-Gupta, A. and He, Z.: "A Comparison of Travel Time and Amplitude Matching for Field-Scale Production Data Integration: Sensitivity, Non-Linearity and Practical Implications," SPE 84570 presented at the 2003 SPE Annual Technical Conference and Exhibition, Denver, CO, October 5-8.
25. Vega, L., Rojas, D. and Datta-Gupta, A., "Scalability of the Deterministic and Bayesian Approaches to Production Data Integration into Field-Scale Reservoir Models," SPE 79666 presented at the 2003 SPE Reservoir Simulation Symposium, Houston, February 3-5.
26. Parker, R.L.: *Geophysical Inverse Theor*y, Princeton University Press, 1994.
27. Paige, C.C. and Saunders, M. A.: "LSQR: An Algorithm for Sparse Linear Equations and Sparse Least Squares," *ACM Trans. Math. Software* (1982) **8**, No. 1, 43.
28. Nolet, G.: "Seismic Wave Propagation and Seismic Tomography," in *Seismic Tomograph*y, G. Nolet (Ed.), D. Reidel, Dordrecht, (1987) 1-23.
29. Qassab, H, Khalifa, M, Pavlas, R., Khargoria, A., He, Z., Lee, S. H. and Datta-Gupta, A.: "Streamline-based Production Data Integration Under Realistic Field Conditions: Experience in a Giant Middle-Eastern Oil Reservoir," SPE 84079 presented at the SPE Annual Technical Conference and Exhibition, Denver, CO, October 5-8, 2003.

Part-III

1. Allison, S. B., "Analysis and Design of Field Tracers for Reservoir Description," MS thesis, The University of Texas at Austin, 1988.
2. Datta-Gupta, A., Yoon, S., Vasco, D.W. and Pope, G.A., "Inverse modeling of partitioning interwell tracer tests: A streamline approach," Water Resources Research, 38(6), 15.1-15.15, 2002.
3. Delshad, M., Asakawa, K., Pope, G. A. and Sepehrnoori, K., "Simulations of Chemical and Microbial Enhanced Oil Recovery Methods," paper SPE 75237, presented at the SPE/DOE Thirteenth Improved Oil Recovery Symposium, Tulsa, OK, 2002.
4. Delshad, M., Pope, G. A. and Sepehrnoori, K., "A compositional simulator for modeling surfactant enhanced aquifer remediation, Part 1 Formulation," Journal of Contaminant Hydrology, 23, 303-327, 1996.
5. Dwarakanath, V., Deeds, N. and Pope, G. A., "Analysis of Partitioning Interwell Tracer Tests," Environmental Science and Technology, 33, 3829-3836, 1999.
6. ECLIPSE Reference Manual (2002a), Schlumberger Geoquest, Geoquest Reservoir Technologies, Houston, TX, 2002.
7. Jennings, J. W, Ruppel, S. C and Ward, W. B., "Geostatistical Analysis of Permeability Data and Modeling of Fluid-Flow Effects in Carbonate Outcrops," SPE Reservoir Engineering, 3(4), August 2000.
8. Jin, M., Delshad, M., Dwarakanath, V., McKinney, D. C., Pope, G. A., Sepehrnoori, K., Tilburg, C. E., and Jackson, R. E., "Partitioning tracer test for detection, estimation, and remediation performance assessment of subsurface nonaqueous phase liquids," Water Resources Research 31(5), 1201-1211, 1995.
9. Jin, M., "A Study of Nonaqueous Phase Liquid Characterization and Surfactant Remediation," Ph.D. dissertation, The University of Texas at Austin, August 1995.
10. Jin, M., Jackson, R. E. and Pope, G. A., "Development of Partitioning Tracer Tests for Characterization of Nonaqueous-Phase Liquid-Contaminated Aquifers," paper SPE 39293, presented at the SPE 72nd Annual Technical Conference & Exhibition, San Antonio, Texas, 1997.
11. Reinsel, M. A., Borkowski, J. J. and Sears J. T., "Partition Coefficients for Acetic, Propionic, and Butyric Acids in a Crude Oil/Water System," Journal of Chemical Engineering Data, 39, 513-516, 1994.
12. Sinha, R., "Simulation of Natural and Partitioning Interwell Tracers to Calculate Saturation and Swept Volumes in Oil Reservoirs," MS thesis, The University of Texas at Austin, December, 2003.
13. Tang, J. S. and Harker, B., "Interwell Tracer Test to Determine Residual Oil Saturation in a Gas Saturated Reservoir. Part I: Theory and Design," The Journal of Canadian Petroleum Technology, 30(4), 34, 1991a.
14. Tang, J. S. and Harker, B., "Interwell Tracer Test to Determine Residual Oil Saturation in a Gas Saturated Reservoir. Part II: Field Applications," The Journal of Canadian Petroleum Technology, 30(3), 76, 1991b.
15. Taylor, P., Larter, S., Jones, M., Dale, J. and Horstad, I., "The effect of oil-water-rock partitioning on the occurrence of alkylphenols in petroleum systems," Geochimica et Cosmochimica Acta, 61(9), 1899-1910, 1997.

16. Nelson, R. A., Geologic Analysis of Naturally Fractured Reservoirs, Gulf Publishing Company, Texas, 1985.
17. Yoon, S., Barman, I., Datta-Gupta, A., and Pope, G. A., "In-Situ Characterization of Residual NAPL Distribution Using Streamline-based Inversion of Partitioning Tracer Tests," paper SPE 52729 presented at the 1999 SPE/EPA Exploration and Production Environmental Conference, Austin, Texas, 28 February-3 March, 1999.
18. Zemel, B., Tracers in the Oil Field, Developments in Petroleum Science, 43, Elsevier Science B. V., Amsterdam, 1995.

LIST OF ACRONYMS AND ABBREVIATIONS

Part-I

D =Depth from datum, L
f = fractional flow, fraction
F_s = shape factor, L^{-2}
k = permeability, L^2
k_r = relative permeability, dimensionless
l = matrix length, L
P = pressure, $ML^{-1}T^{-2}$
P_c = capillary pressure, $ML^{-1}T^{-2}$
P_{gh} = pressure due to a gravity head in fracture system, $ML^{-1}T^{-2}$
q = source term, L^3T^{-1}
Q_∞ = ultimate oil recovery, L^3
Q = cumulative oil recovery, L^3
S = saturation, fraction
S_{orm} = matrix residual oil saturation, dimensionless
$S_{wn\ m}$ = normalized water saturation in matrix, dimensionless
SP = streamline path
t = time, T
u = velocity, LT^{-1}

Part-II

$\boldsymbol{d}$ = data vector
F_w = fractional flow of water
$\mathbf{I}$ = identity matrix
J = misfit function
k = permeability
$\mathbf{L}$ = spatial difference operator
m = reservoir parameter
$\boldsymbol{m}$ = reservoir parameter vector
Ndj= number of dynamic data observations of jth well
Nw = number of wells
R^2 = coefficient of determination
s = slowness
$\mathbf{S}$ = sensitivity matrix
S_w = water saturation
t = time
Δt = travel-time shift
$\Delta\tilde{t}$ = generalized travel-time
y^{obs} = observed response
$\overline{y^{obs}}$ = averaged observed response

y^{cal} = calculated response
β = weighting factor
τ = time of flight

Part-III

C_i = *Concentration of tracer i*

C_{ij} = *Concentration of tracer i in phase j*

C_{iJ} = *Concentration of the injected tracer slug*

C_{niw} = *Normalized water phase tracer*

C_{io} = *Concentration of tracer i in oil*

C_{it} = *Total tracer concentration of tracer i*

C_{iw} = *Concentration of tracer i in water*

C_{iwI} = *Initial concentration of tracer i in water*

C_{iwJ} = *Injected concentration of tracer i in*

f_o = *Fractional flow of oil*

f_w = *Fractional flow of water*

K_i = *Partition coefficient of tracer i*

$\vec{\vec{K}}_{ij}$ = *Dispersion coefficient of tracer i in phase*

m_n = *Mass of tracer produced at producer n*

M = *Total mass of the tracer injected*

m_{0iw} = *Zeroth temporal moment of concentration of tracer i in water*

m_{0i} = *Zeroth temporal moment of tracer i*

m_{1i} = *First temporal moment of tracer i*

n_p = *Total number of phases*

$\vec{N}_i$ = *Flux of tracer i*

q = *Liquid flow rate*

Q = *Injection rate*

Q_o = *Total oil production rate*

R_{fi} = *Retardation factor of tracer i*

S_j = *Saturation of phase j*

$\hat{S}_j$ = *Average saturation of phase j in reservoir*

S_o = *Oil saturation*

$\hat{S}_o$ = *Average oil saturation in reservoir*

$\overline{\hat{S}_o}$ = *Average oil saturation in swept pore*

S_{or} = *Residual oil saturation*

S_w = *Water saturation*

$\hat{S}_w$ = *Average water saturation in reservoir*

t = *Time*

t_{slug} = *Tracer slug time*

$\vec{u}_j$ = *Flux of phase j*

$\overline{V}_i$ = *Mean residence volume of tracer i*

V_s = *Swept pore volume*

V_{slug} = *Volume of tracer slug*

ϕ = *Porosity*